

Deliverable 2.3 Energy Efficient RAN Architecture and Strategies

March 2025



Contractual Date of Delivery:

Actual Date of Delivery:

March 20, 2025

Editor: Keith Briggs (BT)

Authors: Keith Briggs (BT)

Alejandro Blanco (TSA)

Vladica Sark, Mert Özates, Jesús Gutiérrez (IHP)

Miguel Catalán-Cid, David Reiss, Esteban Municio (i2CAT)

German Castellanos, Simon Pryor (ACC)

Anna Umbert, Juan Sánchez-González, Jordi Pérez-Romero,

Oriol Sallent, Olga Ruiz (UPC)

Joss Armstrong (LMI)

Mir Ghoraishi (GIGASYS)

Work Package: WP2

Target Dissemination Level: Public

This work is supported by the Smart Networks and Services Joint Undertaking (SNS JU) under the European Union's Horizon Europe research and innovation programme under Grant Agreement No 101097083, BeGREEN project. Views and opinions expressed are however those of the author(s) only and do not necessarily reflect those of the European Union or SNS-JU. Neither the European Union nor the granting authority can be held responsible for them.



Revision History

Revision	Date	Editor / Commentator	Description of Edits	
0.1	2024-10-30	Keith Briggs (BT) Jesús Gutiérrez (IHP)	Table of contents/ work distribution	
	2024-11-04		Added partner outline plans	
0.2	2024-12-09	Koith Driggs (DT)	Added material on energy score	
0.2	2024-12-12	Keith Briggs (BT)	Added lots of new material	
	2024-12-16		Added some intro material	
0.3	2024-12-18	Miguel Catalan (i2CAT)	Added initial inputs in section 4.8	
0.4	2024-12-20	Anna Umbert (UPC)	Added material to 3.5.4, 4.2, 4.3 and 4.4	
0.5	2024-12-23	Alejandro Blanco (TSA)	Added material to 4.1	
0.6	2025-01-08	Anna Umbert (UPC)	Added material on system-level simulators 3.4.2	
0.7	2025-01-13	Keith Briggs (BT)	Many minor edits	
0.8	2025-02-10	Keith Briggs (BT)	Final edits	
0.9	2025-01-28	Keith Briggs (BT)	Final review	
0.91	2025-02-14	Krishnakant Tiwari (BT)	Independent review	
0.94	2025-02-27	Jesús Gutiérrez (IHP)	Final revision of the document	
0.95	2025-03-15	Mir Ghoraishi (GIGASYS)	Final revision before submission	
1.0	2025-03-20	Simon Pryor (ACC)	Submission to the EC	



Table of contents

List of Figures	6
List of Tables	8
List of Acronyms	9
Executive Summary	
1 Introduction	
2 Simulation frameworks for the study of energy efficiency	
2.1 Introduction and objectives of the chapter	13
2.2 The 3GPP channel models used in this work	
2.3 Definition of the energy score	14
2.4 Descriptions of the simulation software platforms	15
2.4.1 System-level: the AIMM 5G simulator	15
2.4.2 System-level: the UPC 5G simulator	
2.5 Descriptions of the simulation scenarios	16
·	
2.5.1 Cellular reference model	
2.5.2 Adastral Park mockup scenario	
2.5.3 UPC University Campus scenario	
2.5.4 Real dataset-based scenario in Spain	
3 Case Studies Simulation Results	25
3.1 Evaluation of the energy savings by use of a cell-free	architecture25
3.1.1 Evaluation of the number of antennas	25
3.1.2 Cell-free evaluation	27
3.1.3 Conclusions	28
3.2 Assessments of energy savings through relay nodes	29
3.2.1 Considered scenario and assumptions	29
3.2.2 Energy saving results	30
3.2.3 Conclusions	33
3.3 Comparative analysis of RIS and relay nodes for energy	gy saving34
3.3.1 System model	34
3.3.2 Impact of the model parameters	
3.3.3 Analysis in the campus scenario	
3.3.4 Conclusions	
3.4 Implications of operating frequency on power consu	mption45
3.4.1 Considered scenario and assumptions	45
3.4.2 Results	
3.4.3 Conclusions	
3.5 Network optimization given ISAC data	
3.5.1 Considered scenario and assumptions	
3.5.2 Power saving based on user density	
3.6 Limits on energy efficiency for the CRM	
3.7 DU uplink energy efficiency corresponding to the ce	IIular reference model56

D2.3 – Energy Efficient RAN Architecture and Strategies



3.8	Da	ata-driven analysis of energy-QoS trade-off in traffic offloading scenarios	57
	.8.1	Methodology	57
3.9	Pe	erformance assessment of energy savings via A1 policies at Adastral Park	65
3.	9.1	Results	66
3.	9.2	Conclusions	70
4 KI	PI resu	ults	71
5 Sı	umma	ry and conclusions	73
6 R	eferen	nces	75



List of Figures

Figure 2-1 The ETSI RMa (rural macrocell) pathloss models, for LoS, and NLoS	13		
Figure 2-2 The 3GPP UMa (urban macrocell) pathloss models, for LoS, and NLoS			
Figure 2-3 Main components of the AIMM simulator			
Figure 2-4 Cellular reference model (CRM) scenario depiction			
Figure 2-5 Use Case 1 - SFN Energy Management			
Figure 2-6 a) General location of sites in Adastral Park, b) mapping of sites onto the VIAVI RIC Tester			
Figure 2-7 a) Normalised daily traffic based on [8]. b) Traffic and users for the Adastral Park			
Figure 2-8 Adastral Park a) SS-SINR drive test results, b) example of car mobility in Viavi RIC tester			
Figure 2-9 SINR simulation for the emulation radio scenario			
Figure 2-10 UPC Campus Nord scenario			
Figure 2-11 Region covered by the dataset			
Figure 3-1 Number of antennas evaluation			
Figure 3-2 Cell-free vs C-MIMO scenario	27		
Figure 3-3 Cell-free and C-MIMO BER results	28		
Figure 3-4 Spectral efficiency (b/s/Hz) in the ground (Gr) floor (a), first floor (b) and second floor (c) when the BS			
transmitted power is fixed to 38 dBm. Buildings selected for the analysis and relay positions indicated by black do	ots 31		
Figure 3-5 Average energy saving percentages for required bit rate 50 Mbps in different buildings and floors	32		
Figure 3-6 Average energy saving percentages for required bit rate 100 Mbps in different buildings and floors	33		
Figure 3-7 Average energy saving percentages in different buildings and floors as a function of the required bit ra	te for		
the best combination (a) and the worst combination (b)	33		
Figure 3-8 Considered communication options. (a) Reference case. (b) Use of a relay node. (c) Use of a RIS	34		
Figure 3-9 Involved angles in azimuth and elevation for the BS-RIS and RIS-UE links	36		
Figure 3-10 Considered scenario	38		
Figure 3-11 Energy saving percentage achieved for different θ_r values with (a) $L_{BS,RIS}$ =70 dB, (b) $L_{BS,RIS}$ =100 dB			
Figure 3-12 Power consumption difference of the relay with respect to the RIS as a function of the azimuth θ_r Figure 3-13 Impact of the pathloss between BS and RIS/relay in terms of (a) energy saving, (b) PCR metric			
Figure 3-15 Pathloss values (dB) experienced at the ground level with BS2 and studied situations. Locations are in			
ground floor for cases 1, 2, 3, 5, 11, 12, 13, 15, in the 1st floor for cases 4, 6, 7, 10, 14, 16, 17, 20 and in the 2nd fl			
for cases 8, 9, 18, 19	42		
Figure 3-16 PCR metric for the studied situations as a function of the pathloss between BS and RIS/relay (a) and			
between RIS/relay and UE (b)	42		
Figure 3-17 Energy saving with the relay and the RIS for each studied situation			
Figure 3-18 PCR metric at the first floor in A5 building			
Figure 3-19 Percentage of pixels of the ground floor where the RIS requires less power than the relay (blue line) a			
where the relay requires less power than the RIS (orange line) as a function of the RIS pointing angle			
Figure 3-20 Spectral efficiency maps (b/s/Hz) of the campus with (a) 26GHz (a) and (b) 3.72GHz, both with P_T =380			
Figure 3-21 Spectral efficiency maps (b/s/Hz) of the campus with 26 GHz and P_T =65 dBm			
Figure 3-22 Spectral efficiency map (b/s/Hz) of the campus with 26 GHz, beamforming and P _T =38 dBm			
Figure 3-23 Spectral efficiency maps (b/s/Hz) of the campus with 26GHz, beamforming and P _T =42 dBm			
Figure 3-24 Scenario 1 (dense): daytime with 4 BS, 150 users			
Figure 3-25 Scenario 2 (sparse): night-time with 1 BS, 70 users			
Figure 3-26 Average received power per user (daytime)			
Figure 3-27 Average received power per user (night-time)			
Figure 3-28 Scenario 1: daytime with 4 BS, 150 users			
Figure 3-29 Scenario 2 (sparse): night-time with 1 BS, 60 users			
Figure 3-30 CCDF of spectral efficiency for the CRM with RMa-LoS pathloss			
Figure 3-31 CCDF of spectral efficiency for the CRM with RMa-NLoS pathloss			
Figure 3-32 CCDF of spectral efficiency for the CRM with UMa-LOS pathloss			
Figure 3-33 CCDF of spectral efficiency for the CRM with UMa-NLOS pathloss			





Figure 3-34 Energy consumption comparison: 4G vs 5G 3500 MHz carriers	58
Figure 3-35 Utilization comparison: 4G vs. 5G carriers	58
Figure 3-36 Load of a selected cell during the analysed week in percentage of total PRBs: Aggregated 4G (blue), 5G	
(orange), and aggregated plus offloaded demand in 4G (green)	59
Figure 3-37 Average load (blue) and energy consumption (orange) of one 5G 3500 MHz node	60
Figure 3-38 Correlation between load (% of PRBs) and average throughput per UE KPIs – (a) 5G 3500 MHz cell and	(b)
4G 2600 MHz cell	61
Figure 3-39 Traffic offloading and QoS impact characterization pipeline	62
Figure 3-40 Evaluation of Energy-QoS trade-off using 100% threshold: (a) Calculated switch-off time (% of the	
analysed week), (b) Time above defined QoS levels per percentage of cells (CCDF)	63
Figure 3-41 Evaluation of Energy-QoS trade-off using different thresholds: (a) Average switch-off time vs assured	
throughput, (b) Percentage of switching-off time above 10 Mbps level per percentage of cells (CCDF)	64
Figure 3-42 Threshold distribution of the cells for each throughput level. For each throughput level, cases where the	ne
5G cell remains off continuously due to low load are not considered (i.e., no threshold can be inferred)	65
Figure 3-43 General location of sites in Adastral Park, b) mapping of sites on the VIAVI AI RSG Tester	65
Figure 3-44 Dashboard providing energy savings metrics, policies and general cell metrics.	66
Figure 3-45 Energy Saving results for the Adastral Park use case.	67
Figure 3-46 Power consumption results from the Adastral Park use case	68
Figure 3-47 Ratio between the requester traffic and the served traffic in the Adastral Park use case	68
Figure 3-48 Energy score in khos/Liresults for the Adastral Park use case	69



List of Tables

Table 2-1 Telemetry Requirements	18
Table 2-2 Adastral Park Site Coordinates	20
Table 2-3 Dataset Description	23
Table 2-4 4G and 5G Radio Specifications	23
Table 2-5 Relevant KPI Description	24
Table 3-1 Simulation Parameters	29
Table 3-2 Power Consumption Parameters	30
Table 3-3 Model Parameters	38
Table 3-4 Power Consumption for the Same Coverage	47
Table 3-5 Power consumption for the Same Coverage with Beamforming	48
Table 3-6 Performance Metrics after Optimization	52
Table 3-7 Optimized Power Levels in dBm	
Table 3-8 Corresponding Power Levels for a Fixed Rx Power	52
Table 3-9 Minimum Required Transmit Power and Power Consumption Reduction	
Table 3-10 Energy Score Ratios Predicted by The AIMM Simulator for the Cellular Reference Model	
Table 3-11 Estimated Energy Score Ratios for Rx DU Scenarios	57
Table 4-1 BeGREEN KPI Evaluation (based on that in BeGREEN D2 2 [2] and to BeGREEN D5 2 [34])	71



List of Acronyms





SCS	Subcarrier Spacing
SFN	Single Frequency Network
SINR	Signal-to-Interference-plus-Noise Ratio
SNR	Signal-to-Noise-Ratio
SNS JU	Smart Networks and Services Joint Undertaking
TDD	Time Division Duplex
UE	User Equipment
UL	Uplink
UMi	Urban Microcell
vRAN	Virtualized RAN
WP	Work Package



Executive Summary

BeGREEN D2.3 provides evaluation and benchmarking, using simulation techniques, of the energy-saving mechanisms studied in BeGREEN. An end-to-end (E2E) system-level software simulator has been developed, so that the different energy-efficiency mechanisms in various parts of the network can be tested simultaneously, and in interaction with each other. The term 'system-level' means that all important network components are simulated, but for those at the link level (especially for radio links), approximations are used.

The simulator was used to emulate cellular deployments utilizing the different architectures studied so far in BeGREEN, while implementing the different mechanisms. In this way, the forecasts on how real systems with the proposed novel mechanisms behave are obtained. This will enable us to predict the energy efficiency levels that can be achieved. Several energy-saving-focused experiments were carried out, where their findings are:

- 1. Cell-free architecture reduces the transmit power by 30 dB compared to collocated MIMO.
- 2. An energy savings of 90% is achieved by placing relays on floors of buildings with poor coverage.
- 3. It is observed that RIS provides higher energy savings when the pathloss is lower than 90 dB while for higher values, relays are suitable for energy-saving purposes.
- 4. The findings in the network optimization given sensing data in terms of power consumption demonstrate that, by turning off some of the BSs and turning on the optimal BS given a certain scenario, the power consumption can be reduced by 15% to 50%, depending on the performance metric to optimize.
- 5. The achievable fundamental limits on energy score improvements were analysed in a simulated and realistic 5G system.
- 6. A UL-DU energy score improvement of approximately 40% compared to legacy architectures can be achieved.
- 7. Network-wide cell switch-off opportunities ranging from 17% to 79% while ensuring data rates of 25 Mbps and 5 Mbps, respectively, are shown.
- 8. By dynamically adjusting transmission power and selectively deactivating Radio Units (RUs) during low-demand periods, energy savings of up to 84% were achieved.



1 Introduction

This document, Begreen D2.3, builds upon the foundation laid out in Begreen D2.1 [1], which provides a comprehensive overview of the state-of-the-art Radio Access Networks (RANs) from an energy efficiency (EE) perspective.

Expanding upon this groundwork, BeGREEN D2.2 [2] provided an initial analysis of the Key Performance Indicators (KPIs) of the project, Key Value Indicators (KVIs), and societal Key Values (KVs). BeGREEN D2.2 [2] proposed a suite of mechanisms to bolster RAN energy efficiency. Finally, we proposed an evolved architecture to integrate these mechanisms seamlessly in BeGREEN D2.2.

Extending the valuable findings for energy reduction in the RAN, BeGREEN D2.3 aims to provide RAN energy-saving mechanisms with a broader scope. While in BeGREEN D2.2 four mechanisms were evaluated independently, this BeGREEN D2.3 provides a common framework for simulation purposes. In particular, it is considered a common scenario called the cellular reference model where the results of link-level simulators are evaluated using the same reference scenario.

In addition, we propose the AIMM simulator that emulates a cellular radio system roughly following 5G concepts and channel models. AIMM is a system-level simulator that allows us to implement energy-reduction algorithms in large-scale 5G networks.

Finally, BeGREEN D2.3 assesses nine different energy-saving studies. Our observations are quite diverse, and we conclude that we reduce energy consumption at different levels of the RAN by:

- 1. using cell-free architectures,
- 2. using relays and Reconfigurable Intelligent Surfaces (RIS),
- 3. sensing the environment,
- 4. minimizing the transmitting power of different base stations (BSs),
- 5. switching off cells, and
- 6. policies that adjust transmit power and deactivate Radio Units (RUs).

Begreen D2.3 is structured in five chapters, with the main body of the content being in Chapters 2 and 3. Chapter 1 is an overall introduction. Chapter 2 proposes a set of simulation frameworks to study the minimization of energy consumption in the network. Chapter 3 presents the simulation results from studies of nine separate scenarios. Finally, Chapter 4 provides the updated KPIs and Chapter 5 concludes the document.



2 Simulation frameworks for the study of energy efficiency

2.1 Introduction and objectives of the chapter

This section describes the two main types of simulation software used in the energy-minimization studies employed in this document. It is important to be very clear about the strengths and weaknesses, and the differences between these two types. These are, in fact, mutually supportive but largely non-overlapping.

- 1. <u>Link-level simulators</u>: these typically have very accurate models of the radio channel, as well as modelling at least part of the protocols stack, including packet buffering and resource-block allocation. However, simulations of this type are computationally very intensive, and it is not feasible to simulate an entire network to this level of detail.
- 2. <u>System-level simulators</u>: these typically use a more approximate model of the radio channel in order to speed up simulations of large networks. In practice the loss of detail in modelling the radio channel is not significant, because the average performance is still correctly captured.

2.2 The 3GPP channel models used in this work

It is an important principle of radio simulation work that radio channel models (also called pathloss models) conform to agreed standards. This is so that meaningful comparisons can be made between different scenarios. In this work we use the following channel models from standards documents.

- 1. RMa: the Rural Macrocell model from ETSI standard 38.901 v18.0.0, Table 7.4.1-1, p.27 [3]. There are Line-of-Sight (LoS) and Non-Line-of-Sight (NLoS) variants, as plotted in Figure 2-1.
- 2. UMa: the Urban Macrocell dual-slope pathloss model, from 3GPP standard 36.873, Table 7.2-1 [4]. Again, there are LoS and NLoS variants, as plotted in Figure 2-2.
- 3. UMi: the Urban Microcell model, from 3GPP TR 38.901 v18.0.0, section 7.4 [3].
- 4. InH: the 3D-InH indoor pathloss model, from 3GPP standard 36.873, Table 7.2-1 [5].

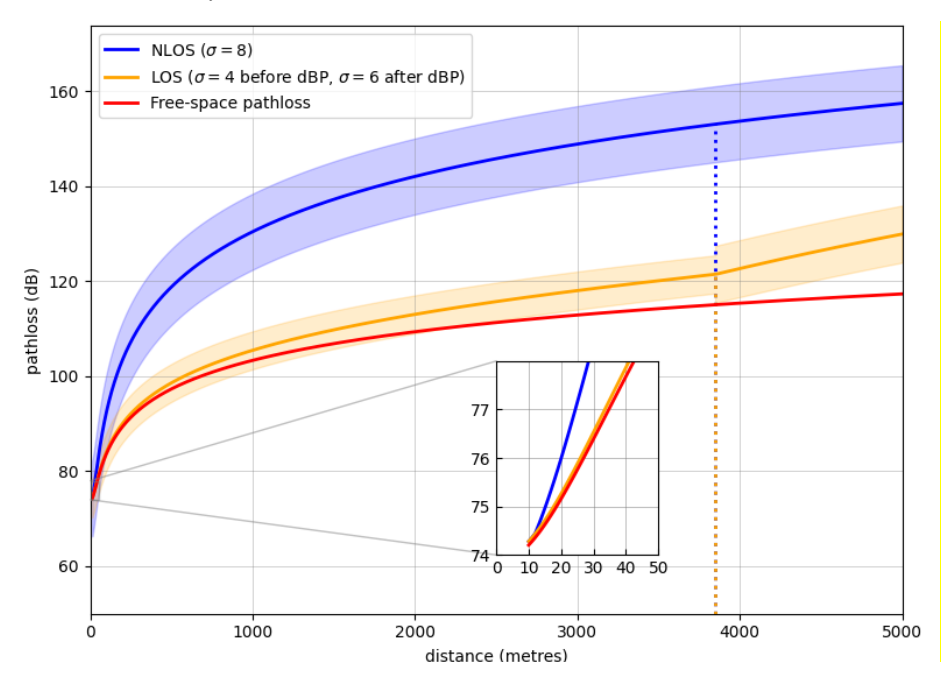


Figure 2-1 The ETSI RMa (rural macrocell) pathloss models, for LoS, and NLoS



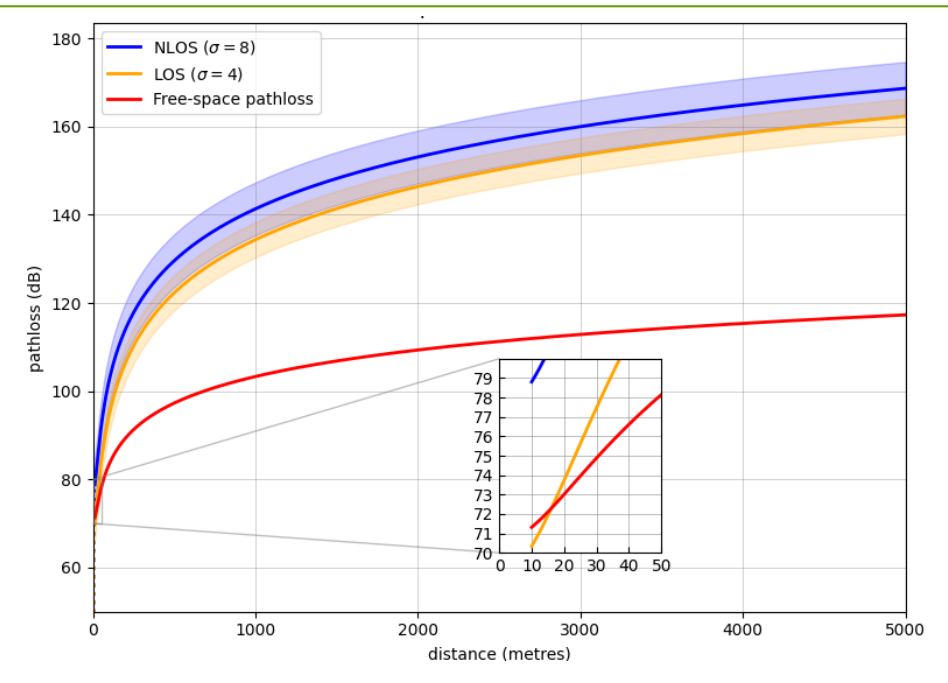


Figure 2-2 The 3GPP UMa (urban macrocell) pathloss models, for LoS, and NLoS

2.3 Definition of the energy score

Though the definition of energy score has been covered in BeGREEN WP4, and published in BeGREEN D4.2 [6], some expansion is needed here to clarify details sufficiently, in order to have a fully precise definition which can be implemented in the code of the various simulations.

The NGNM 5G whitepaper (2015) defined energy efficiency as "the number of bits that can be transmitted per Joule of energy, where the energy is computed over the whole network, including potentially legacy cellular technologies, radio access and core networks, and data centres".

The BeGREEN project uses the same definition but renames the same concept as *energy score*. An equivalent definition may be obtained by the following algebraic manipulations:

energy score = (bits transmitted)/(Joules expended) (averaged over the time considered)

- = (bits transmitted in 1 second)/(Watt-seconds expended in 1 second)
- = (throughput in bits/s)/(Watt-seconds expended in 1 second)

Thus, the units can be written as either bits/J, or bits/s/W. The second way is more useful, because the NGMN definition does not mention time. An "instantaneous" value for the energy score (a short-time-period average), in practice over short interval such as 1 second, is easier to implement in simulation code.

At all times, when using this definition, we need to make clear the part of the network over which it is being applied; that is, we must specify the source and destination of the bits being transferred.

In many of the simulation results to be presented here, a ratio of energy scores is used before and after optimization. The *energy score ratio* will be our overall metric for the quality of an energy-minimization strategy.

The following potential deficiencies of the definition should be kept in mind:

- 1. It values all bits equally there is no notion of any utility function in the definition.
- 2. It also values all energy equally a more precise model would include an energy utility function to capture the idea that some energy has higher value, or has higher monetary or environmental cost,



than other energy.

- 3. What happens when the data transmitted and the energy consumption are both zero (e.g., due to an optimization action switching off a cell)?
- 4. What happens when switching off a cell results in very low baseline energy consumption and zero traffic? According to the formula, this would yield an energy score of zero, which is worse than transmitting 1 bit while consuming a huge amount of energy.

Future work may well come up with a revised definition of energy score, which considers these deficiencies. However, for the present work, we have found the simplest definition to be sufficient.

2.4 Descriptions of the simulation software platforms

2.4.1 System-level: the AIMM 5G simulator

The AIMM simulator¹ emulates a cellular radio system roughly following 5G concepts and channel models. The intention is to have an easy-to-use and fast system written in pure Python with minimal dependencies. It is especially designed to be suitable for interfacing to AI engines such as TensorFlow or PyTorch (though these have not been used in BeGREEN), and it is not a principal aim for it to be extremely accurate at the level of the radio channel.

The AIMM simulator uses a discrete event simulation framework. Internally, a queue of pending events (such as periodic UE reports) is maintained, but this is invisible to the programmer (see Figure 2-3). All functions and classes have default arguments appropriate to the simulation of a 5G macrocell deployment at 3.5 GHz. This means that setting up a simple simulation is almost trivial, but also means that care is needed to set parameters correctly for other scenarios. Subbanding of the channel is implemented on all Cell objects, but the number of subbands may be set to 1, effectively switching off this feature.

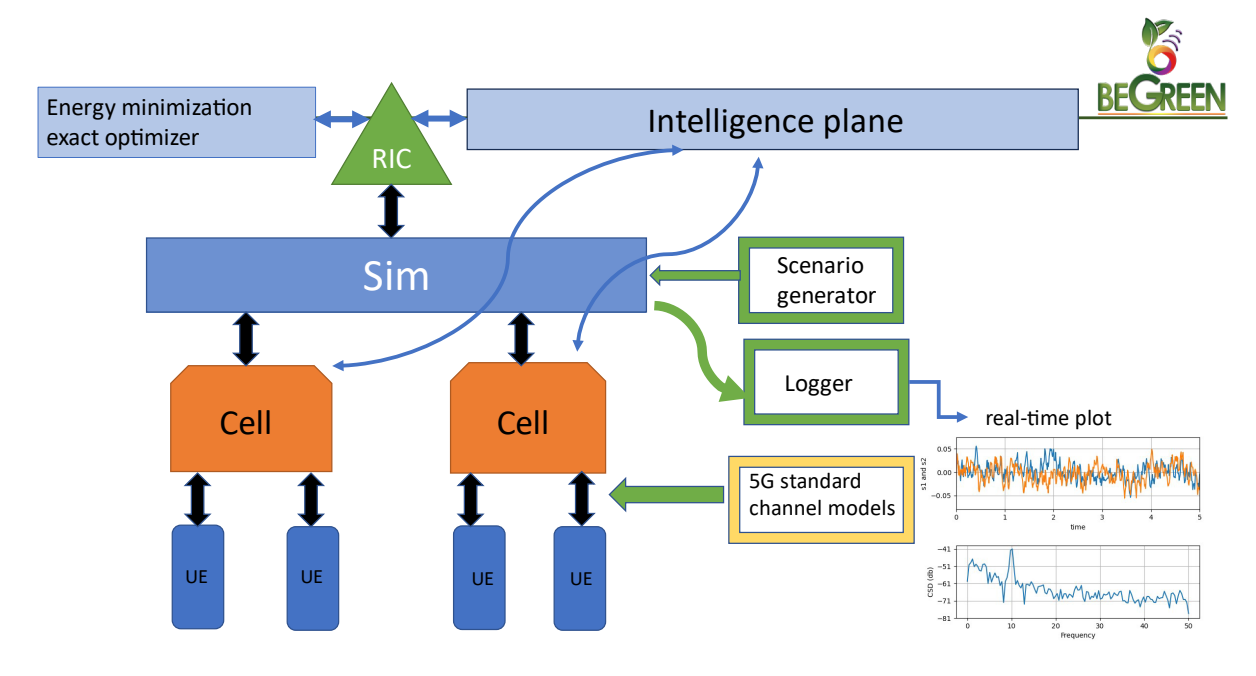


Figure 2-3 Main components of the AIMM simulator

-

¹ https://github.com/keithbriggs/AIMM-simulator



The AIMM simulator normally operates without a graphical user interface, and simplest writes logfiles for subsequent analysis. The default logfile format is tab-separated columns, with purely numerical data. These files can then be easily processed with shell utilities such as cut, head, tail, etc., or read into, for example, python, MATLAB, or R scripts. However, a custom logger can be implemented to create a logfile in any desired format.

The diagram below shows the main components of the AIMM simulator, with the two added BeGREEN-specific components of the exact optimizer – conceptually a Radio Intelligent Controller (RIC) xApp – and the BeGREEN Intelligence Plane (conceptually a set of interfaces between energy-management algorithms, implemented on top of standard O-RAN interfaces).

2.4.2 System-level: the UPC 5G simulator

The *Universitat Politècnica de Catalunya* (UPC) 5G simulator is a system-level simulator developed with Matlab. It allows defining an urban environment composed of buildings and streets, in which a number of base stations and relays can be deployed at specific positions. For each base station or relay, it computes the propagation losses according to a selected propagation model, which can be UMa or UMi for outdoor base stations or relays or InH for indoor relays. The computation also includes shadowing with 2D spatial correlation, outdoor-to-indoor (O2I) losses, and identification of LoS and NLoS areas. Based on the propagation loss the simulator also obtains other metrics such as the SINR and spectral efficiency. All these computations are performed on a pixel basis, where the default size of the pixel is 1m × 1m. Inside the buildings the computations are also performed on different floors.

The simulator also allows modelling a number of User Equipments (UEs) whose locations are selected according to a specific spatial distribution that can be either homogeneous, or defined based on real measurements such as those of [7]. UEs can remain stationary at fixed locations, either indoor or outdoor, or they can move around the scenario (e.g. pedestrians moving around the streets). UEs can connect to the base stations and relays to get service during a certain session time. Moreover, some of the UEs can be configured to act as relay UEs, thus providing connectivity to other UEs.

The studies presented in BeGREEN WP2 exploit the pixel-based propagation and spectral efficiency computations considering the UPC university campus scenario described in section 2.5.3. In turn, the capabilities of UE generation are used for the results presented in the BeGREEN WP4 studies.

2.5 Descriptions of the simulation scenarios

In BeGREEN D2.1 [1] the RAN was identified as the most power-consuming element with up to 73% of the total power consumption. Therefore, reducing the energy consumption of the RAN will significantly reduce the total consumption. To this end, four mechanisms were identified, i.e., (1) D-MIMO deployments, (2) Sensing-aided resource allocation of radio resources, (3) B5G RAN enhanced through relay nodes, and (4) Energy-aware computing allocation in virtualized RAN (vRAN). The following descriptions target these objectives.

2.5.1 Cellular reference model

For this section, we have defined at cellular reference model (CRM) as follows: there are either 7 or 19 cells in a regular hexagonal array, as depicted in Figure 2-4. Cell spacing is a model parameter. There are a number of UEs, typically 100, distributed randomly and uniformly over the covered area. A Poisson Point Process (PPP) model is chosen, as commonly used in this type of modelling. This implies that the model parameter is the *mean number* of UEs per unit area, not the exact number. The pathloss model will be one of the ETSI or 3GPP standard types, defined above.



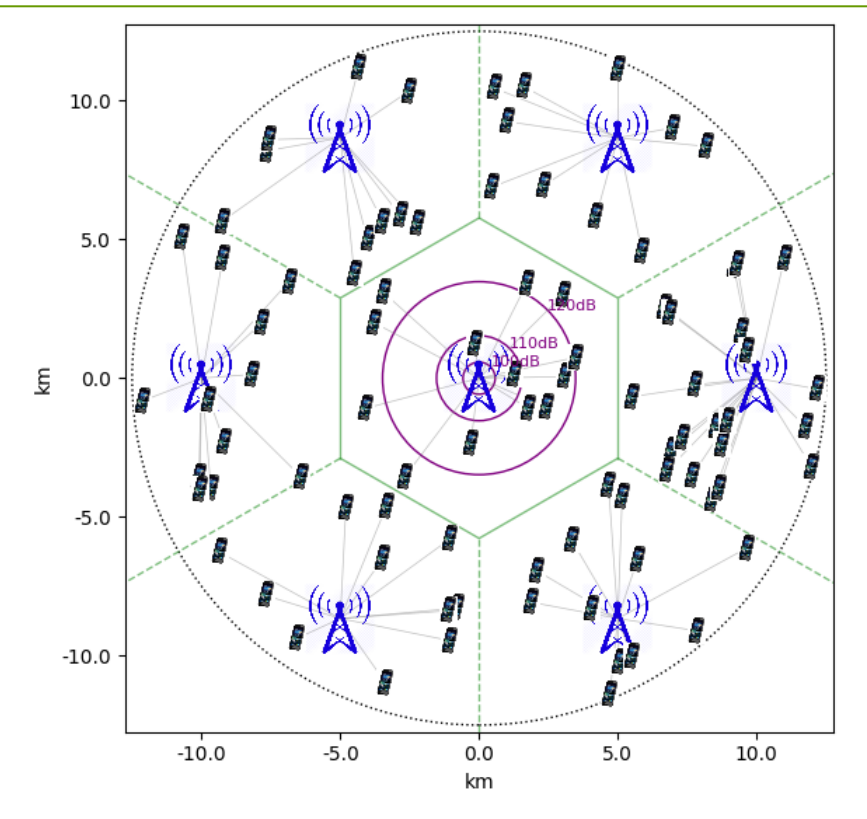


Figure 2-4 Cellular reference model (CRM) scenario depiction

Next, we describe one of the approaches to the estimation of the theoretically attainable energy savings obtainable by reducing transmit powers in cellular systems such as 5G. This is useful in providing a baseline value for evaluating the performance of heuristic methods in real systems. Several steps are required to set this up:

- 1. Definition of a system model. This needs to balance the requirement of being sufficiently generic that a reasonable mathematical model can be based on it, with the requirement of not being so over-simplified that it is unrealistic.
- 2. Construction of a mathematical model based on the system model.
- 3. Definition of the optimization problem (objectives and constraints), built on the mathematical model.
- 4. Solution of the optimization problem.

The steps will now be detailed.

- 1. We define a CRM as above. The pathloss model will be one of the ETSI or 3GPP standard types.
- 2. The mathematical model will be based on Shannon's formula, which we express here in a vectorized form suitable for efficient computation with numerical Python. The variables in the model are:
 - (a) The pathgain matrix G. The pathgain is defined as the reciprocal of the pathloss, and the (i,j) element of G is defined as the pathgain between cell i and UE j.
 - (b) The transmit power of the cells forms a vector denoted p.
 - (c) The channel noise power-density is denoted σ . The value of the parameter is critical and will be discussed further below.
 - (d) The spectral efficiencies of the downlink (DL) channels to the UEs form a vector denoted s. The units are bits/s/Hz.



With these definitions, the formulas below can be produced.

$$s_{j} = \log_{2} \left(1 + \frac{p_{i}G_{ij}}{\sigma + \sum_{k \neq i} p_{k}G_{kj}} \right)$$

$$= \log_{2} \left(\frac{\sigma + \sum_{k} p_{k}G_{kj}}{\sigma + \sum_{k} p_{k}\tilde{G}_{kj}} \right)$$

$$s = \log_{2} \left(\frac{\sigma + p^{T}G}{\sigma + p^{T}\tilde{G}} \right) = \log_{2} \left(\frac{\sigma + G^{T}p}{\sigma + \tilde{G}^{T}p} \right)$$

- 3. There are many possible variations on the optimization problem. The general idea will be that we want to minimize power, but obviously we must impose some constraints, otherwise the optimization process will simply set all transmit powers to zero (*p*=0). Another requirement is that we stay within the class of optimization problems, which have good algorithms available for their solution. We emphasize that the purpose of this work is to get benchmark results, so that we want to solve the problems with exact algorithms, not heuristics which come with no guarantees. Generally, this means that we want a convex problem, but some non-convex types such as quasiconvex (which includes fractional-linear), pseudoconvex, or difference-of-convex may be tractable. After much experimentation, we found that the following problem can be solved effectively and corresponds to a plausible real-world problem: we will minimize total power, subject to constraints which express that the minimal Signal-to-Interference-plus-Noise-ratio (SINR) is above some preset threshold. This is a strong constraint: it implies that we want all UEs (however badly positioned) to get above so pre-decided minimal level of service. Note that putting a constraint on the minimal spectral efficiency results in a non-convex problem and turns a problem which is easy to solve into a very hard one. Thus, we do not attempt this.
- 4. The optimization problems of the previous paragraph can be solved with the open-source software *cvxpy*, which we found to be very fast and reliable. Results are presented below in the form of complementary cumulative distribution functions (CCDFs) of UE spectral efficiencies, with the upper 0.9 quantile of this distribution marked.

2.5.2 Adastral Park mockup scenario

This section describes the proposed scenario for the Adastral Park simulation using a Single Frequency Network (SFN) for coverage and energy optimization. The EMS is in charge of integrating data coming from the simulator (a software system emulating the radio environment and its scenarios) and controlling the radio environment in order to reduce the energy consumption while maintaining the Quality of Service (QoS) within the system.

<u>General System KPIs:</u> The KPIs provided by the RIC Tester system used by the EM algorithms are described in Table 2-1.

Table 2-1 Telemetry Requirements

Name	3GPP Name	Unit
DL Total PRB Usage	RRU.PrbTotDl	#PRB
UL Total PRB Usage	RRU.PrbTotUl	#PRB
Average DL UE throughput in gNB	DRB.UEThpDl	Mbps



Average UL UE throughput in gNB	DRB.UEThpUI	Mbps
Number of active UE per cell	DRB.MeanActiveUe	#UE
Power Consumption (avg)	PEE.AvgPower	W
Energy consumption	PEE.Energy	kWh
Mean Transmission power of an NR Cell	CARR.MeanTxPwr	dBm
Packet drop rate	DRB.RlcPacketDropRateDl	%
DL Avail PRB Usage	RRU.PrbAvailDl	#PRB
UL Avail PRB Usage	RRU.PrbAvailUl	#PRBs
DL Usedl PRB Usage	RRU.PrbUsedDl	#PRBs
UL Usedi PRB Usage	RRU.PrbUsedUl	#PRBs

<u>QoS Score</u>: The QoS.Score defined in the RIC Tester as VIAVI.QoS.Score, is the ratio between the Actual throughput versus the target throughput per UE. This value is averaged at the network level to calculate the degradation of the system based on the actions used to perform energy savings.

QoS. Score =
$$\frac{\text{Average DL UE Throughput}}{\text{Target DL UE Throughput}}$$
 (2-1)

This use case consists of a SFN environment with 6 omnidirectional antennas covering an area of 1.5 km² in the 3.8 GHz band. The use case is defined to support coverage with the same n77 for all sites aiming to reduce the number of cells powered on in low traffic times. The goal is to establish a robust single-frequency network (SFN) and implement dynamic transmission power management. By optimising coverage for small cells within the SFN, this use case aims to reduce overall RAN energy consumption. As shown in Figure 2-5, the main objective is to evaluate the traffic of the network and, during predicted low traffic hours, reduce the number of active sites by powering down RUs and compensating the coverage holes with increases in other sites' Tx Power. Similarly, during predicted higher traffic hours, powered-down sites can be reactivated.

The general deployment scenario is based on the Adastral Park site belonging to BT at Martlesham Heath in the UK. Originally, six sites at Adastral Park were identified. Their locations are shown in Figure 2-6. These sites were then used to define the simulation environment. All sites are configured to operate at 3.8208 GHz with 40 MHz of bandwidth using Time Division Duplex (TDD) mode (7D1S2U). The RUs are configured to transmit at a maximum of 37 dBm per site, and each site uses an omnidirectional antenna deployed at 5 m of elevation. The RUs are placed on lampposts in Adastral Park.



Figure 2-5 Use Case 1 - SFN Energy Management



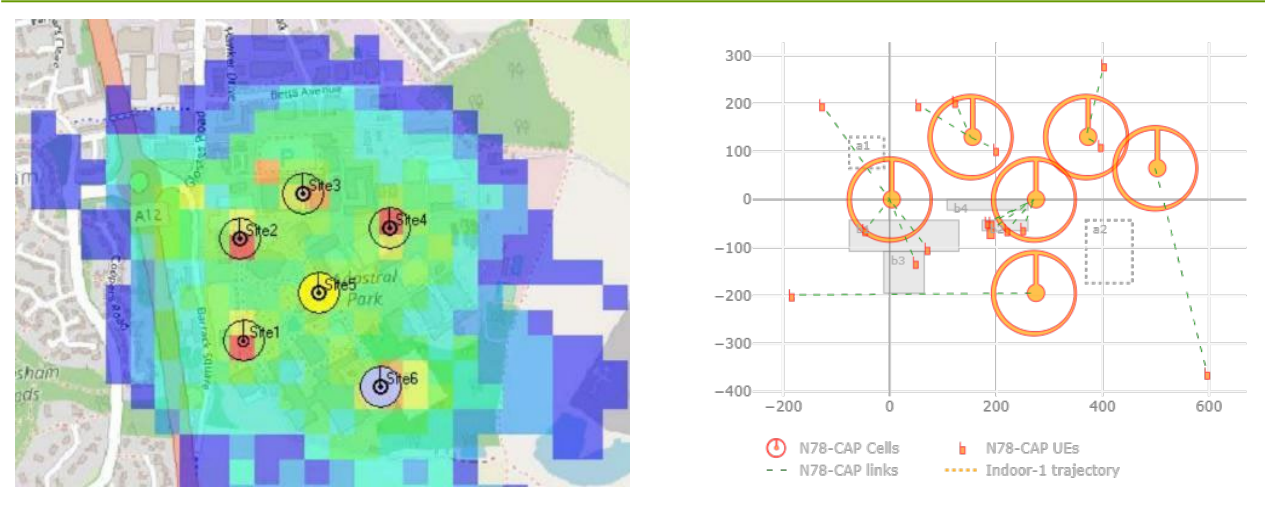


Figure 2-6 a) General location of sites in Adastral Park, b) mapping of sites onto the VIAVI RIC Tester

Table E E Maastrai i ark site coordinates				
Site Coordinates				
1	52.057126	1.279536		
2	52.058963	1.279567		
3	52.059710	1.281488		
4	52.059043	1.283988		
5	52.057935	1.281825		

Table 2-2 Adastral Park Site Coordinates

Ideally, for test purposes we would use the following representative traffic profiles and mobility patterns within Adastral Park:

- The area covered by this scenario is approximately 1.5 km².
- A maximum of 32 simultaneous users per cell (based on [8]).
- The traffic per user varies, ranging from 5 Mbps to 20 Mbps, depending on individual user requirements.
- The whole network traffic can be modelled as per Figure 2-7 a), to emulate the traffic of a realistic network (based on [8]).
- Figure 2-7 b) shows the anticipated number of parallel users and the mean traffic per user over time.

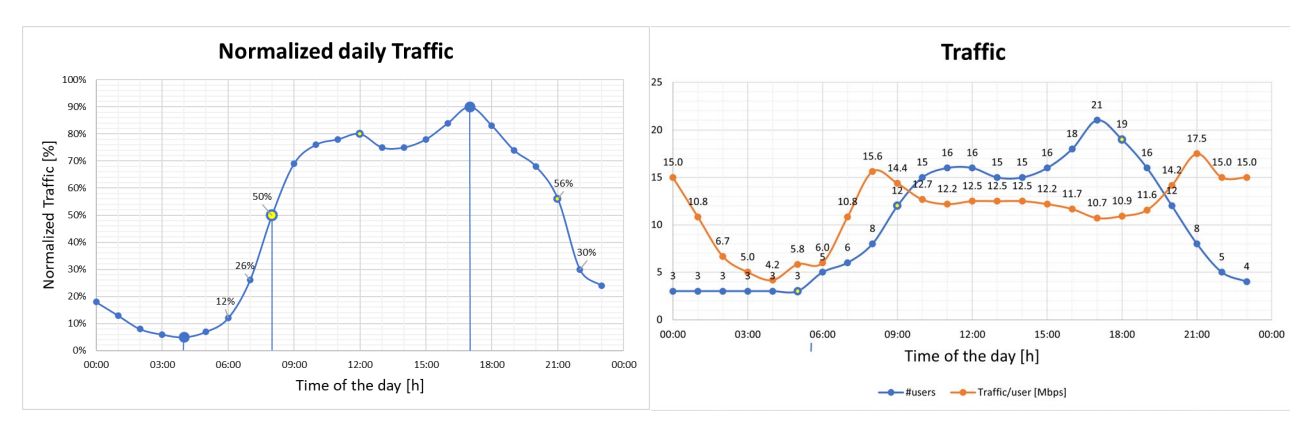


Figure 2-7 a) Normalised daily traffic based on [8]. b) Traffic and users for the Adastral Park



The mobility patterns and the locations of the users can be categorised as follows:

- 1. 30% of users are pedestrians who move outdoors, at speeds of 2 km/h to 5 km/h.
- 2. 50% of users are static indoors.
- 3. 20% of users move on bikes or cars at speeds of 20 km/h to 30 km/h.

The paths for the car and bike users follow the path presented on the drive test described in Figure 2-8a. In particular, they will move between a1 and a2 (VIAVI RIC Tester) shown in Figure 2-8 b). Figure 2-9 presents the expected SINR of the system and the Modulation and Coding Scheme (MCS) – SINR used for the system based on Table 5.1.3.1-2 in 3GPP TS 38.214 [9].



Figure 2-8 Adastral Park a) SS-SINR drive test results, b) example of car mobility in Viavi RIC tester

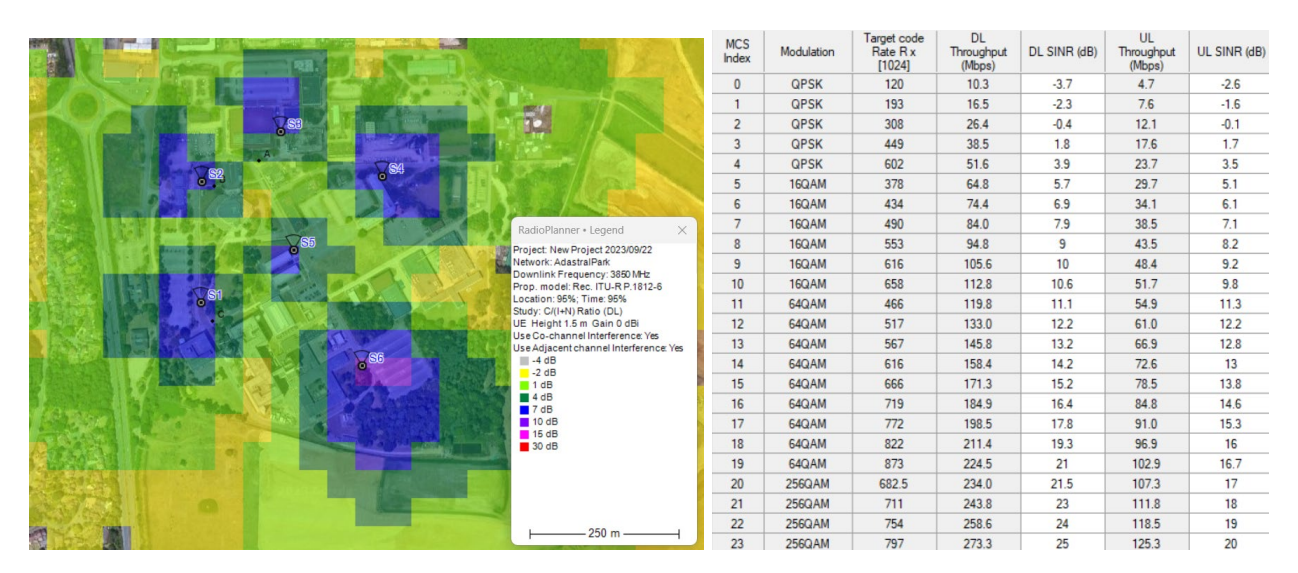


Figure 2-9 SINR simulation for the emulation radio scenario

2.5.3 UPC University Campus scenario

This scenario corresponds to the Campus Nord of UPC in Barcelona. The considered environment is a 350×125 metre area with 25 buildings of three floors as depicted Figure 2-10, where the modelled area corresponds to the rectangle highlighted in red. The names of the considered buildings A1, ..., D6 are also included in the figure. 5G NR coverage on the campus is provided by three outdoor macrocells of a public MNO in band n78 (3.3-3.8 GHz). The locations of these macrocells are shown in Figure 2-10.





Figure 2-10 UPC Campus Nord scenario

The UMa propagation model of 3GPP TR 38.901 at 3.7 GHz is considered for evaluating the propagation conditions at the different locations of the modelled area, subdivided into square pixels of 1 m \times 1 m. The computation of the pathloss includes both outdoor-to-outdoor and penetration losses as well as 2D-spatially correlated shadowing.

Depending on the considered study, the simulation environment of this scenario may include a number of relay stations deployed at indoor or outdoor locations and working at different frequencies than the base stations. The propagation model for the relay stations can be selected as the UMi model from 3GPP TR 38.901 (section 7.4) [3] in case they are deployed outdoor, or as the InH model, in which case they are deployed indoors.

2.5.4 Real dataset-based scenario in Spain

In this section, we describe the dataset being leveraged to implement a data-driven analysis of the energy-QoS trade-off in real 5G Non-Stand Alone (NSA) traffic offloading scenarios, detailed in Section 3.8. The dataset, provided a Spanish Mobile Network Operator (MNO), includes an extensive set of KPIs collected from the RAN of a real cellular deployment. This deployment spans a large metropolitan area in Spain, encompassing both urban and suburban environments, as illustrated in Figure 2-11. The analysed region is divided into two distinct areas: a dense urban zone within the city covering approximately 14 km² and a larger region of about 100 km² that includes multiple cities with mixed urban and suburban characteristics.



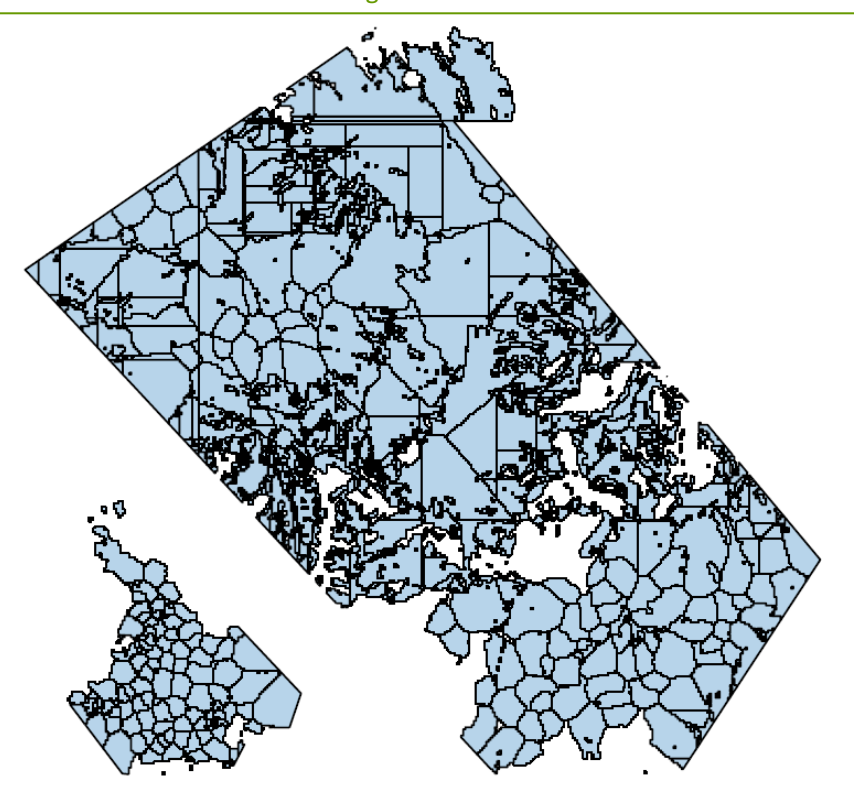


Figure 2-11 Region covered by the dataset

The dataset includes information from all Radio Access Technologies (RATs) deployed by the operator: 2G, 3G, 4G, and 5G. It covers two consecutive months of data, along with some additional non-consecutive weeks, with a granularity of 15 minutes, i.e., the KPIs are reported as averages over 15-minute intervals. The number of KPIs, cells, carriers, and sites vary across RATs, as summarized in Table 2-3. Notably, 4G accounts for the largest share of cells and sites, as is expected in an NSA scenario. For simplicity, the term "node" is used throughout the document to refer to the group of cells or sectors associated with a specific carrier at a site.

Table 2-3 Dataset Description

Technology	#Sites	#Cells	#KPIs	#Carriers
2G	250	742	205	2
3G	299	1900	838	2
4G	312	3427	1314	5
5G	220	1271	679	3

Table 2-4 4G and 5G Radio Specifications

Carrier	Bandwidth	scs	UL/DL PRBs	Duplexing
4G 700 MHz	10	15	50/50	FDD
4G 800 MHz	10	15	50/50	FDD
4G 1800 MHz	20	15	100/100	FDD
4G 2100 MHz	10	15	50/50	FDD
4G 2600 MHz	20	15	100/100	FDD
5G 3500 MHz	100	30	68/205	TDD



Table 2-4 summarizes the key radio features of 4G and 5G cells included in the NSA deployment. The number of Uplink (UL) and DL Physical Resource Blocks (PRBs) is derived from 3GPP specifications, based on bandwidth and Subcarrier Spacing (SCS) configurations. For 5G cells, a 25%/75% UL/DL ratio is assumed, aligned with the operator's configuration, which corresponds to a TDD pattern of *DDDSU*. The special slot "S" in this pattern is configured with 10 DL symbols, a 2-symbol Guard Period, and 2 UL symbols [10]. These differences between 4G and 5G are considered in the traffic offloading process, as discussed in subsequent sections.

The evaluation of the proposed traffic offloading strategy focuses on a subset of KPIs summarized in Table 2-5. Energy-related KPIs are used to estimate the baseline consumption of 5G nodes and the potential energy savings, while the other KPIs support the implementation of the offloading strategy and its impact assessment on QoS. The analysis focuses on the DL direction, as it represents the most demanding traffic flow. It is assumed that successful offloading of DL traffic also ensures feasibility for UL traffic, as the aggregated UL load of 4G and 5G remained below 50% of the available 4G resources.

Table 2-5 Relevant KPI Description

Name	Description	Technology
Consumed Energy	Energy consumption of the nodes (Wh)	5G
Daily Consumption	Daily aggregated energy consumption (kWh)	5G, 4G
Average DL Load	Average DL load of the past 15-minute interval (%)	5G, 4G
Average DL Throughput per UE	Average throughput per user equipment (UE) in the past 15-minute interval (Mbps)	5G, 4G
Average RRC Connected UEs	Average number of 5G RRC-connected UEs, without specifying their states	5G
Cell Name	Name, RAT, carrier, and sector of a given cell	5G, 4G

To simplify the analysis and reduce processing time, the study focuses on data from a specific week. The analysis showed that KPI behaviour was consistent across weeks, displaying cyclic patterns strongly correlated to day-night variations. By using a full week, the analysis captures differences between weekdays and weekend days, particularly Sundays, when network demand tends to decrease.



3 Case Studies Simulation Results

3.1 Evaluation of the energy savings by use of a cell-free architecture

Distributed MIMO (D-MIMO) systems aim to provide a homogenous quality link over the cell while benefiting from transmitting multiple streams simultaneously. A cell-free system is a step forward since it inherently uses D-MIMO technology, and it removes the physical cell boundaries by taking the best Access Points (APs) for a specific user. This system is also called user-centric since it is designed to maximize the performance of every user.

To the best of our knowledge, some manuscripts delve into reducing the energy of a cell-free system. The authors in [11] derived a closed-form expression for the spectral efficiency of a cell-free system. Furthermore, the authors proposed two AP selection schemes, in which each user chooses a subset of APs, to reduce the power consumption caused by the backhaul links. In [12], the authors solve the combinatorial problem of associating APs to UEs by developing a novel alternating optimization algorithm. The solution was evaluated in a simulated indoor factory environment. The work [13] reduces the total power consumption for a given minimum target spectral efficiency of the system by temporarily switching off a set of APs that are not contributing to overall system performance. Although several works evaluate cell-free systems for energy reduction purposes, their evaluations do not consider the realistic scenarios that an operator needs to deploy as it is done in this BeGREEN D2.3.

In BeGREEN D2.2, we showed that D-MIMO significantly outperforms collocated MIMO (C-MIMO) in terms of bit error rate (BER) while requiring lower transmit power. In this work, we delve into cell-free technology for energy reduction. To do so, we first estimate the minimum number of transmit antennas that provide the maximum performance. This number is a tradeoff between system performance and energy reduction as it tries to maximize both. Second, we extensively evaluate a cell-free system with a C-MIMO system using the cellular reference model (described in Section 2.5.1) in a dense urban environment in the city center of Madrid. Our evaluation shows three main findings.

- 1. Compared with C-MIMO, a cell-free system reduces the transmit power up to 30 dB without degrading the performance.
- 2. Cell-free provides functional BER for 8 MIMO streams which implies that it is feasible for high-data-rate applications.
- 3. Cell-free transmission adds flexibility in terms of how many APs are selected for MIMO transmission. The number of transmit antennas can be reduced considerably compared to the number of antennas that a regular C-MIMO base station has. We observe that 8, 12, and 16 are the minimum number of antennas that maximize performance for 2, 4, and 8 streams, respectively.

3.1.1 Evaluation of the number of antennas

We aim to find the lowest number of APs that provide equal or even better performance than using all APs available. To this end, we analyse the attenuation of the link between the UE and the AP since the lower the attenuation, the higher the link quality. Hence, our strategy is two-fold, we reduce the number of APs for energy-saving purposes and maximize performance since we reduce interference by switching off unreliable APs.

The D-MIMO system discussed in BeGREEN D2.2 is evaluated in terms of the number of active antennas to empirically select the optimal number of active antennas. In BeGREEN D2.2, the number of antennas for the D-MIMO system was 32. Then, we analyse the system from 32 antennas to the number of streams with a step of two antennas. For instance, if the number of streams is 4, we evaluate the system with a minimum of 4 antennas to meet requirements.



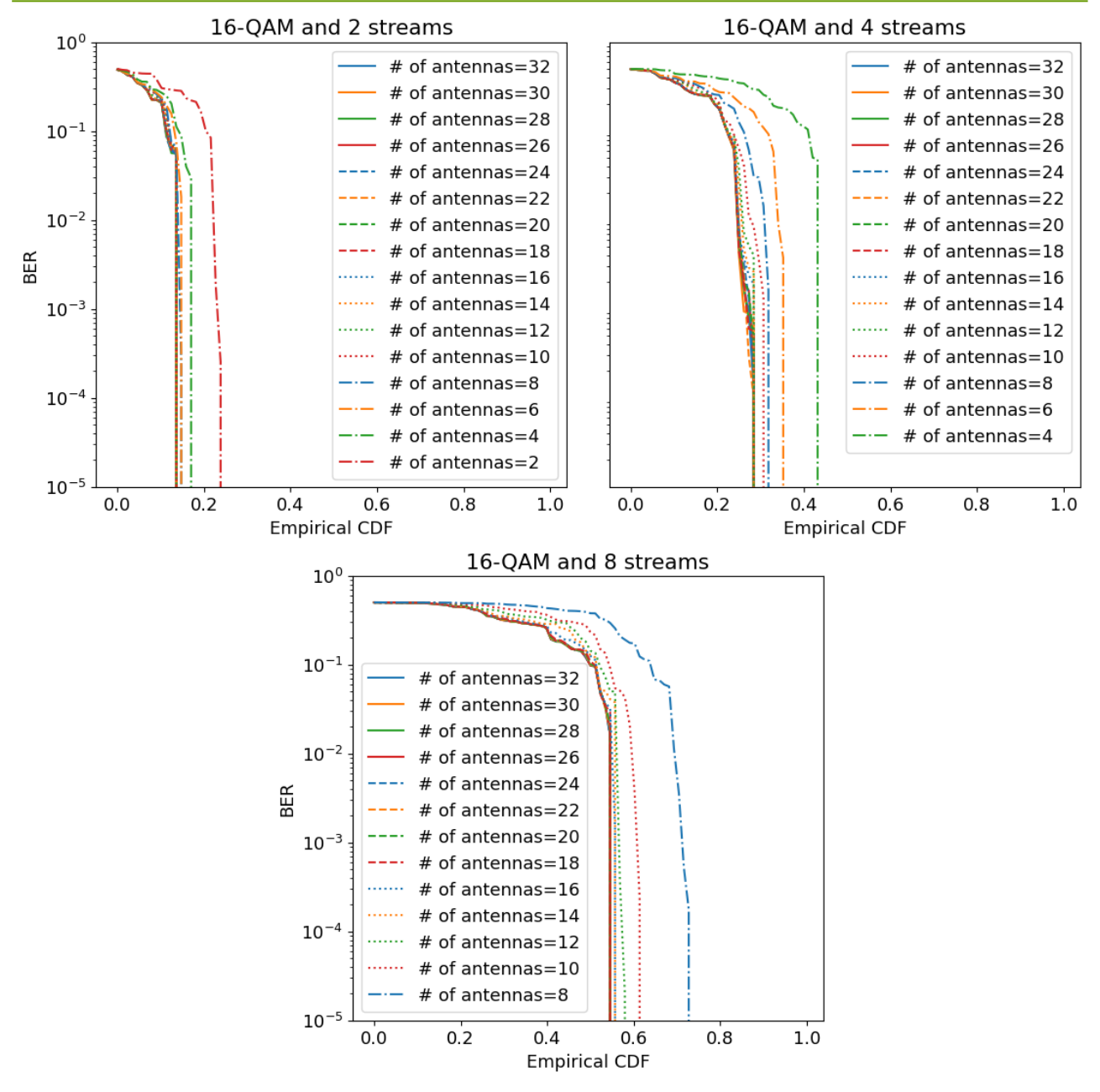


Figure 3-1 Number of antennas evaluation

To assess the system, we remove the antennas with the highest attenuation until we get only the antennas with the best quality link. Note that we assess only how many antennas are needed, when testing it in real deployments the operator needs to translate it to the number of APs. In this evaluation, each AP has two antennas.

The results of this evaluation are shown in Figure 3-1. For the sake of understanding, we only show the results of 16-QAM and for 2, 4, and 8 streams, respectively. For all cases, we can see that using the same number of antennas as the number of streams leads to the worst results. As long as the number of antennas increases, the performance also increases. However, the performance converges to a point where it does not improve when more antennas are added. This points out that the APs with high attenuation do not make any valuable contributions. We conclude that the optimal number of antennas is 8, 12, and 16 for 2, 4, and 8 MIMO streams, respectively.



3.1.2 Cell-free evaluation

The scenario is depicted in Figure 3-2. For the C-MIMO case, this scenario is composed of seven base stations which are represented by the orange dots following the cellular reference system. The radius of the base station is 150 m. For the cell-free case, the APs are the blue dots, and 56 APs are deployed. As in BeGREEN BeGREEN D2.2, each C-MIMO base station has 32 antennas, so the whole C-MIMO system has 224 antennas. The cell-free system has the same number of antennas as each AP comprises 4 antennas. Note that the positions of the base stations for the C-MIMO case are APs for cell-free as well. The green dots represent the 700 user positions, which were randomly placed across the whole study area.

As described in BeGREEN D2.2, we transmit bits in a 5G-compliant system and compute the BER for every user position. To do so, we simulate the wireless link at a central frequency of 3.5 GHz with a bandwidth of 10 MHz and a subcarrier spacing of 15 kHz. We vary the transmit power, the number of MIMO streams, and the number of bits for QAM. We evaluate the performance of both systems, C-MIMO and cell-free for the 700 positions of the UE. We apply four transmit powers, p1, p2, p3, and p4. p1 is the lowest transmit power, p2 is 10 dB higher than p1, p3 is 10 dB higher than p2 and the same for p4. p4 represents the maximum transmit power of a regular MIMO 5G base station. Regarding the number of MIMO streams and the modulation, we evaluate performance for 2, 4, and 8 streams and 4-QAM, 16-QAM, and 64-QAM, respectively.



Figure 3-2 Cell-free vs C-MIMO scenario



To make a fair energy-consumption comparison between the two systems, we assume that the total power budget of C-MIMO is spread uniformly across all the cell-free APs. In addition, we have considered interference from adjacent base stations for the C-MIMO case. In BeGREEN D2.2 we did not do it because the scenario was a single base station. For the cell-free case, we do not consider interference since the transmission is coordinated among different APs. We select the best APs according to their attenuation as done in the previous evaluation. The DL is analysed here as this link that consumes the most power in the RAN.

The results of this evaluation are shown in Figure 3-3. In general, we observe that the C-MIMO results for this scenario are worse than the Sol scenario of BeGREEN D2.2 because of the interference from the adjacent base stations.

As in BeGREEN D2.2, the higher the modulation and the number of streams, the higher the BER. Concerning energy reduction, C-MIMO with the highest transmit power (p4) in most cases has more limited performance than cell-free with the lowest transmit power (p1). This points out that a cell-free architecture reduces the transmit power by 30 dB compared with a traditional MIMO deployment. In addition, the cell-free system provides functional BER for 8 streams which makes this technology suitable for high-data-rate applications.

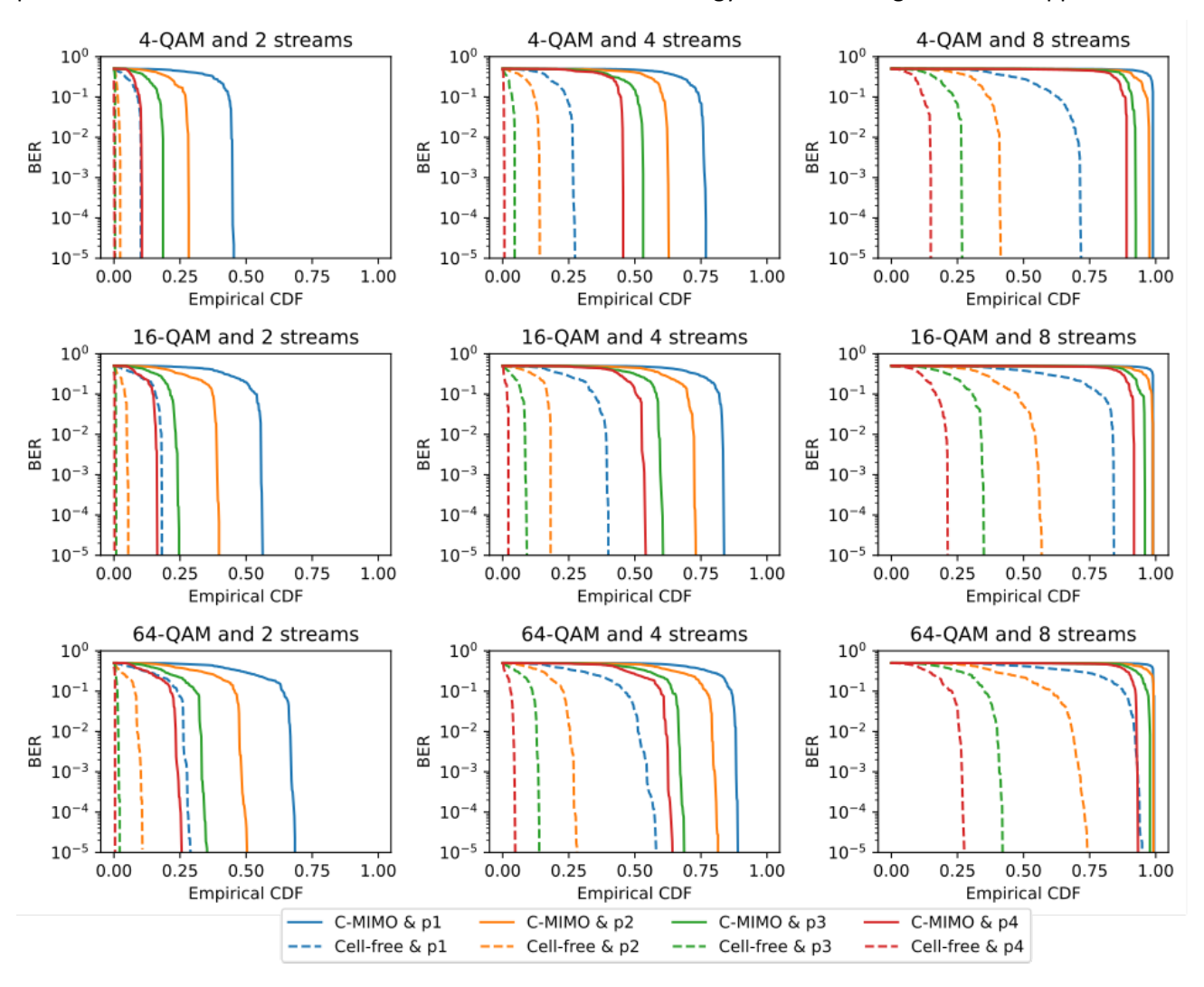


Figure 3-3 Cell-free and C-MIMO BER results

3.1.3 Conclusions

In this work, we have evaluated how a cell-free system reduces energy consumption. To do so, we have



compared a cell-free system to a traditional C-MIMO deployment in a realistic urban-dense scenario. The two systems were compared in terms of the transmit power and BER. Three main findings were observed. First, the transmit power can be reduced by up to 30 dB without degrading performance using a cell-free architecture. Second, cell-free provides functional performance for 8 streams. Third, cell-free offers flexibility in terms of the number of transmit APs, hence the number of transmit antennas can be reduced.

This analysis has been carried out for research purposes, and we did not consider the economic cost of deploying more APs.

3.2 Assessments of energy savings through relay nodes

Begreen D2.1 [1] and Begreen D2.2 [2] considered a RAN enhanced with relay nodes as means of reducing the energy consumption in the network, thanks to improving the coverage conditions experienced by the UEs, which in turn reduce the required transmitted power. In this respect, Section 3.3.1 of Begreen D2.2 presented a model to assess the required transmission power of a BS and a relay to achieve a given downlink bit rate. From this transmission power, the model also provided the total power and energy consumption in the network, the energy efficiency and the energy saving achieved by means of the relay with respect to a reference case without relays. This model was used to quantify the improvements which can be obtained by locating fixed relays in two buildings of the UPC campus scenario by means of simulations. Starting from these results, this section presents an extension of the analysis considering different buildings and floors of the campus as well as different configurations of the power consumption model parameters and the required bit rate in order to consolidate the conclusions obtained in Begreen D2.2.

3.2.1 Considered scenario and assumptions

The simulations for this study were carried out by reproducing the scenario of the UPC Campus Nord in Barcelona as explained in Section 2.5.3. The university campus comprises 24 buildings of 3 floors whose names are shown in Figure 2-10. The coverage is provided by three BSs operating at frequency 3.72 GHz in band n78 using Time Division Duplex (TDD). The simulation parameters considered by the model of section 3.3.1 of BeGREEN D2.2 [2] are given in Table 3-1.

Based on the model considered in BeGREEN D2.2, the total power consumption when a UE is connected through the relay is given by:

$$P_{TOT} = a_{BS}P_{T,BS} + P_{0,BS} + a_{R}P_{T,R} + P_{0,R}$$

where $P_{T,BS}$ and $P_{T,R}$ are, respectively, the transmitted power by the BS and the relay in order to provide the UE with a given bit rate. The terms a_{BS} , a_R , represent the scaling factors between the power consumption and the transmitted power for the base station and the relay, respectively, and the terms $P_{0,BS}$, $P_{0,R}$, represent the power consumption at zero RF output power associated to circuits, signal processing, etc., for the base station and relay. Similarly, for the reference case without relays the total power consumption only includes the terms $a_{BS}P_{T,BS}+P_{0,BS}$ where in this case $P_{T,BS}$ is the power transmitted by the BS to provide the UE with the required bit rate considering that the UE is served directly by the BS without any intermediate relay.

In the results of BeGREEN D2.2 a total of eight different combinations of the power consumption model parameters a_{BS} , a_R , $P_{0,BS}$, $P_{0,R}$ were studied based on different references. It was found that the energy savings obtained from the relay were very sensitive to these parameters. Thus, in order to assess the margin of variations of the energy saving, this study will focus on two combinations, which correspond to the one that provided the highest energy savings observed in BeGREEN D2.2, referred to as "best" combination, and the one with the lowest energy savings, referred to as "worst" combination. The parameters of these combinations are shown in Table 3-2.



Parameter		Value	
Propagation Model	BS	UMa - 3GPP TR 38.901	
	Relay	InH - 3GPP TR 38.901	
Antenna Gain	BS	G_{BS} = 10 dB	
	Relay	$G_R = 3 \text{ dB}$	
	UE	<i>G_{UE}</i> = 3 dB	
Bandwidth	BS	B _{BS} = 20 MHz	
	Relay	<i>B_R</i> = 20 MHz	
Noise Power	BS-UE link	<i>P_{N,UE}</i> = -92 dBm	
	BS-Relay link	P _{N,R} = -92 dBm	
	Relay-UE link	$P_{N, R,UE}$ = -92 dBm	
Efficiency factor (ε)	BS	$\varepsilon_{BS} = 0.59$	
	Relay	ε _R = 0.59	

Table 3-2 Power Consumption Parameters

	BS			Relay		
Combination	a _{BS}	P _{0,BS} (W)	Ref.	a _R	P _{0,R} (W)	Ref.
Best	28.4	156.38	[14]	4	6.8	[15]
Worst	2.8	84	[15]	20.4	13.91	[16]

3.2.2 Energy saving results

The analysis conducted here involved placing a fixed relay at selected locations of different floors in different buildings of the campus. For this purpose, a first study has been conducted to identify the regions with poor coverage and choose the relay locations. Figure 3-4 plots the spectral efficiency at the different pixels of the campus when assuming a fixed transmitted power of the BSs equal to 38 dBm and without any relays. Results are presented for the ground (Gr) floor, the first and the second floors of the buildings. The white areas correspond to those with spectral efficiency lower than 1 b/s/Hz assumed to be in outage. It is observed that these areas are located inside the buildings. Based on these results, a set of 10 buildings and floors, which are highlighted in the figure, have been selected for the study representing different building sizes and distances to the BSs (see Figure 2-10 for the positions of the BSs and names of the buildings). These buildings have the characteristic that they include significantly large outage areas while at the same time they have some positions with good coverage level where a relay can be placed. In this respect, the figure also indicates with black dots the positions where the relay has been placed. The selection of these relay positions has been done after a detailed analysis of each building and floor, choosing a location with sufficiently high spectral efficiency and being sufficiently close to the outage area.



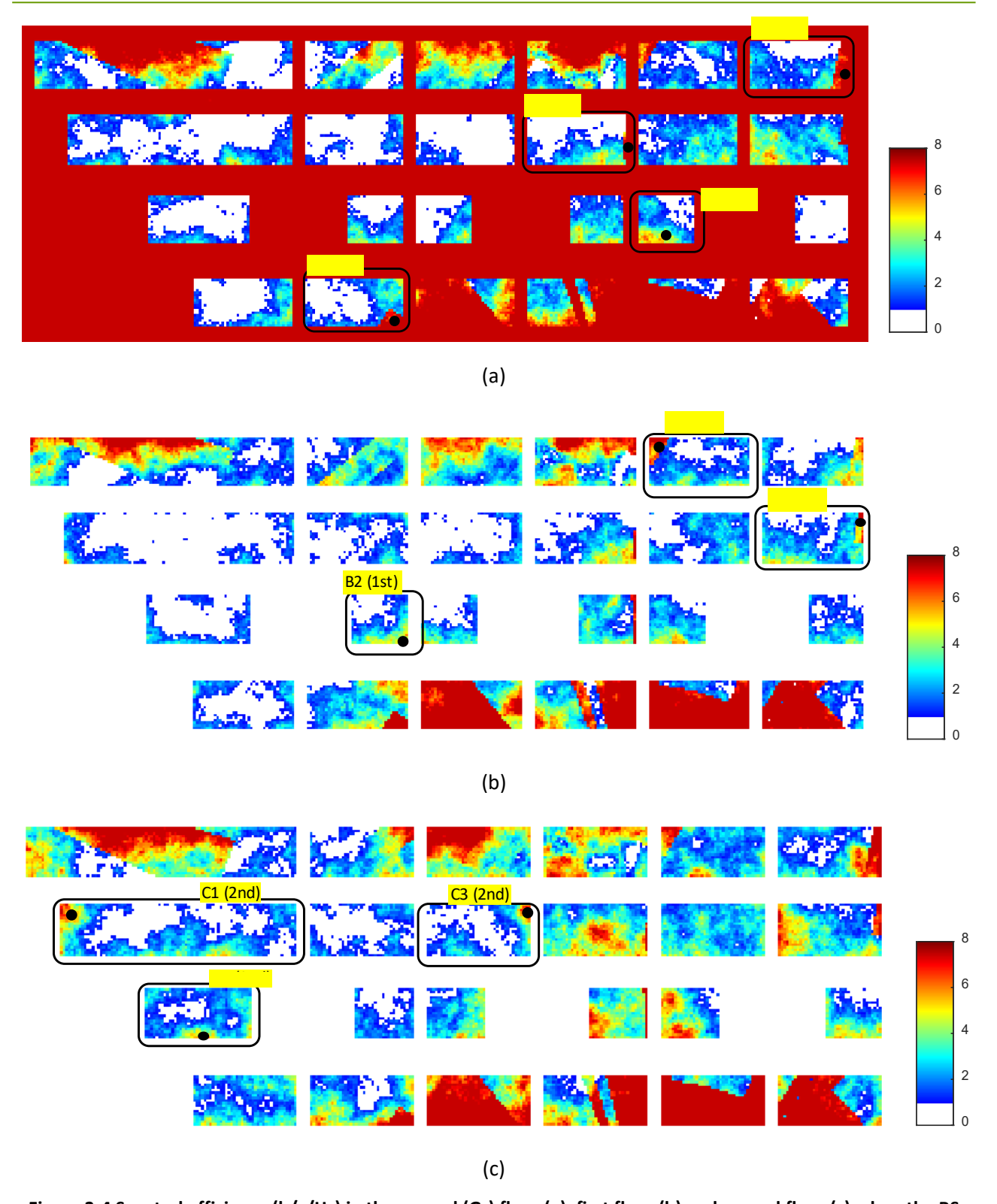


Figure 3-4 Spectral efficiency (b/s/Hz) in the ground (Gr) floor (a), first floor (b) and second floor (c) when the BS transmitted power is fixed to 38 dBm. Buildings selected for the analysis and relay positions indicated by black dots

For each selected floor or building, the energy savings achieved at each pixel of the floor have been obtained by comparing the required transmitted power and power consumption when a UE located at the pixel connects directly to the BS or when it connects through the relay. Then, the average energy saving is obtained by averaging the values of energy saving for all the pixels of the floor.

Figure 3-5 plots the average energy savings that are obtained for a required bit rate of 50 Mbps with the



combinations of power consumption parameters of Table 3-2 that provide the best and the worst savings for the selected buildings and floors. Focusing first on the best combination, it is observed in Figure 3-5 that the energy savings range between approximately 70% and 85% depending on the considered building and the average for all buildings is 80%. The buildings and floors with the largest energy savings of 85 % are the ground floor of A2 and C4 buildings and the second floor of C3 building. They are all characterized by large outage areas in Figure 3-4 and at the same time by having the relay placed in a position with high spectral efficiency. In contrast, the lowest savings are found in the ground floor of building B5 (energy saving of 71%) and in the first floor of building B2 (energy saving 73%). Looking at Figure 3-4, these two buildings are characterized by a smaller outage area and also by a smaller spectral efficiency at the position of the relay. Regarding the worst combination, Figure 3-5 reflects that in this case the variation of the savings across buildings is between 43% and 60%, exhibiting a similar variation trend, like the best combination but now with smaller savings. Indeed, the highest and lowest energy savings are obtained in the same buildings or floors than with the best combination. Taking the average for all buildings the energy saving with the worst combination is 52%.

To assess the behaviour when increasing the bit rate, Figure 3-6 plots the average energy savings for different buildings when considering a required bit rate of 100 Mbps. It is observed that now the difference between the best and the worst and between combinations becomes smaller than in the case of 50 Mbps of Figure 3-5. Specifically, for the best combination, the variation of energy saving across buildings is between 86% and 96%, with an average across buildings of 91% while for the worst combination the energy savings vary between 74% and 92% with an average of 85%. The variations between buildings are similar to the ones observed for 50 Mbps, with the ground floor of C4 building and the second floor of C3 building providing the highest energy saving with the best combination and the ground floor of building B5 and first floor of building B2 exhibiting the lowest energy saving.

To gain further insights on the effect of the bit rate, Figure 3-7 plots the average energy savings in the considered buildings as a function of the required bit rate for the two combinations of power consumption model parameters. Results reflect a similar behaviour like the one observed in the results of BeGREEN D2.2-Section 3.3.1.2, noting that the energy savings increase with the required bit rate with all the analysed buildings and exhibiting similar trends. For the case of the best combination, it is seen in Figure 3-7a that the energy savings is positive for the whole range of bit rates. In contrast, for the worst combination, depicted in Figure 3-7b, it is found that positive savings are achieved for bit rates higher than approximately 10 Mbps, while for lower bit rates the energy saving is negative, meaning that the reference case without relays requires less power consumption.

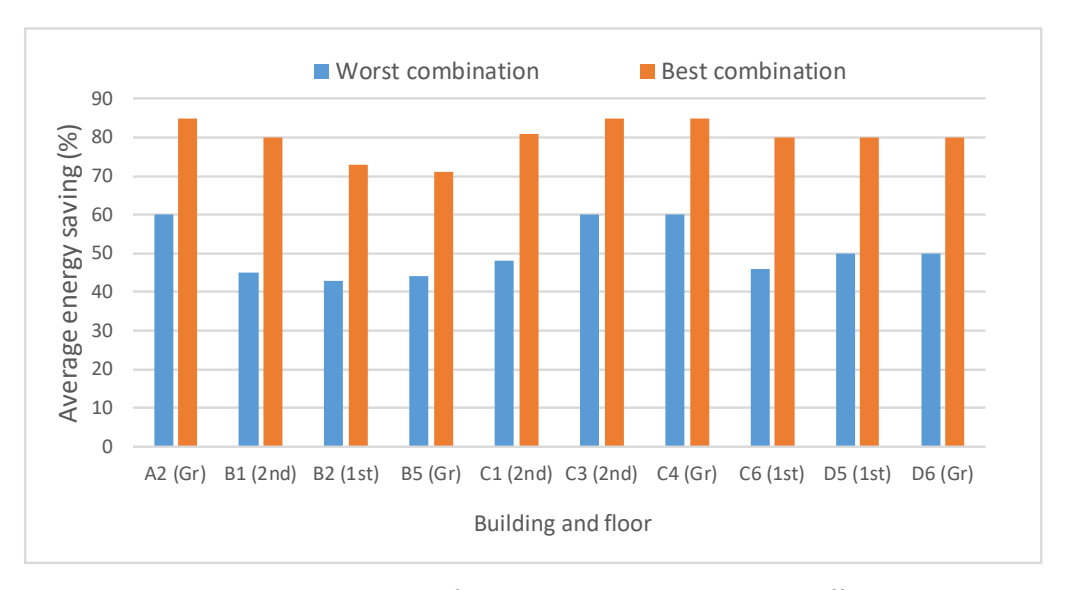


Figure 3-5 Average energy saving percentages for required bit rate 50 Mbps in different buildings and floors





Figure 3-6 Average energy saving percentages for required bit rate 100 Mbps in different buildings and floors

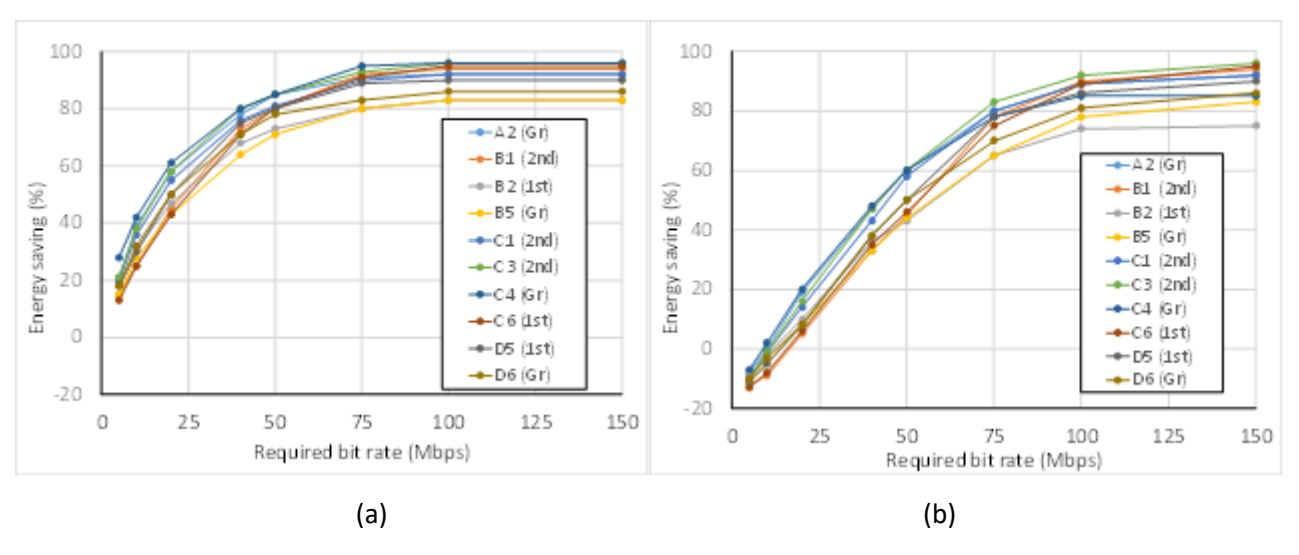


Figure 3-7 Average energy saving percentages in different buildings and floors as a function of the required bit rate for the best combination (a) and the worst combination (b)

3.2.3 Conclusions

The interest in using relays to enhance mobile networks has recently re-emerging as a result of recent initiatives such as the Integrated Access and Backhaul (IAB) and the UE-to-Network relaying. While the relay nodes have been traditionally considered as a tool to enhance the coverage conditions, they can also contribute to reducing the energy consumption in the network. In this direction, BeGREEN has studied in this section and in section 3.3.1 of D2.2 the evaluation of the energy savings and EE improvements achievable through the usage of relay nodes. The results have been obtained by means of simulations recreating a realistic scenario corresponding to the university campus of UPC in Barcelona, considering the real positions of the 5G NR BSs that cover the campus.

The performed analysis has demonstrated that, by properly placing relays in floors of buildings with poor indoor coverage conditions, significant energy savings can be found with respect to the case of not using a relay. These savings increase with the required bit rate and become relevant for bitrates approximately above 10 Mbps. Specifically, in global terms, the results have shown that, for a bit rate of 50 Mbps, the energy saving average across different buildings and floors is 80% for the best combination of power consumption model parameters, namely the linear coefficient of the transmitted power and the power



consumption at zero RF power, while it reduces down to 52% for the worst combination. In turn, when increasing the bit rate to 100 Mbps the average energy saving becomes 91% for the best combination and 85% for the worst one.

3.3 Comparative analysis of RIS and relay nodes for energy saving

The BeGREEN architecture presented in BeGREEN D2.1 [1] identifies two mechanisms for coverage enhancement and consequent transmission power reduction, namely the use of relay nodes and the use of Reconfigurable Intelligent Surfaces (RISs). In previous BeGREEN D2.2 [2] and BeGREEN D3.2 [17], these two techniques have been studied separately. Then, this section presents a comparative study of both techniques conducted over the same scenario and assumptions attending to the particularities of each one in terms of how they alter the radio propagation environment and their energy savings. We study the different tradeoffs and practical benefits as a function of different factors such as location deployment, RIS' codebook configuration, pathloss values or power consumption model parameters.

Some previous works compare RISs with traditional relays. Some of them focus on RIS vs. amplify-and-forward (AF) relays, with AF relays generally outperforming RIS in spectral efficiency but RIS offering better energy efficiency [18]. Large RISs can potentially surpass AF relays in signal-to-noise ratio (SNR) [19]. RIS has also been compared to decode-and-forward (DF) relays, with RIS achieving higher energy efficiency at high data rates, though requiring many elements [20][21]. In comparison with full-duplex relays, a RIS generally lags in data rate unless it has many elements, but it outperforms DF relays in energy efficiency [22][23][24]. Finally, a study in London [25] explores deploying RISs in urban areas with poor coverage, finding it to be a cost-efficient alternative to traditional network expansions, though not matching conventional technologies in coverage and data rate.

In contrast to these previous works, the study presented here goes a step further by considering different aspects not addressed in the literature. First, we consider more accurate RIS modelling based on physical constraints of actual RIS equipment. In particular, we consider a codebook characterized using a RIS prototype [26]. Second, we analyze the impact of aspects that are underexplored in the literature, such as the values of the power consumption model parameters of the considered equipment, the impact of the radiation pattern in different directions in accordance with the measurement-based RIS model or the impact of the propagation losses between the BS and the RIS/relay. Finally, this section also presents a comparison of RISs and relays in a realistic scenario that represents the university campus of UPC in Barcelona. It includes different buildings and combines indoor and outdoor propagation effects to assess the best approach for different conditions and under realistic locations.

3.3.1 System model

Let us assume the downlink communication between a BS and a UE which requires a specific bit rate Relay UE (RUE). To enhance the coverage experienced by the UE, the possibility of deploying a relay node or a RIS at a given position is considered. This is illustrated in Figure 3-8, which shows the different communication options.

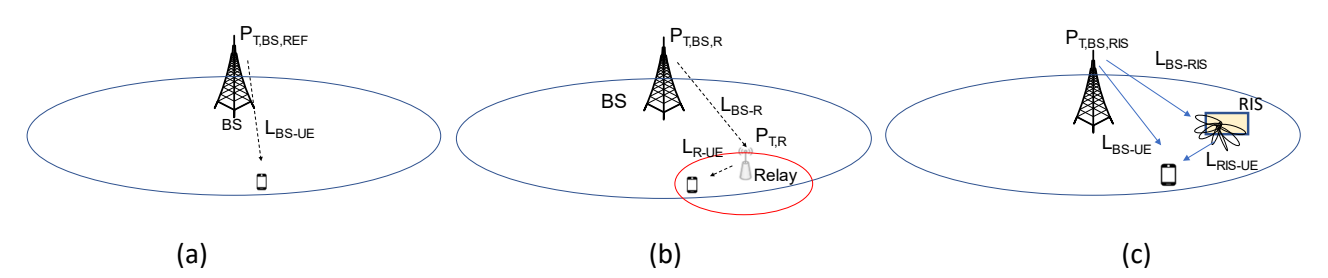


Figure 3-8 Considered communication options. (a) Reference case. (b) Use of a relay node. (c) Use of a RIS.



Figure 3-8 (a) considers the reference case in which the UE is directly connected to the BS without the support of any relay or RIS. The total propagation loss between the BS and the UE is L_{BS-UE} and the required transmitted power at the BS to support the bit rate is denoted as $P_{T,BS,REF}$. The relationship between the transmitted power and the bit rate of the UE is given by the Shannon formula as:

$$R_{UE} = B_{BS} \cdot \varepsilon_{BS} \cdot \log_2 \left(1 + \frac{P_{T,BS,REF} G_{BS} G_{UE}}{P_{N,UE} L_{BS-UE}} \right) \quad \triangleright \quad P_{T,BS,REF} = \left(2^{\frac{R_{UE}}{B_{BS} \cdot \varepsilon_{BS}}} - 1 \right) \frac{P_{N,UE} L_{BS-UE}}{G_{BS} G_{UE}}$$

where G_{BS} , G_{UE} are the gains of the antennas of the BS and the UE, B_{BS} is the transmission bandwidth, $P_{N,UE}$ is the noise power at the UE measured over this bandwidth and ε_{BS} is an efficiency factor $0 < \varepsilon_{BS} \le 1$ that accounts for the overheads associated to cyclic prefix, reference signals, control plane signaling, etc.

Then, following the power consumption model that has been used for similar studies in BeGREEN D2.2-Section 3.3.1 [2], the total power consumption at the BS in the reference case becomes:

$$P_{TOT,REF} = a_{BS}P_{T,BS,REF} + P_{0,BS}$$

where a_{BS} is the scaling factor that determines the contribution of the transmitted power and $P_{0,BS}$ the consumption at zero RF output power due to circuits, signal processing, etc.

Figure 3-8 (b) considers the situation where a relay node is deployed at a certain position. The UE is served by the relay node and connects to the BS in two hops, namely the UE-Relay link with propagation loss L_{R-UE} and the BS-Relay link with propagation loss L_{BS-R} . As in the studies of relays done in BeGREEN D2.2, the decode-and-forward relay is considered with out-of-band operation, i.e. the UE-Relay and BS-Relay links operate at different frequencies. Following the same model that was explained in section 3.3.1 of D2.2, the transmitted power by the BS in this case, denoted as $P_{T,BS,R}$, is determined by the power required to provide the bit rate R in the BS-Relay link, that is:

$$P_{T,BS,R} = \left(2^{\frac{R_{UE}}{B_{BS} \cdot \varepsilon_{BS}}} - 1\right) \frac{P_{N,R} L_{BS-R}}{G_{BS} G_{R}}$$

where G_R is the antenna gain of the relay and $P_{N,R}$ the noise power of the relay receiver in the link BS-Relay.

Similarly, the transmitted power of the relay node is given by the power required to provide the bit rate in the Relay-UE link, that is:

$$P_{T,R} = \left(2^{\frac{R_{UE}}{B_R \cdot \varepsilon_R}} - 1\right) \frac{P_{N,UE,R} L_{R-UE}}{G_R G_{UE}}$$

where B_R is the transmission bandwidth in the Relay-UE link, $P_{N,UE,R}$ is the noise power at the UE measured over this bandwidth and ε_R is the efficiency factor that accounts for the overheads.

The total power consumption is the aggregate of the power consumed by the BS and the relay, given by:

$$P_{TOT,REL} = a_{BS}P_{T,BS,R} + P_{0,BS} + a_{R}P_{T,R} + P_{0,R}$$

where a_R and $P_{0,R}$ are, respectively, the scaling factor of the transmitted power and the power consumption at zero RF power for the relay.

Figure 3-8c shows the situation in which a RIS is deployed to enhance the coverage conditions experienced by the UE. In this case, L_{BS-RIS} and L_{RIS-UE} denote, respectively, the propagation losses in the links BS-RIS and RIS-UE. RISs are structures designed to alter the reflection behavior of impinging radio waves without requiring complex RF chains. A RIS board is usually arranged as a planar antenna array with $N=N_i \times N_j$ unit cells (e.g. patch antennas) separated by a fixed sub-wavelength distance.



The ability of the RIS to reflect the received signal from a BS in the direction of the UE depends on the phase shifts applied by its elements. Figure 3-9 depicts the reference system of the RIS based on a horizontal coordinate system. We denote the azimuth angles between the BS-RIS and RIS-UE as θ_t and θ_r , respectively. They are defined with respect to right-hand side part of a RIS board in the range of [-180°, 0°]. Similarly, we denote ϕ_t and ϕ_r , respectively, as the elevation with respect to the perpendicular of the RIS in the range [-90°, +90°]. In practice, the range of operation of an RIS is limited to [-150°, -30°] in the azimuth and [-45°, +45°] in the elevation range [26].



Figure 3-9 Involved angles in azimuth and elevation for the BS-RIS and RIS-UE links

The received power at the UE in the presence of the RIS, denoted as $P_{R,UE}$, results from the aggregation of the direct path between the BS-UE and the reflected path at the RIS and is given by:

$$P_{R,UE} = P_{T,BS,RIS}G_{BS}G_{UE} \left\| \frac{D(\theta_r, \phi_r)^* \cdot \Theta \cdot D(\theta_t, \phi_t)}{\sqrt{L_{BS-RIS}L_{RIS-UE}}} + \frac{1}{\sqrt{L_{BS-UE}}} \right\|^2$$

where $D(\theta_t, \phi_t)$ and $D(\theta_r, \phi_r)$ are $\mathbb{C}^{1 \times N}$ vectors corresponding to the array response of the RIS in the directions BS-RIS and RIS-UE, respectively. The term Θ is a diagonal $N \times N$ matrix defined as:

$$\Theta = \operatorname{diag}[e^{j\theta_1}, \dots, e^{j\theta_N}]$$

where the values θ_n $n \in \{1,...,N\}$ are the phase shifts configured for each one of the N RIS elements. The element in the cell of row i and column j is mapped to index $n=n_i+(n_j-1)\cdot N_i \ \forall n_i \in \{1,...,N_i\}, \ n_j \in \{1,...,N_j\}.$ Θ is selected from a codebook to maximize the reflected power from the direction of the impinging signal towards the desired direction.

The received power $P_{R,UE}$ can be compacted to follow a similar expression like in the reference case as:

$$P_{R,UE} = \frac{P_{T,BS,RIS}G_{BS}G_{UE}}{L_{RIS}}$$

with LRIS defined as:

$$L_{RIS} = \frac{1}{\left\| \frac{D(\theta_r, \phi_r)^* \cdot \Theta \cdot D(\theta_t, \phi_t)}{\sqrt{L_{BS-RIS} L_{RIS-UE}}} + \frac{1}{\sqrt{L_{BS-UE}}} \right\|^2}$$

The transmitted power required by the BS in order to provide the required bit rate R_{UE} is given by:



$$P_{T,BS,RIS} = \left(2^{\frac{R_{UE}}{B_{BS} \cdot \varepsilon_{BS}}} - 1\right) \frac{P_{N,UE} L_{RIS}}{G_{BS} G_{UE}}$$

The total power consumption is the aggregate of the power consumed by the BS and the power consumed by the RIS, denoted as P_{RIS} . This yields:

$$P_{TOT,RIS} = a_{BS}P_{T,BS,RIS} + P_{0,BS} + P_{RIS}$$

To conduct the comparison between RIS and relays, a set of KPIs is considered. Firstly, the energy or power saving with respect to the reference case is defined for the relay and the RIS respectively as:

$$ES_{REL}(\%) = 100 \left(\frac{P_{TOT,REF} - P_{TOT,REL}}{P_{TOT,REF}} \right)$$

$$ES_{RIS}(\%) = 100 \left(\frac{P_{TOT,REF} - P_{TOT,RIS}}{P_{TOT,REF}} \right)$$

In turn, the power consumption reduction (PCR) of the relay with respect to the RIS is defined as:

$$PCR(\%) = 100 \left(\frac{P_{TOT,RIS} - P_{TOT,REL}}{P_{TOT,RIS}} \right)$$

Note that PCR>0% means that the relay requires less power than the RIS, while PCR<0% means that the RIS requires less power than the relay.

3.3.2 Impact of the model parameters

The results presented in this section intend to assess how the different model parameters of the considered scenario with RIS or relays impact the achieved energy savings. To that end, the three cases illustrated in Figure 3-8 are considered, assuming that the relay and the RIS are placed at the same location, so that $L_{BS-RIS}=L_{BS-R}$ and $L_{RIS-UE}=L_{R-UE}$. The specific scenario is illustrated in Figure 3-10. The RIS codebook for reflecting a signal to a specific direction has been computed analytically and validated from measurements on actual RIS equipment [26]. To assess the impact of the azimuth angle between the UE and the RIS, it is assumed that the RIS codebook is optimized to reflect the BS power in the direction of a receiver located at azimuth -120° and elevation-20°, while the actual azimuth θ_r of the UE is varied as seen in Figure 3-10. In turn, different values of the propagation loss L_{BS-RIS} between the BS and the RIS or relay are considered, to account for different distances between them. The values of the parameters considered in the evaluation are presented in Table 3-3, indicating those that are varied. Regarding the parameters of the power consumption model for the BS and the relay, eight possible combinations are tested, based on different values extracted from references [14], [15], [16].



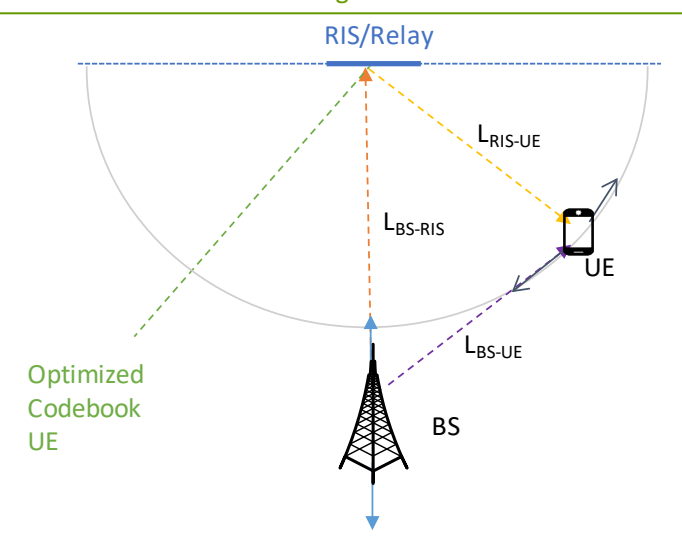


Figure 3-10 Considered scenario

Table 3-3 Model Parameters

Parameter		Value
Antenna gain	$G_{BS} = 10 \text{ dB}, G_R = 3$	dB , $G_{UE} = 3 dB$
Bandwidth	$B_{BS} = [20, 100] \text{ MHz}$	$a, B_R = 20 \text{ MHz}$
Noise Power	$P_{N,UE} = P_{N,R} = N_o B_{BS},$	$P_{N,R,UE} = N_o B_R$ with N_o =-168 dBm/Hz
Efficiency factor	$\varepsilon_{BS} = \varepsilon_R = 0.59$	
Bit rate	50 Mb/s	
Angles	BS-RIS: θ_t =-90°, ϕ_t =	5°
Angles	RIS-UE: θ_r varied, ϕ	-=-20°
Propagation losses	$L_{BS-RIS} = L_{BS-R}$ varied,	$L_{RIS-UE} = L_{R-UE} = 70 \text{ dB}, L_{BS-UE} = 140 \text{ dB}$
	10×10 elements	
RIS	Codebook optimize	ed for a receiver at azimuth -120°, elevation -20°
	P _{RIS} =62 mW	
	Combination 1	a_{BS} =28.4, $P_{0,BS}$ =156.38 W, a_{R} =20.4, $P_{0,R}$ =13.91 W
	Combination 2	a_{BS} =28.4, $P_{0,BS}$ =156.38 W, a_R =4, $P_{0,R}$ =6.8 W
	Combination 3	<i>a</i> _{BS} =4.7, <i>P</i> _{0,BS} =130 W, <i>a</i> _R =20.4, <i>P</i> _{0,R} =13.91 W
Power consumption	Combination 4	a _{BS} =4.7, P _{0,BS} =130 W, a _R =4, P _{0,R} =6.8 W
parameters of BS and relay	Combination 5	a _{BS} =2.8, P _{0,BS} =84 W, a _R =20.4, P _{0,R} =13.91 W
	Combination 6	a _{BS} =2.8, P _{0,BS} =84 W, a _R =4, P _{0,R} =6.8 W
	Combination 7	a_{BS} =2.57, $P_{0,BS}$ =12.85 W, a_{R} =20.4, $P_{0,R}$ =13.91 W
	Combination 8	<i>a</i> _{BS} =2.57, <i>P</i> _{0,BS} =12.85 W, <i>a</i> _R =4, <i>P</i> _{0,R} =6.8 W



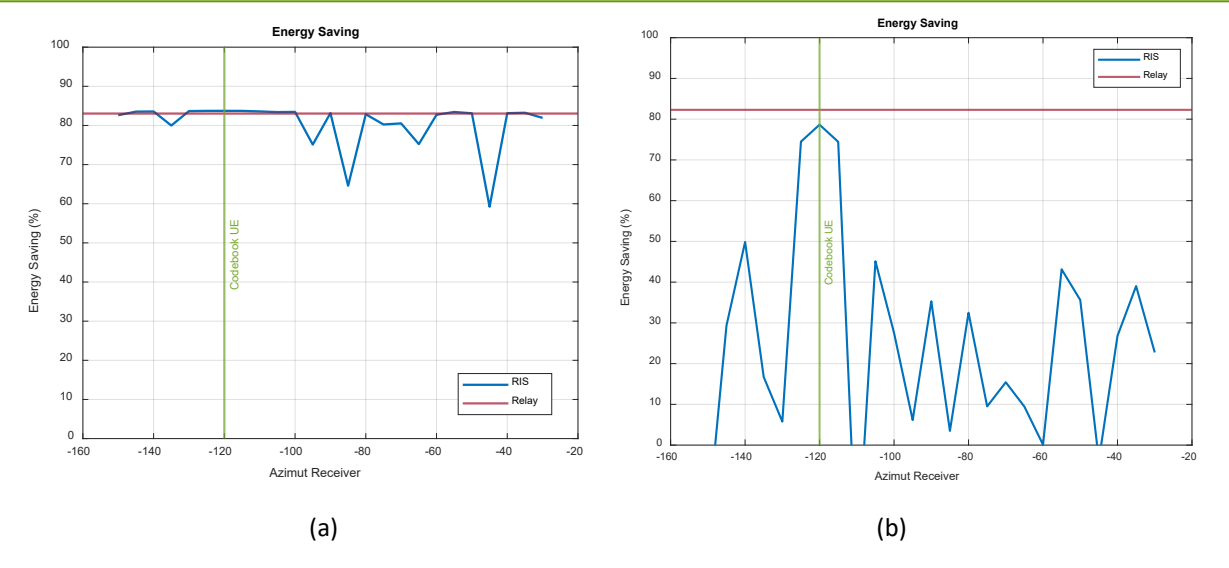


Figure 3-11 Energy saving percentage achieved for different θ_r values with (a) $L_{BS,RIS}$ =70 dB, (b) $L_{BS,RIS}$ =100 dB

Figure 3-11 shows the energy saving values achieved with the relay and the RIS with respect to the reference case as a function of the azimuth angle θ_r of the UE. Two values of the pathloss between BS and RIS/relay are considered. In particular, Figure 3-11 (a) shows the case L_{BS-RIS} = 70 dB, which could correspond e.g. to a distance of 30 m with a UMi model in LoS, so that the RIS or relay is located close to the BS. In turn, Figure 3-11 (b) shows the case L_{BS-RIS} = 100 dB, which could correspond e.g. to a distance of 500 m with a UMa model in LoS. Results consider bandwidth B_{BS} =20 MHz and combination 1 of power consumption parameters. It is observed that the energy saving achieved with the relay is very similar in both cases. In turn, when using the RIS, the energy savings reduce significantly when the pathloss between the BS and the RIS increases. Besides that, with the RIS, the energy savings fluctuate a lot depending on the azimuth angle, capturing the radiation pattern of the RIS. This is particularly noticeable for L_{BS-RIS} = 100 dB, in which the maximum energy saving is only achieved in a range of approximately +/- 5° around the direction of -120° that corresponds to the maximum reflected power according to the codebook configuration (denoted as "Codebook UE" in the figure). In the rest of the directions, the energy savings reduce by more than one half and are much lower than those of the relay.

The comparison between the relay and the RIS in terms of the PCR metric is shown in Figure 3-12 considering the two situations L_{BS-RIS} = 70 dB and L_{BS-RIS} = 100 dB as well as two different bandwidths of the BS, namely B_{BS} =20 MHz and B_{BS} =100 MHz. When the RIS or relay are close to the BS, corresponding to the low pathloss value of 70 dB, there are several angles in which the RIS achieves lower power consumption than the relay, i.e. PCR<0%, mostly in a span of +/- 30° around the angle of -120° where the RIS reflects the highest power power (denoted as "Codebook UE"). In these cases, the power consumption with the relay case is up to about 9% higher than with the RIS. Outside these angles, the performance of the RIS degrades with a lot of fluctuations depending on the angle, and the relay starts to go better, i.e. PCR>0% with values that can be up to 56% for a bandwidth of 20 MHz and 18% for a bandwidth of 100 MHz.

When the RIS or relay is farther from the BS, i.e. pathloss of 100 dB in Figure 3-12, the effect of the RIS is only noticeable in an angle of about +/- 5° around the angle of -120°. Still, in this region the RIS performs very similar to the relay (PCR \sim 0%) for B_{BS} =100 MHz and worse than the relay (PCR \sim 17%) for B_{BS} =20 MHz. For the rest of angles, the PCR fluctuates between 65-85% for 20 MHz and between 30-60% for 100 MHz.



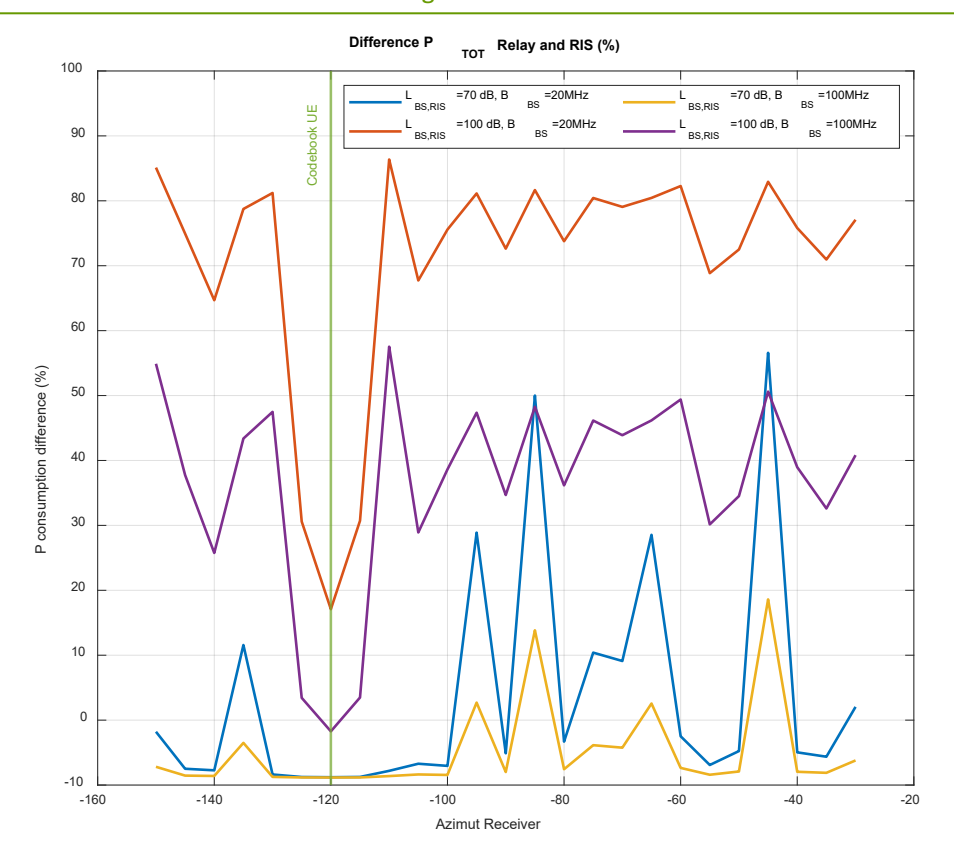


Figure 3-12 Power consumption difference of the relay with respect to the RIS as a function of the azimuth θ_r

To further assess the impact of the propagation losses, or equivalently distance, between the BS and the relay/RIS, Figure 3-13 (a) plots the energy saving with respect to the reference case achieved by the RIS and by the relay as a function of L_{BS-RIS} when the UE is located at the optimum angle of -120° according to the RIS codebook configuration. B_{BS} =20 MHz and combination 1 of power consumption parameters are considered. Similarly, Figure 3-13 (b) presents the PCR to quantify the comparison between RIS and relay. It is observed that the RIS provides higher savings than the relay (PCR ~ -9%) for L_{BS-RIS} <90 dB, and these are kept more or less constant. Instead, the relay provides higher savings for approximately 90 dB< L_{BS-RIS} <140 dB. In this range, the PCR reaches a maximum of about 70% at around L_{BS-RIS} =125 dB and then it starts to decrease abruptly. For pathloss above 140 dB, both techniques bring very little or no energy savings with respect to the reference case.

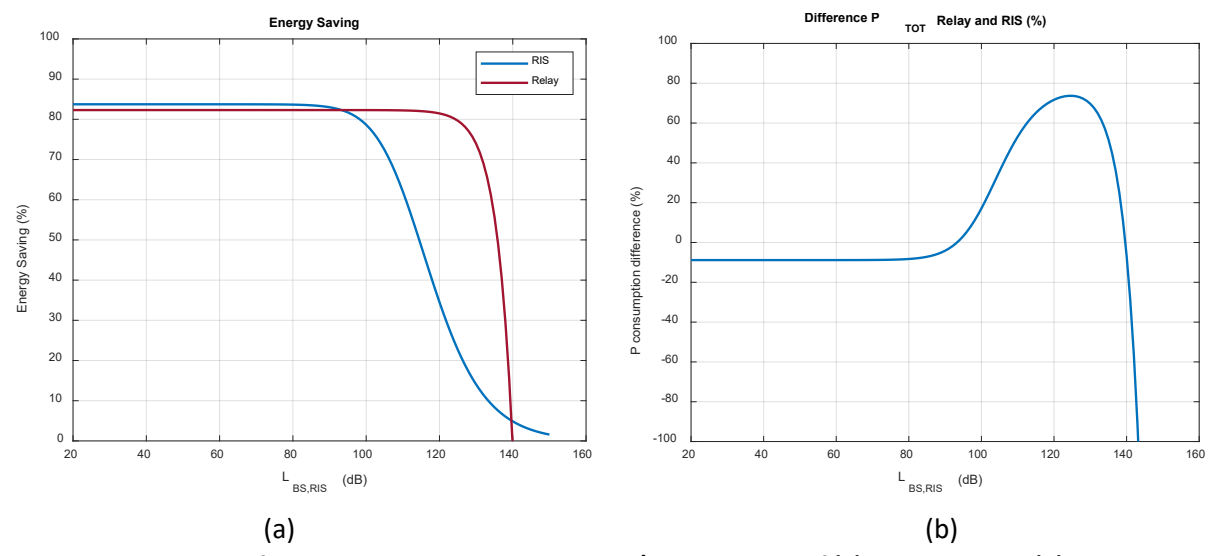


Figure 3-13 Impact of the pathloss between BS and RIS/relay in terms of (a) energy saving, (b) PCR metric



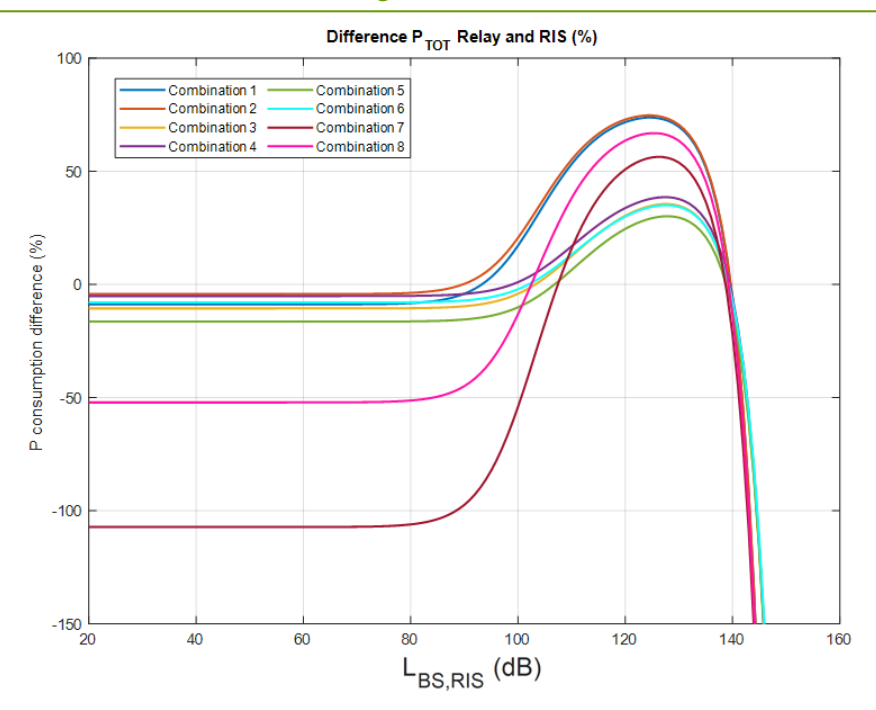


Figure 3-14 Impact of the power consumption model parameters on the PCR metric

The effect of the power consumption model parameters of the BS and relay is shown in Figure 3-14. It plots the PCR metric as a function of the pathloss L_{BS-RIS} between the BS and the RIS/relay for the different combinations of power consumption model parameters indicated in Table 3-3. The figure considers that the UE is located at the optimum angle -120° based on the RIS codebook and that the bandwidth of B_{BS} =20 MHz. It is observed that the improvements of the RIS with respect to the relay are very sensitive to the power consumption model parameters. For low pathlosses up to L_{BS-RIS} =90 dB the RIS outperforms the relay (i.e. PCR<0%). However, there are larger differences for the cases with lower $P_{0,BS}$, i.e. combination 7, which leads to a PCR of about -110%, and combination 8, which shows a PCR of about 50%. In the other cases PCR combinations are around -10%. In turn, for L_{BS-RIS} >90 dB the relay starts to perform better and achieves PCR > 0% for all combinations. The maximum values of the PCR are obtained for the pathloss of approximately 125 dB and range from 25% for combination 5 up to 70% for combinations 1 and 2.

3.3.3 Analysis in the campus scenario

This section presents the results of the comparison between the use of RIS and relays considering the UPC Campus Nord scenario described in section 2.5.3. An analysis of the pathloss values in this scenario reflects that the poor coverage areas that experience high pathloss values are located indoors. In this respect, Figure 3-15 plots the pathloss experienced at the different locations of the campus in the ground level with the base station BS2 that is the one that serves a largest area in the campus (see Figure 3-15 for the overall view of the campus and the location of each BS). Asit can be observed, the outdoor pathloss values are approximately below 110 dB in most of the cases, while the indoor pathloss are larger than 130 dB in many positions. Then, the first study consisted of analyzing 10 indoor positions with poor coverage at different floors of the buildings that are closer to BS2 and analyzing two alternatives to enhance the coverage of each one, namely the use of an indoor or an outdoor RIS/relay. This leads to the 20 situations depicted in Figure 3-15, each one represented by an arrow in which the tip is the UE position and the circle the RIS/relay position (indoor for situations 1 to 10 and outdoor for situations 11 to 20). The RIS codebook is always configured to reflect the maximum power in the direction of the UE. The propagation losses of the link RIS/relay-UE are obtained with the Indoor Hotspot (InH) model and the UMi respectively for indoor and outdoor RIS/relays. The rest of the simulation parameters are the same as in Table 3-3 with B_{BS} =20 MHz and combination 1 of power consumption parameters.



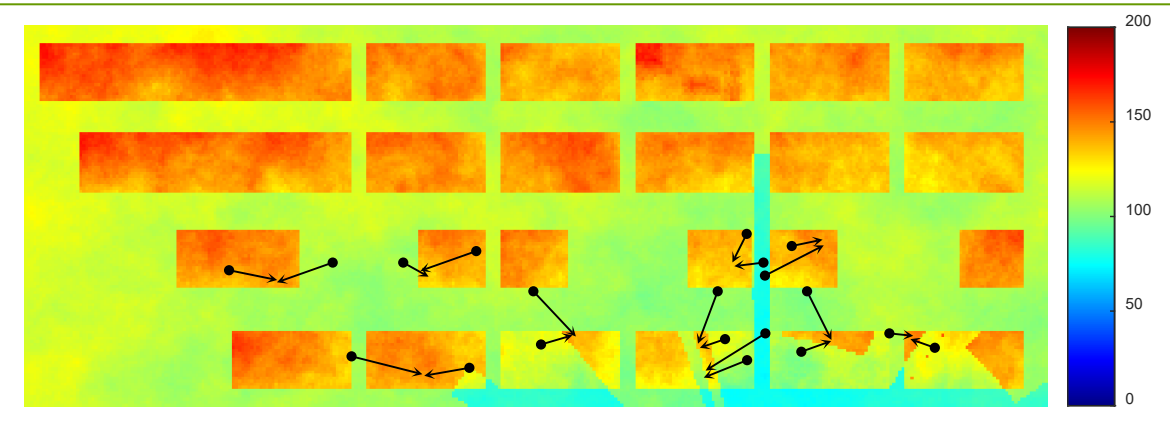


Figure 3-15 Pathloss values (dB) experienced at the ground level with BS2 and studied situations. Locations are in the ground floor for cases 1, 2, 3, 5, 11, 12, 13, 15, in the 1st floor for cases 4, 6, 7, 10, 14, 16, 17, 20 and in the 2nd floor for cases 8, 9, 18, 19

Figure 3-16 depicts the PCR metric for each situation as a function of the pathloss between the BS and the RIS/relay in Figure 3-16 (a) and as a function of the pathloss between the RIS/relay and the UE in Figure 3-16 (b). In turn, the energy savings with respect to the reference case for the relay and the RIS are depicted in Figure 3-17.

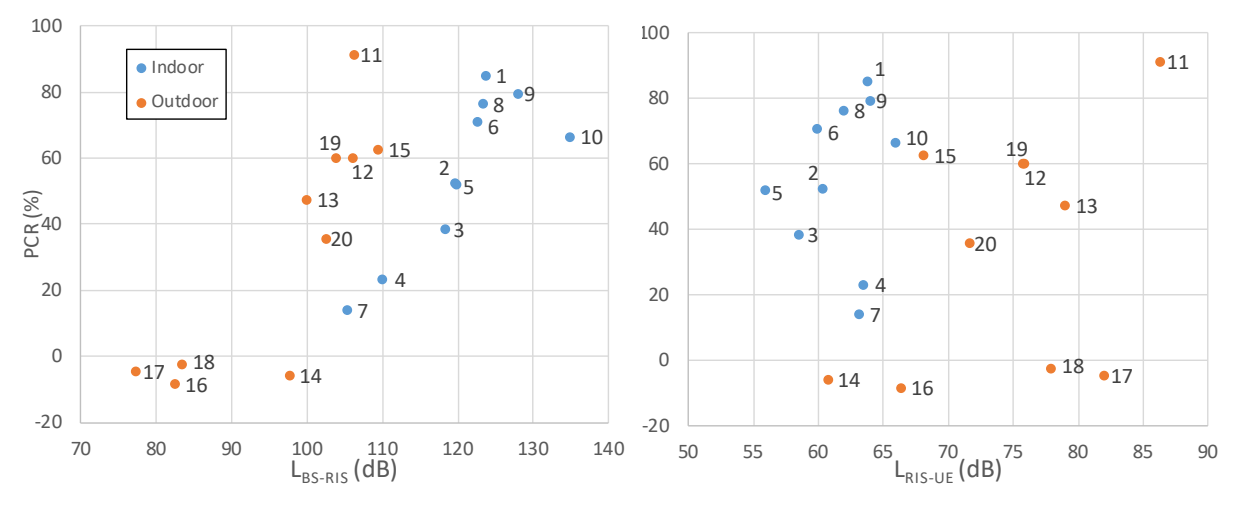


Figure 3-16 PCR metric for the studied situations as a function of the pathloss between BS and RIS/relay (a) and between RIS/relay and UE (b)

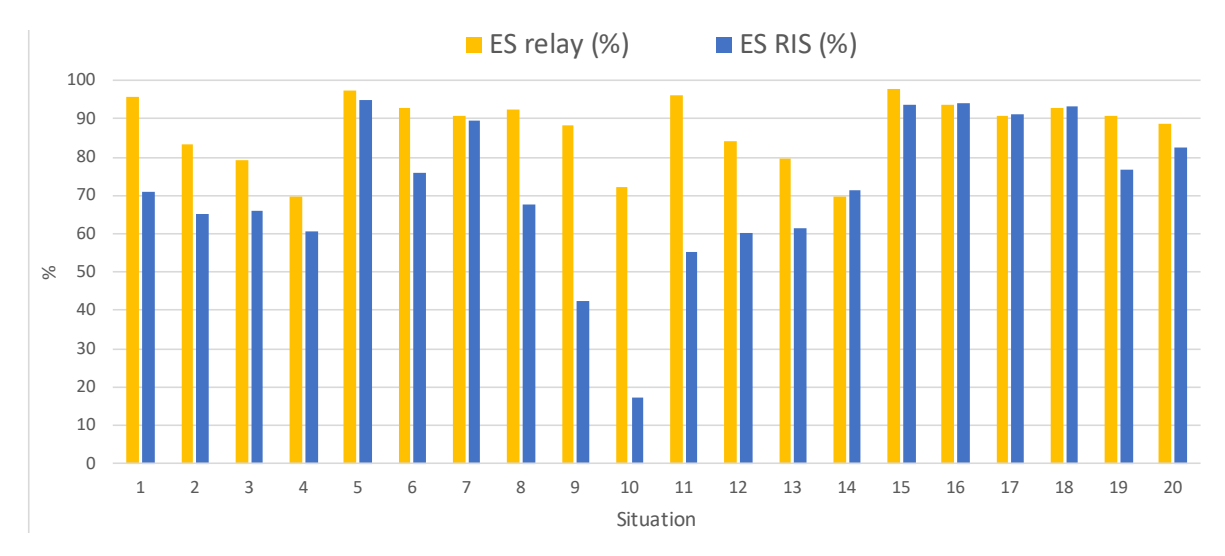


Figure 3-17 Energy saving with the relay and the RIS for each studied situation



It is observed that in all the situations with an indoor RIS/relay the relay outperforms the relay, i.e. PCR>0% in Figure 3-16 and ESREL>ESRIS in Figure 3-17. The main reason is the large pathloss between the BS and the RIS/relay that exists in these situations. Indeed, this corroborates the results in the previous section (see Figure 3-13) that indicate that the RIS needs to have a good pathloss with the BS (e.g. lower than ~90 dB, which is hardly found in indoor locations) to achieve higher energy savings than the relay. In turn, looking at the situations 11 to 20 in which the RIS/relay is outdoor, it is observed in Figure 3-16a that the pathloss L_{BS} -RIS is in general smaller than when it is indoor and, as a result, in situations 14, 16, 17, 18 the RIS requires less power than the relay, i.e. PCR<0%. Among them, the situations 16, 17 and 18 are characterized by very low values of L_{BS-RIS} < 85 dB, while the situation 14 has a larger value of L_{BS-RIS} (~97 dB) but in contrast the pathloss L_{RIS-UE} is much lower than in the other situations (see Figure 3-16b). In turn, the rest of outdoor situations with PCR>0% are characterized by lower values of LBS-RIS than for the indoor situations but by higher values of L_{RIS-UE} , leading eventually to a better performance of the relay. In terms of energy savings with respect to the reference case, it is seen in Figure 3-17 that in all the situations the RIS and the relay achieve significant savings, being more than 90% in some of them. In most of the situations, the energy savings of the relay are larger than those of the RIS, while in the abovementioned four situations with PCR<0% the energy saving of the RIS is slightly higher than that of the relay.

To get further insights into one of the situations with PCR<0%, a more detailed analysis of the RIS/relay used in situation 14 is conducted. In this case, the RIS/relay is deployed close to the wall of building B5 to improve a coverage hole at the first floor of building A5. The RIS reflects the signal of BS2 and is initially configured with a codebook to point in the direction shown in Figure 3-15 that corresponds to azimuth θ_r =-80°. Figure 3-18 plots the map of the first floor of building A5 with the value of the PCR metric for each pixel. This has been obtained considering a UE located at the pixel and assessing the required power consumption when it is connected through the relay or through the RIS. The pixels in which the RIS results in less power consumption than the relay (i.e. PCR<0%) is the grey area at the central upper part of the building, which represents approximately 5% of the pixels in the ground floor. The lowest PCR value achieved in these pixels is around -7.7% (i.e. the relay requires 7.7% more power than the RIS). These pixels belong to the area with poor coverage from the base station and fall around the azimuth angle where the RIS reflects most of the power based on its codebook configuration. In contrast, the rest of pixels in yellow/green in the upper part of the building are those of the coverage hole in which the use of the relay leads to a lower power consumption than the RIS and represent approximately the 21% of the pixels. In the rest of pixels of the building where the coverage of the base station is sufficiently good there are no differences between relay and RIS (i.e., PCR ~0%) because in this area none of the two approaches lead to energy savings with respect to the reference case without RIS/relay. This area represents approximately 74% of the building.



Figure 3-18 PCR metric at the first floor in A5 building



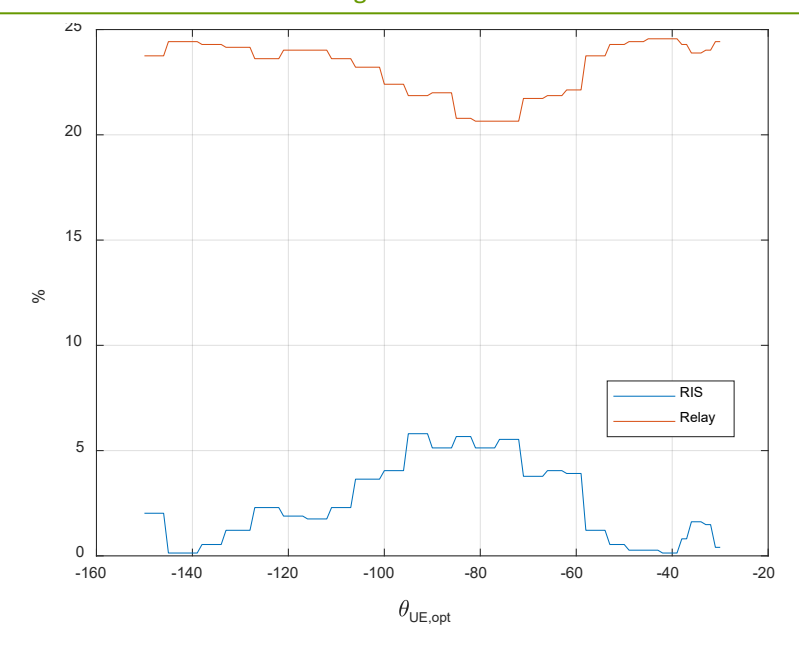


Figure 3-19 Percentage of pixels of the ground floor where the RIS requires less power than the relay (blue line) and where the relay requires less power than the RIS (orange line) as a function of the RIS pointing angle

To assess the effect of the pointing direction of the RIS based on its codebook configuration, Figure 3-19 plots in blue the percentage of pixels of the ground floor of the building in which the RIS requires less power than the relay and there is energy saving with respect to the reference case. Similarly, it plots in orange the percentage of pixels in which the relay requires less power than the RIS and there is energy saving with respect to the reference case. These percentages are presented as a function of the RIS pointing direction. It is observed that in all the cases, the relay leads to lower consumption in a larger number of pixels than the RIS, with a percentage that fluctuates between 21% and 25% depending on the pointing direction. Instead, the percentage of pixels in which the RIS outperforms the relay varies between 0 and 6%, exhibiting the highest values when the pointing direction is between -100° and -70° approximately. In these cases, the RIS reflects the power to a larger part of the poor coverage area. In the rest of pixels of the building that are not included in the percentages of Figure 3-19 neither the RIS nor the relay achieve significant energy savings with respect to the reference case. These represent approximately 76% of the pixels.

3.3.4 Conclusions

This section has presented a comparison between the use of a RIS or a relay in terms of the achievable energy savings with respect to the case in which none of these elements is used to enhance the coverage in certain areas. Results have shown that both RIS and relays can achieve substantial energy savings with respect to this reference case. In particular, values of energy savings of up to approximately 80% have been found with some configurations.

The comparison between the two depends on several factors. In general, the RIS achieves higher savings than the relay when the pathloss between the RIS and the base station is low, e.g. around 70 dB, and the UE is located in an angular region of approximately +/- 30° with respect to the RIS pointing angle. In this case, it has been observed that the power consumption of the RIS is about 9% better than that of the relay. Instead, when the pathloss between the RIS and base station increases up to approximately 90 dB, the improvements of the RIS are only observed when the UE is in the RIS pointing angle with a margin of only +/- 5°. For larger pathloss values, the relay outperforms the RIS. Similarly, when the UE is outside the indicated angular ranges, the relay also outperforms the RIS, with differences in power consumption that can be as high as 70-80%.

It has also been found that the comparison between RIS and relay is very sensitive to the power consumption model parameters that characterize the consumption at zero RF power and the scale factor with the



transmitted power. Depending on how these parameters are set, it is found that for low pathloss values between the RIS and the base station (i.e. lower than 90 dB) the RIS can outperform the relay with differences that range between 10% and 110%, while for high pathloss values (i.e. higher than 90 dB) the relay outperforms the RIS with differences that range from 25% to 70%.

The analysis conducted in the UPC campus scenario has led to the observation that in most of the analyzed situations the relay provides higher energy savings than the RIS. The reason is that the areas with poor coverage in the campus are located indoor and an indoor RIS to cover these areas would experience an excessive pathloss with the BS. Thus, the RIS only is able to provide better savings than the relay in very specific conditions of outdoor RIS. In these cases, the RIS improvements over the relay are observed mostly in a small area around the RIS pointing direction.

3.4 Implications of operating frequency on power consumption

The progressive increase in operating frequencies towards millimeter waves (mmWaves) that is expected for certain 5G deployments and for beyond 5G systems to better deal with the highly increasing demand for bandwidth hungry applications will bring important challenges from the coverage perspective. These frequencies are more susceptible to blockage by physical objects such as buildings, trees, and other obstacles, than traditional sub-6 GHz frequencies. Therefore, this will reduce the received signal strength leading to coverage holes, which can impact the QoS experienced by end-users. To compensate for these degradations, the use of higher transmitted powers together with network densification will be required, thus increasing the overall energy consumption in the network. In this context and trying to address some of the comments raised by the BeGREEN External Advisory Board (EAB), this section intends to present an assessment of the power consumption increases that will be needed to maintain the coverage conditions when increasing the operating frequency of the network.

3.4.1 Considered scenario and assumptions

The study is conducted in the UPC Campus Nord scenario presented in section 2.5.3 considering the real positions of the 3 closest BSs that provide 5G NR coverage. Based on the total pathloss L in a pixel for a given BS, the downlink spectral efficiency in bits/s/Hz is computed using the Shannon formula as:

$$S = \log_2 \left(1 + \frac{P_T G_{BS} G_{UE}}{P_N L} \right)$$

where P_T is the transmitted power, G_{BS} and G_{UE} are the antenna gains and P_N is the noise power at the receiver. The resulting spectral efficiency from the above expression is bounded by a maximum value S_{max} =7.4063 b/s/Hz based on the possible modulation and coding schemes considered in Table 5.1.3.1-2 of 3GPP TS 38.214. This computation assumes ideal intercell interference coordination among the involved macrocells.

Initially, the BS transmission power is set to P_T =38 dBm and the antenna gains are G_{BS} =10 dB and G_{UE} =3 dB. Moreover, the results are presented assuming a total bandwidth B of 20 MHz and the resulting noise power P_N is equal to -92dBm.

3.4.2 Results

Figure 3-20 shows the resulting spectral efficiency maps obtained at the ground floor of the campus for the cases that the operating frequency is 3.72 GHz and when it is increased to 26 GHz assuming that the BS transmitted power is the same in both cases. As can be observed, the frequency increase reduces significantly the coverage and spectral efficiency. Assuming that outage occurs when spectral efficiency is lower than 1 b/s/Hz, it is observed that most of the indoor positions are in outage at 26 GHz and the outdoor spectral efficiency is reduced in most areas.



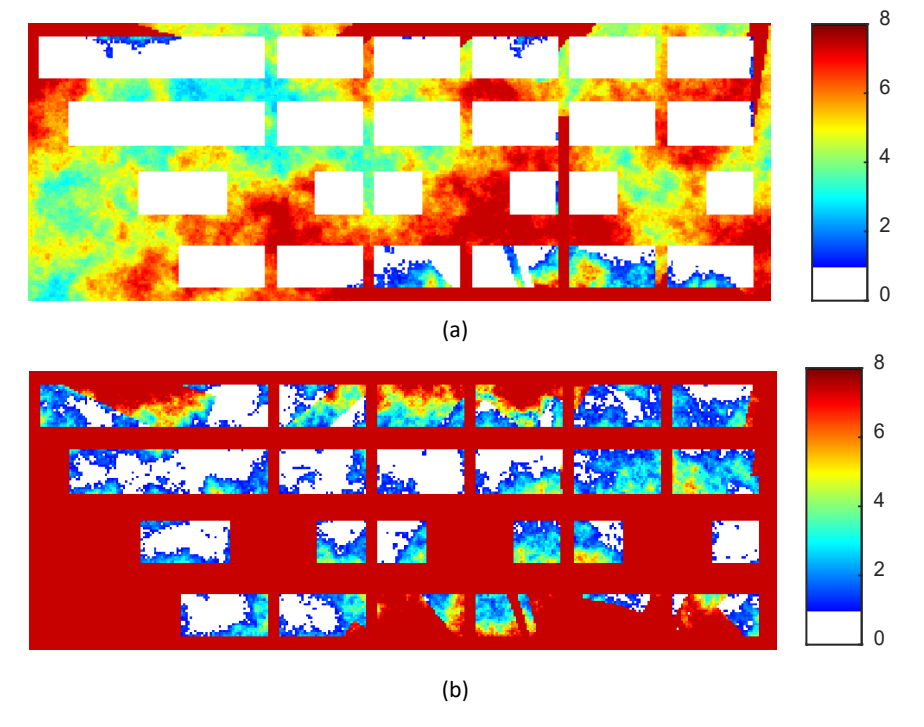


Figure 3-20 Spectral efficiency maps (b/s/Hz) of the campus with (a) 26GHz (a) and (b) 3.72GHz, both with P_T =38dBm

Specifically, the spectral efficiency reduction reaches up to 66% at outdoor positions when the frequency is increased to 26 GHz. Furthermore, at the indoor positions that are not in outage the reduction can be up to 83%.

To maintain the same coverage conditions when increasing the frequency to 26 GHz, the transmission power needs to be increased in such a way that it compensates the increase in propagation losses. Specifically, according to the UMa model of 3GPP TR 38.901, the propagation losses are affected by the frequency in two components:

- Pathloss: The pathloss in dB increases with the operating frequency f in GHz based on the term $20\log_{10}f$. Then, when passing from 3.72 GHz to 26 GHz there is a pathloss increase of approximately 17 dB.
- (O2I) penetration losses, which are aggregated to the pathloss for indoor positions. These losses are defined as:

$$O2I = 5 - 10\log_{10} \left(0.7 \cdot 10^{\frac{-L_{IIRglass}}{10}} + 0.3 \cdot 10^{\frac{-L_{concrete}}{10}} \right)$$

$$L_{IIRglass} = 23 + 0.3 f$$

$$L_{concrete} = 5 + 4 f$$

In this case, it is obtained that increasing the frequency from 3.72 GHz to 26 GHz increases the O2I losses by approximately 10 dB.

Therefore, if no other conditions are changed, in order to obtain the same spectral efficiency in outdoor areas, the transmission power would need to be increased in 17 dB when the frequency is 26 GHz, and to also achieve the same spectral efficiency at indoor areas, the needed increment would be 27 dB. To illustrate this, Figure 3-21 shows the spectral efficiencies in the case of 26 GHz and P_T =65 dBm, corresponding to the power increase of 27 dB with respect to the case of 3.72 GHz. We observe that the resulting spectral efficiency is the same as in the case of 3.72 GHz and 38 dBm from Figure 3-20b.

Frequ 3.72

26 GHz



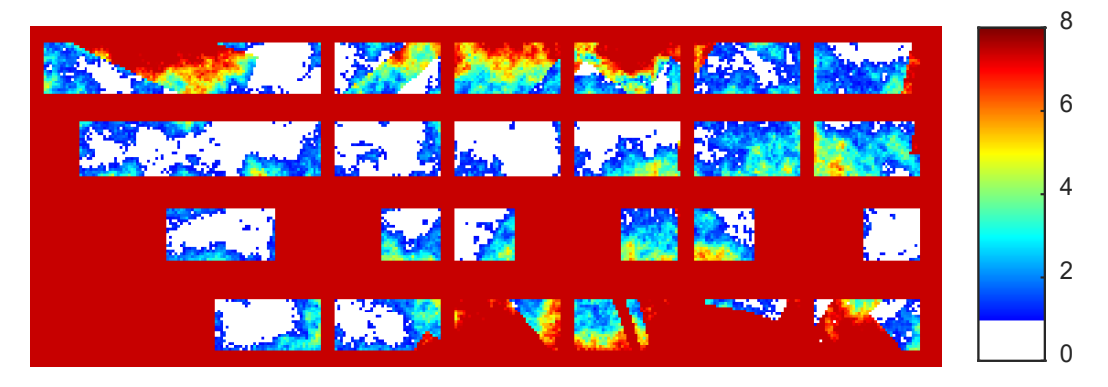


Figure 3-21 Spectral efficiency maps (b/s/Hz) of the campus with 26 GHz and P_T=65 dBm

To assess the corresponding increase in total power or energy consumption we can consider the same model used in previous studies (see e.g. section 3.3.1 of BeGREEN D2.2 [2]). Specifically, the total power consumption becomes $P=a_{BS}\cdot P_T+P_{0,BS}$ where a_{BS} is the scaling factor of the transmitted power and $P_{0,BS}$ the consumption at zero RF output power due to circuits, signal processing, etc. Assuming $a_{BS}=4.7$ and $P_{0,BS}=130$ W for a macrocell from [15][15], the corresponding power consumption per BS for the two considered frequencies is shown in Table 3-4. It is observed that there is a power increase in a factor 94 to maintain the same coverage with 26 GHz than with 3.72 GHz if no other parameters are modified.

uency	Transmitted power	Consumed power per BS
? GHz	38 dBm	160 W

14993 W

Table 3-4 Power Consumption for the Same Coverage

65 dBm

In addition to increasing the power, the possibility of using beamforming at mmWaves can be also considered as a means of overcoming the pathloss increases. To model this, the simulations have considered an increase of the antenna gains for the case of 26 GHz. Specifically, using the antenna model from a 3D beamformer of Atoll planning tool that was studied in [27], the antenna gain at the BS with beamforming is assumed to be GBS=26 dB. Similarly, the antenna gain for the UE with beamforming is assumed to be GUE=10 dB. Ideal beam steering is assumed in the simulations. Figure 3-22 plots the resulting spectral efficiency in the campus with f=26 GHz, beamforming and with the same transmitted power PT=38 dBm like in the 3.72 GHz case. Comparing this result with the case without beamforming in Figure 3-20 (a), it is observed that the spectral efficiency is significantly increased and it is quite close to the one obtained with 3.72 GHz in Figure 3-20 (b). In particular, all the outdoor positions obtain the same spectral efficiency as with 3.72 GHz, but there are still many indoor positions in outage.

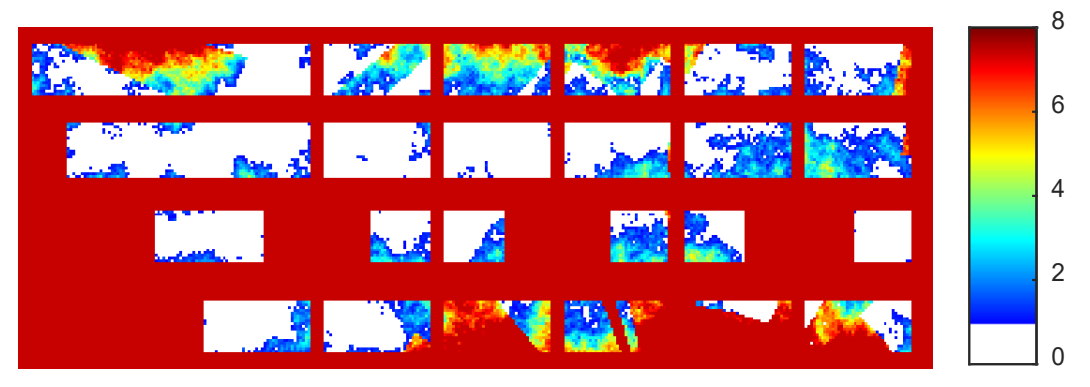


Figure 3-22 Spectral efficiency map (b/s/Hz) of the campus with 26 GHz, beamforming and P₁=38 dBm



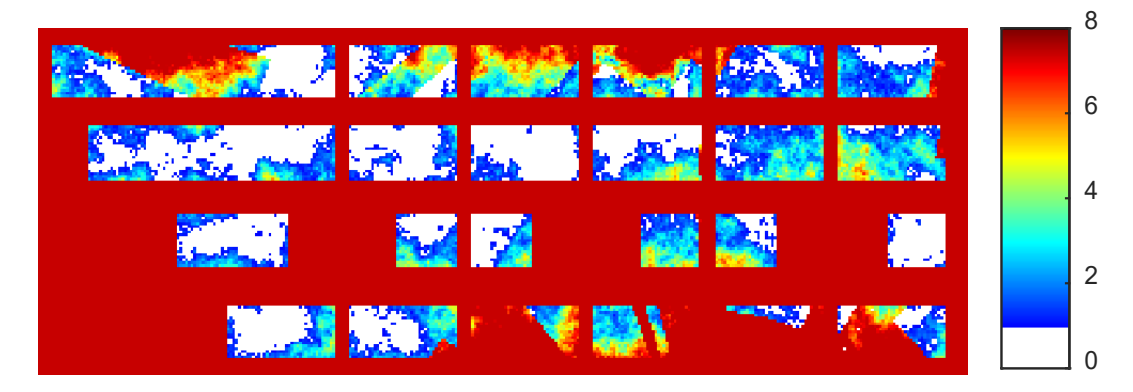


Figure 3-23 Spectral efficiency maps (b/s/Hz) of the campus with 26GHz, beamforming and P_T=42 dBm

Now we can compute the power increase that will be needed in case of having beamforming at 26 GHz to achieve the same coverage as in the 3.72 GHz case. Based on the previous computations without beamforming, the required power increase was 27 dB. With beamforming, part of this increase is provided by the new antenna gains. Specifically, the BS antenna gain has increased from 10 dB to 26 dB and the UE antenna gain from 3 dB to 10 dB. This represents a total gain of 16+7=23 dB. Thus, the required transmission power increase with beamforming is only of 27 dB-23 dB=4 dB, corresponding to a total transmitted power of P_T =42 dBm.

Figure 3-23 plots the spectral efficiency map with 26 GHz, beamforming and transmitted power 42 dBm. It can be seen that the obtained maps are almost identical to the case of 3.72 GHz from Figure 3-20b. This means that if beamforming is applied, an increase of 4 dB in the transmission power is enough to achieve the same coverage with 2 6GHz and with 3.72 GHz.

Table 3-5 presents the increase in total consumed power per BS to keep the same coverage at 3.72 GHz and 26 GHz with beamforming. Now, it is observed that the increase is only a factor 1.28, corresponding to 28%.

Frequency	Transmitted power	Consumed power per BS
3.72 GHz	38 dBm	160 W
26 GHz	42 dBm	204 W

Table 3-5 Power consumption for the Same Coverage with Beamforming

3.4.3 Conclusions

This section has studied the impact of increasing the operating frequency of the base stations that provide coverage in a given area to work with millimetre waves. The results found in the UPC campus scenario have revealed that to keep the same indoor and outdoor coverage conditions when moving from 3.72 GHz to 26 GHz, a transmitted power increase of 27 dB is required to compensate the higher pathloss and outdoor-to-indoor propagation losses. As a result, the total power consumption per base station increases in a factor 94. However, in addition to increasing the transmitted power, it is also possible to exploit other features such as beamforming. When doing this, it has been found that a transmitted power increase of 4 dB is sufficient to maintain the same coverage, which leads to a total power consumption increase in a factor of only 1.28.

3.5 Network optimization given ISAC data

Efficient management of radio resources is an important topic in RANs. By optimizing the parameters of the resources in the network, it is possible to get better spectral efficiency, QoS, throughput, etc., or to reduce the energy consumption while achieving the same performance. There is a vast literature on this resource allocation, and some surveys summarizing those works can be found in [28] and [29].



This investigation is on how to reduce power consumption in the network. It is assumed that the location information of the devices is extracted by the RUs that feature sensing capabilities. The user density is presented in the area using a heatmap and optimize the power consumption via the postprocessing of the heatmap. Namely, using the location information, we perform link budget calculations and try to minimize the total transmitted power based on the user density while getting the same performance criteria, such as minimum receive power, average receive power, and outage probability.

3.5.1 Considered scenario and assumptions

The following scenarios are assumed, i) (Figure 3-24) a dense scenario with many users (daytime), ii) (Figure 3-25) is a sparse scenario with fewer users (night-time). We assume that there are four BSs in the network, where all of them are turned on and transmitting with full power. In the nighttime, we turn off all BSs except one of them and increase its transmitting power. Note that we decide which BS remains active on based on the sensing information and link budget calculation. It is shown that by leaving active the optimal BS, the power consumption can be reduced while satisfying the same QoS. Moreover, the unequal power allocation between the BSs is analysed and that some improvement can be achieved by unequal power allocation through numerical optimization. The link budget calculation is the following:

$$P_{RX} = P_{TX} + G_{TX} - L_{TX} - L_{FS} - L_M + G_{RX} - L_{RX}$$

$$L_{FS} = 20\log_{10}(d) + 20\log_{10}(f) + 20\log_{10}\frac{4\pi}{c}$$

where:

• P_{RX} : received power (dBm)

• P_{TX} : transmitted power (dBm)

• G_{TX} : transmitter antenna gain (dB)

• L_{TX} : transmitter losses (dB)

• L_{FS} : free-space pathloss (dB)

• L_M : misc. losses (dB)

• G_{RX} : receive antenna gain (dB)

• L_{RX} : receiver losses (dB)

• d: Distance

• *f*: Frequency

The system parameters that will be generally used are:

• Threshold for outage = -22 dB

• Average tx power P_{TX} (dBm) = 47 (50.11W)

f = 1 GHz

Transmit antenna gain (dBi) = 3;

• Receive antenna gain (dBi) = 3;

• Idle power P_{idle} (dBm) = 30 (1W);

• Number of BS $N_{BS} = 4$;

Area size: 1 km²

Being the total transmit power calculated as $N_{BS} * P_{TX}$.



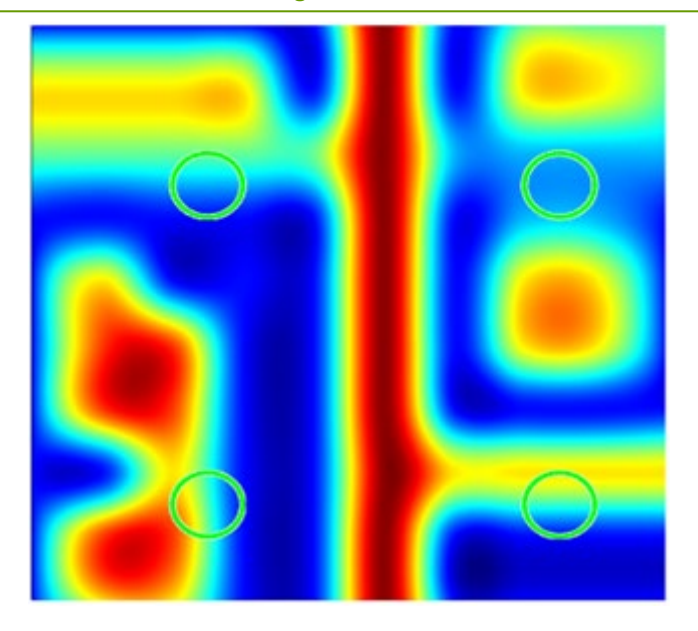


Figure 3-24 Scenario 1 (dense): daytime with 4 BS, 150 users

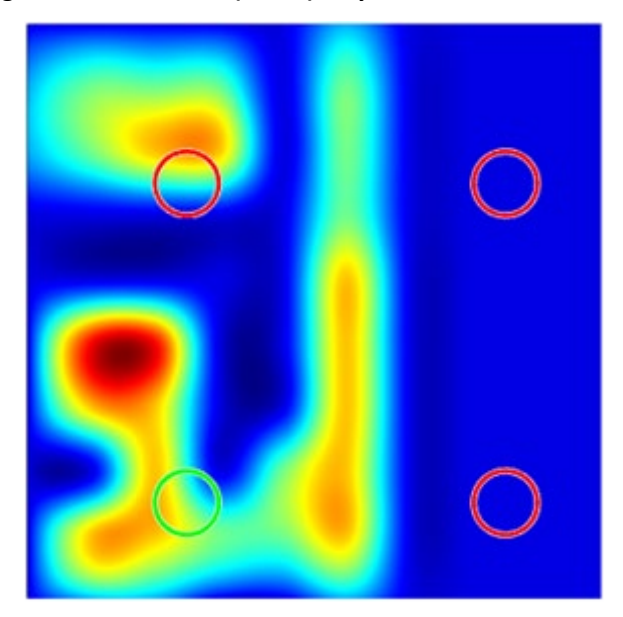


Figure 3-25 Scenario 2 (sparse): night-time with 1 BS, 70 users

3.5.2 Power saving based on user density

It is assumed that the UE locations are known thanks to the sensing capabilities.

In the daytime, we consider a scenario with 150 users. In this case, we have 4 BSs turned on with a transmit power of 50 W. Then, the total transmitted power becomes:

$$P_{TX-tot}$$
 (day) = 4* (50.11) \approx 200 W

The received power of the user is calculated, ignoring the losses except the free space pathloss. In this scenario, the average minimum rx power is -23.94 dBm, and the average rx power is -17.84 dBm.

Also, a sample set of received power levels of the users are depicted in Figure 3-26.



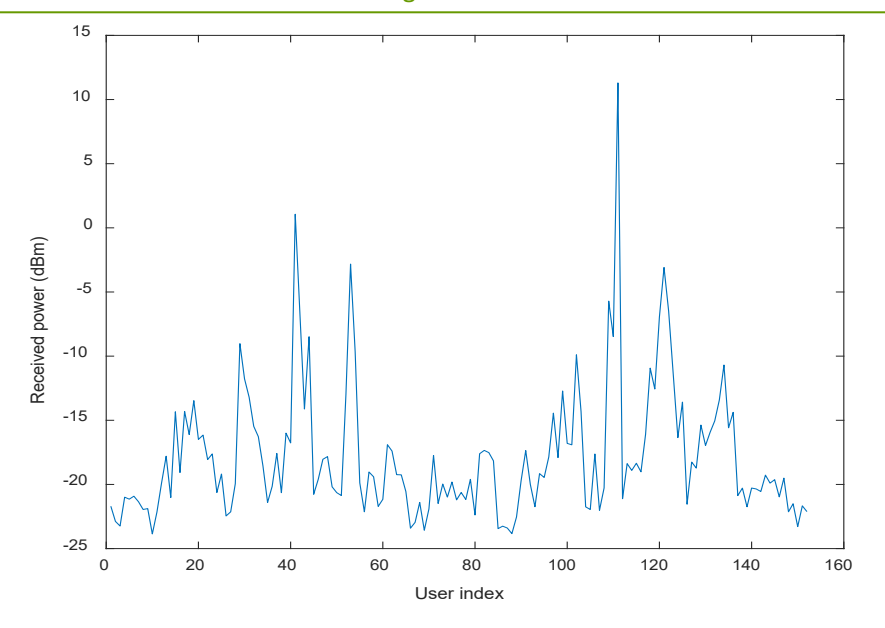


Figure 3-26 Average received power per user (daytime)

In the night-time, the user density decreases and there are 70 users. To get power savings, in this case, we turned off three of the BSs and increased the power of the remaining BS to increase coverage. We keep turned on the BS minimizing the outage probability and maximizing the average and minimum received power of the users. With an increased power level to 50 dBm (100W), the total transmitted power becomes:

$$P_{TX-tot}$$
 (night) = 100W

Here, the average minimum rx power is -28.07 dBm, and average rx power is -19.08 dBm. Also, with a power threshold with -26 dBm, the outage power probability is 0.11.

To summarize, with some sacrifice in the performance, we can get a power saving of more than 50%.

A sample set of the power levels in the night-time is depicted in Figure 3-27.

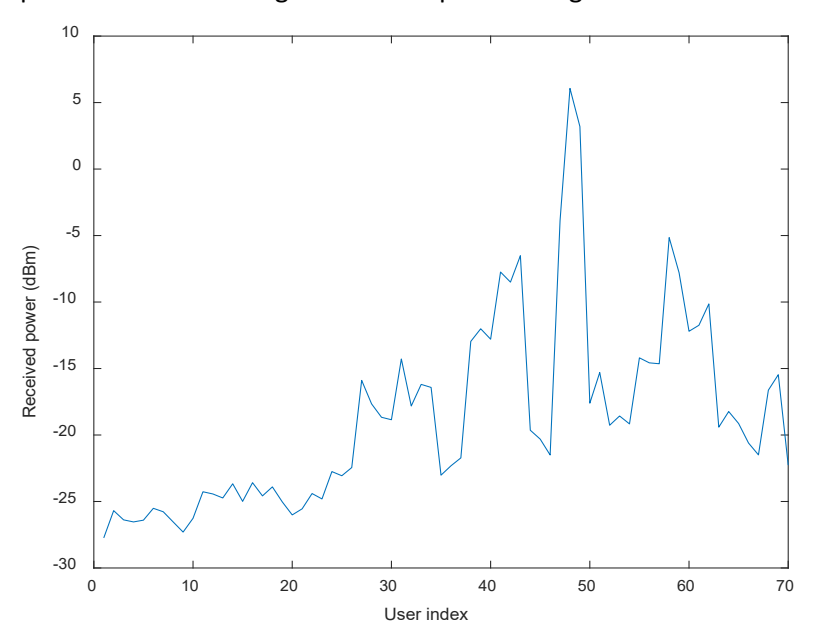


Figure 3-27 Average received power per user (night-time)



3.5.2.1 Unequal power allocation in Scenario 1

We also investigate the potential advantages of unequal power allocation of BSs in the network by Monte Carlo simulations. We simulate a set of discrete power levels between 43 and 51 dBm for BS s and compare it to the case that the transmit power of all BS s is 47 dBm.

The optimized values of the performance metrics and corresponding optimal power levels regarding those performance metrics are indicated in Table 3-6 and Table 3-7, respectively.

Finally, we investigate the minimum power levels with unequal power allocation to get the same average receive power for the case of equal power allocation and the transmit power of each BS is 47 dBm. Note that in terms of minimum rx power, equal power allocation is almost optimal. To get an average rx power of about -17.69 dBm, the corresponding power levels are included in Table 3-8.

Therefore, the average tx power of the BSs is reduced by 46 dBm.

Table 3-6 Performance Metrics after Optimization

	Outage prob. (Threshold = -22 dBm)	Minimum received power (dBm)	Average received power (dBm)
Equal power allocation	0.1206	-23.56	-17.69
Unequal power allocation (optimized)	0.0761	-23.13	-16.74

Table 3-7 Optimized Power Levels in dBm

Performance metric	BS 1 (upper left)	BS 2 (lower left)	BS 3 (upper right)	BS 4 (lower right)
Outage prob.	43	49	47	49
Minimum rx power (dBm)	47	48	45	48
Average rx power (dBm)	43	51	43	51

Table 3-8 Corresponding Power Levels for a Fixed Rx Power

	BS 1	BS 2	BS 3	BS 4
Average rx power (dBm)	41	51	41	51

3.5.2.2 Further simulations on reducing power consumption

In this part, we perform simulations on the received power level in the daytime and night-time scenarios as well as finding the power level in the night-time scenario satisfying the same performance constraints as the day-time scenario. We aim to show that by turning off some of the BSs in an optimal way based on the user density and increasing the transmit power of the remaining BS, power consumption can be reduced while getting the same performance. In our simulations, we consider the scenarios depicted in Figure 3-28 and Figure 3-29.

We keep the BS highlighted in green turned on, based on our simulations in which we calculate the outage probability, minimum received power, and average received power through Monte Carlo simulations. We observe that keeping the BS in the lower left side of the area turned on is optimal in terms of all of these performance metrics with the changing user density and distribution in the night-time.

In the day-time scenario, we assume that each of the BSs transmits with a maximum power of 50W. For the sake of simplicity, we assume that they transmit with the maximum power all the time, which leads to a total power consumption of 200 W. With this setup, the average of minimum rx power is -23.94 dBm, the average rx power is -17.84 dBm and the outage probability with a threshold of -23 dBm is 0.0433.



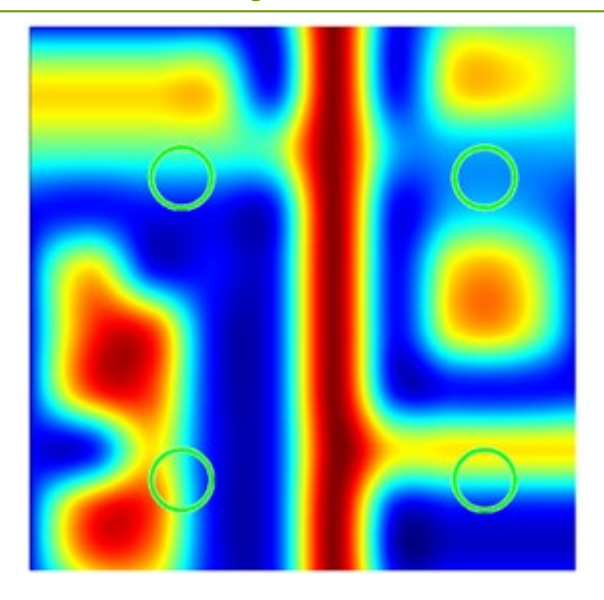


Figure 3-28 Scenario 1: daytime with 4 BS, 150 users

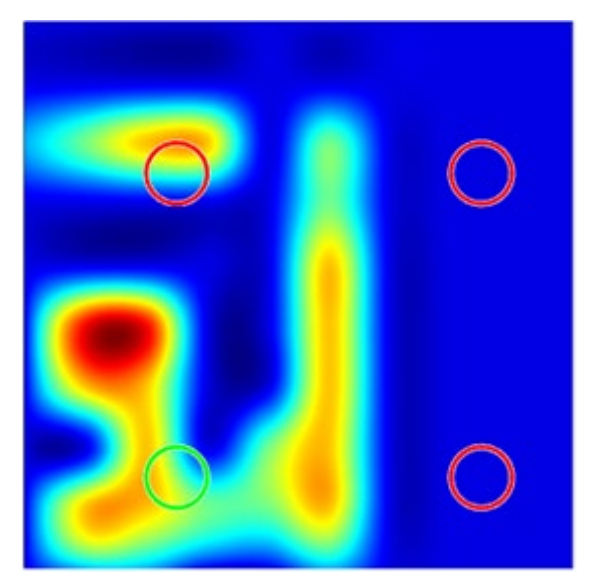


Figure 3-29 Scenario 2 (sparse): night-time with 1 BS, 60 users

The transmit power of the BS the is swept in the nighttime to find the minimum power level that we can get the same outage probability, minimum rx power and average rx power with the daytime. For each of these three performance criteria, the minimum required transmit power is different, which are summarized in Table 3-9 along with the power consumption reduction:

Table 3-9 Minimum Required Transmit Power and Power Consumption Reduction

Performance metric	Required tx power	Reduction w.r.t. day-time
Outage prob.	170 W	15%
Minimum rx power	158 W	21%
Average rx power	100 W	50%

3.5.3 Conclusions

Our results show that by turning off some of the BSs and turning on the optimal BS based on the scenario, the power consumption can be reduced by 15% to 50% depending on the performance metric.



3.6 Limits on energy efficiency for the CRM

Using the AIMM Simulator as previously described, the following main steps were followed:

- 1. We set up an instance of the CRM with 7 cells in a hexagonal arrangement, and a mean number of 100 UEs. The system dimensions were as in Figure 2-4.
- 2. Initial transmit powers were set to the equal value of 140 W for the rural cases, and 14 kW for the urban cases.
- 3. Run the simulation on the AIMM Simulator to determine the UE throughputs. This will use real MCS schemes, resource allocation, etc., as implemented in the AIMM Simulator.
- 4. Using the exact optimization algorithm, minimize total transmit power, subject to lower-bound constraints of -1 dB on SINR of every UE.
- 5. Set the network to use the new optimized transmit powers.
- 6. Run the simulation once more and compare distribution (over UEs) and quantiles of the throughputs.

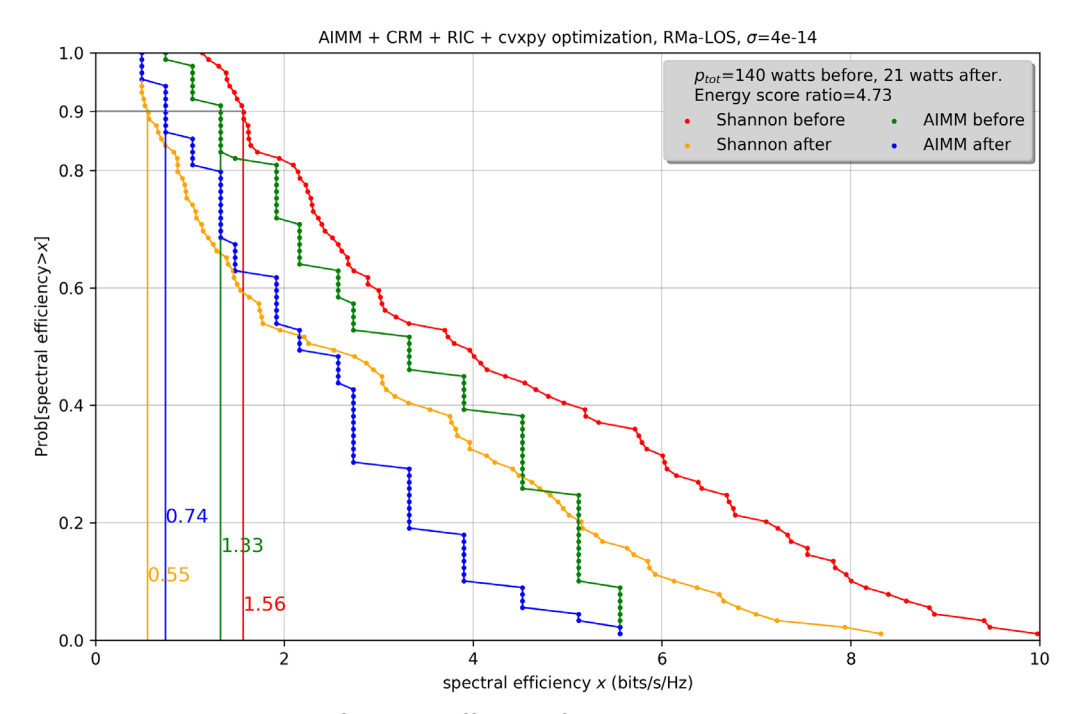


Figure 3-30 CCDF of spectral efficiency for the CRM with RMa-LoS pathloss



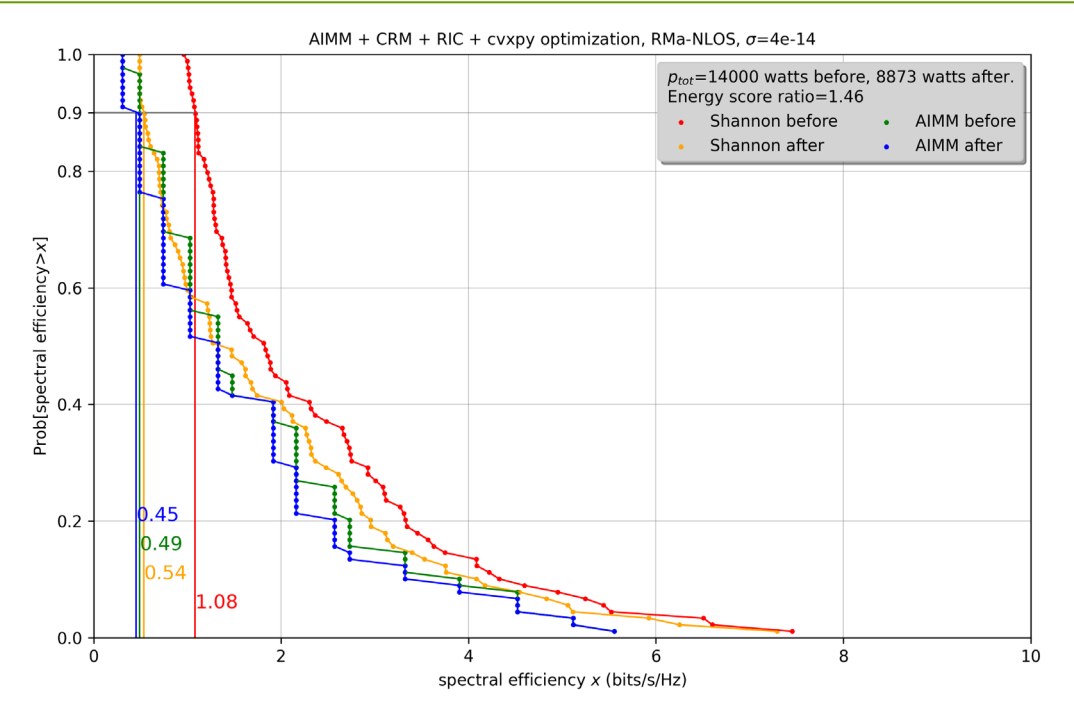


Figure 3-31 CCDF of spectral efficiency for the CRM with RMa-NLoS pathloss

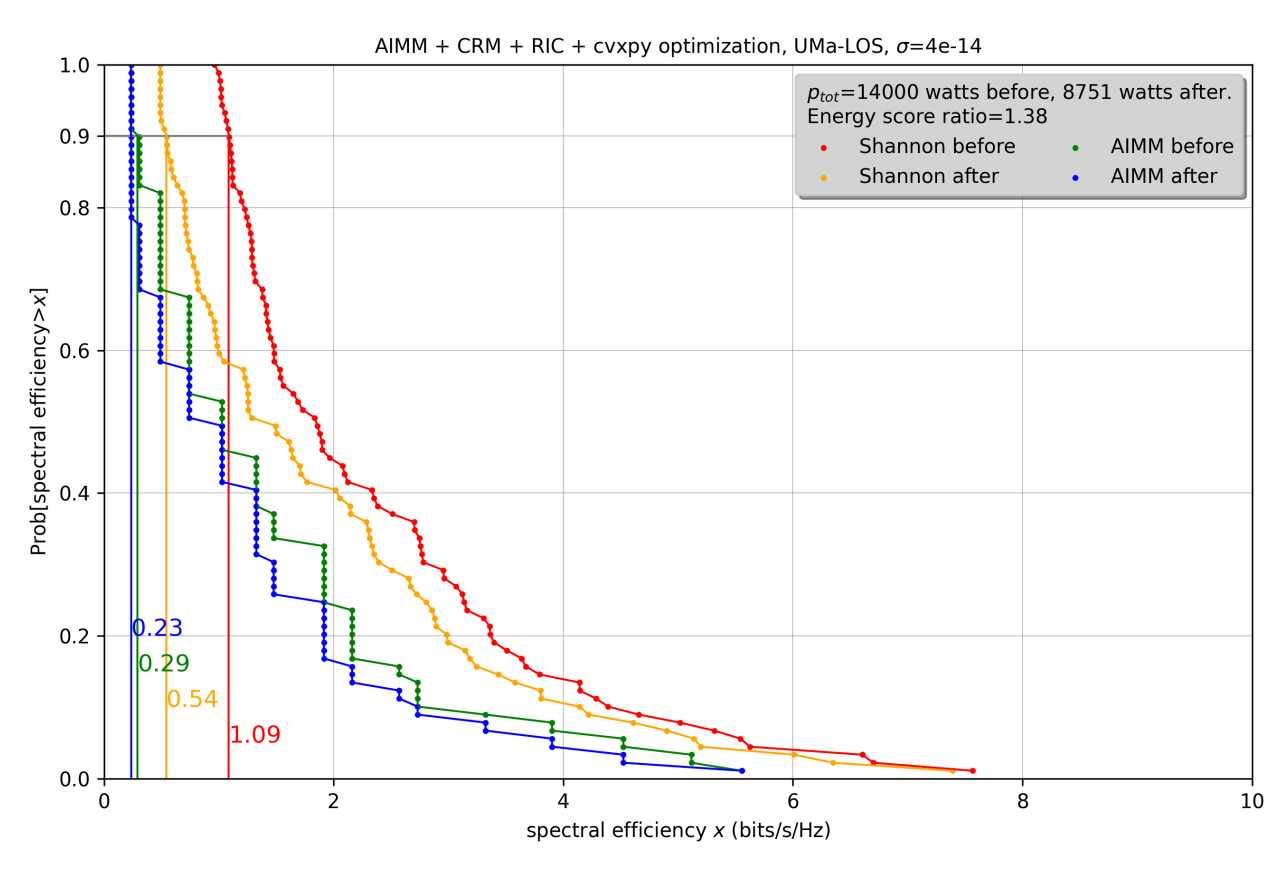


Figure 3-32 CCDF of spectral efficiency for the CRM with UMa-LOS pathloss



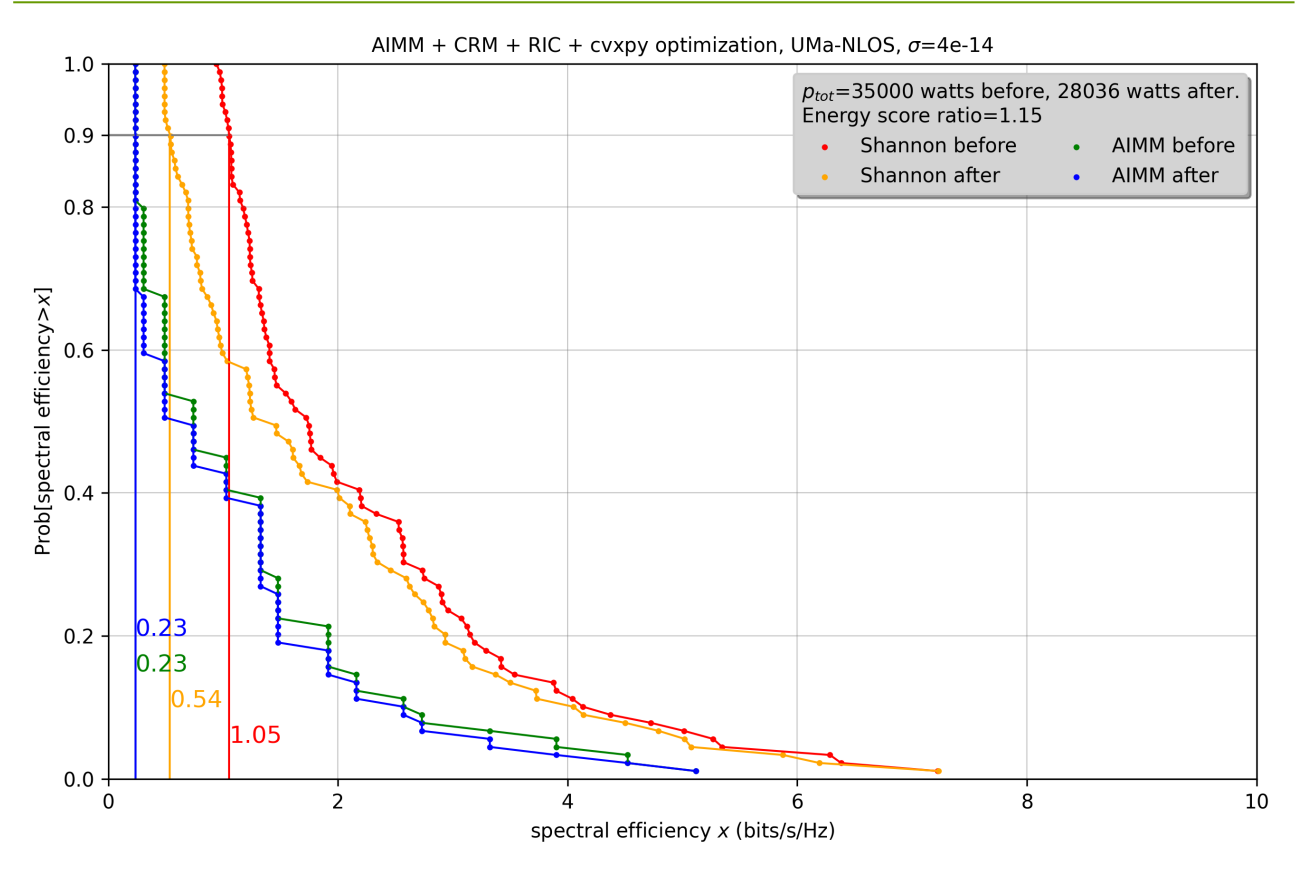


Figure 3-33 CCDF of spectral efficiency for the CRM with UMa-NLOS pathloss

Table 3-10 Energy Score Ratios Predicted by The AIMM Simulator for the Cellular Reference Model

Scenario	Energy score ratio
RMa-LoS	4.73
RMa-NLoS	1.46
UMa-LoS	1.38
UMa-NLoS	1.15

The actual results for the four scenarios are in Figure 3-30, Figure 3-31, Figure 3-32, and Figure 3-33, and are summarized in Table 3-10. An important main conclusion is that larger energy savings are obtainable in the lower pathloss scenarios.

3.7 DU uplink energy efficiency corresponding to the cellular reference model

As part of BeGREEN WP3, we demonstrated how novel architectures can decrease power consumption compared to legacy x86 architectures for UL receiver processing [17]. We would like to estimate the achievable UL receiver energy consumption improvement, which matches the AIMM scenarios presented in section 3.6, focusing on the DL transmitter. We can derive an estimate for the UL spectral efficiency from the DL spectral efficiency by parameter adjustment. We assume that the maximal Tx power level in the DL is 23 dB higher than in the UL, and that the DL noise figure in the DL is 2 dB lower than in the UL. Table 3-11 shows some UL receiver example scenarios, their energy score ratios, and their correspondence DL spectral efficiency which is in the range of 2.6 to 6.3 b/s/Hz. These values have the best match with the AIMM RMa-NLoS scenario, and they show an energy score improvement of about 40%.



Table 3-11 Estimated Energy Score Ratios for Rx DU Scenarios

Scenario	Modulation	UL SPEF (bits/sec/Hz)	Corresponding DL SPEF (bits/sec/Hz)	Energy Score Ratio
1	QPSK	0.3	2.6	1.3
2	64QAM	2.6	4.0	1.4
3	256QAM	4.2	6.3	1.5

3.8 Data-driven analysis of energy-QoS trade-off in traffic offloading scenarios

In this section, we analyze the trade-off between energy consumption and QoS in a real 5G NSA scenario when applying a traffic offloading strategy to enable the dynamic deactivation of 5G cells. The study is based on a real dataset, which was described in Section 2.5.4. Specifically, we use data from various cell KPIs to simulate traffic offloading, assessing the potential energy-saving benefits and the impact on QoS. The findings from this analysis on energy-saving opportunities were utilized to evaluate potential AI/ML and data-driven strategies for energy-efficient 5G carrier on/off switching, as reported in BeGREEN D4.2 [6]. In the upcoming BeGREEN D4.3, these results will be extended by integrating the QoS trade-offs into the AI/ML-driven strategies.

The section is organized into two main parts: (i) The methodology for analysing energy-saving opportunities and QoS trade-offs, and (ii) The results of the analysis.

3.8.1 Methodology

This section presents the data-driven 5G NSA traffic offloading strategy developed to explore opportunities for enhancing RAN energy efficiency. A specific cell is analyzed to illustrate the potential energy-saving benefits, while overall results are presented in Section 3.8.2. First, the energy consumption and utilization of 4G and 5G cells are evaluated, providing initial insights into the potential benefits of switching off 5G sectors and offloading their traffic to 4G. Then, the methodology for the proposed traffic offloading strategy is described, aiming to characterize the upper bound of energy-saving opportunities. Next, the process for estimating energy savings based on the KPIs available in the dataset is detailed. Finally, the methodology to assess the impact of the offloading strategy on QoS is described.

3.8.1.1 Energy consumption and utilisation analysis

On/off cell switching strategies usually target deactivating the capacity layer [30]. In the analysed NSA scenario, the capacity layer corresponds to the 3500 MHz 5G carrier, which offers the highest bandwidth, as detailed in Figure 3-34. The remaining 5G carriers (700 MHz and 2100 MHz) are deployed using Dynamic Shared Spectrum (DSS), sharing radio equipment with 4G and therefore cannot be independently deactivated. Additionally, their utilization is marginal compared to the 3500 MHz carrier.

Figure 3-34 illustrates the daily energy consumption of the nodes, comparing the aggregate consumption of all 4G carriers to that of the 5G 3500 MHz carrier. The average energy consumption for both is similar, although the 4G carriers exhibit greater deviation due to varying numbers of carriers across sites. Note that 5G typically offers higher bandwidth than the aggregate bandwidth of the 4G carriers, highlighting the potential for higher energy efficiency of 5G technology [30]. Note that, despite the higher bandwidth offered by 5G, it shows a significantly lower utilization compared to the most heavily used 4G carriers, as depicted in the CCDF in Figure 3-35. The CCDF highlights the percentage of time each carrier exceeds specific load levels, being 5G utilization often comparable to or lower than the least-utilized 4G carriers. Furthermore, it falls below the overall 4G utilization, which is calculated as the total aggregated 4G resource demand divided by the total available 4G resources.



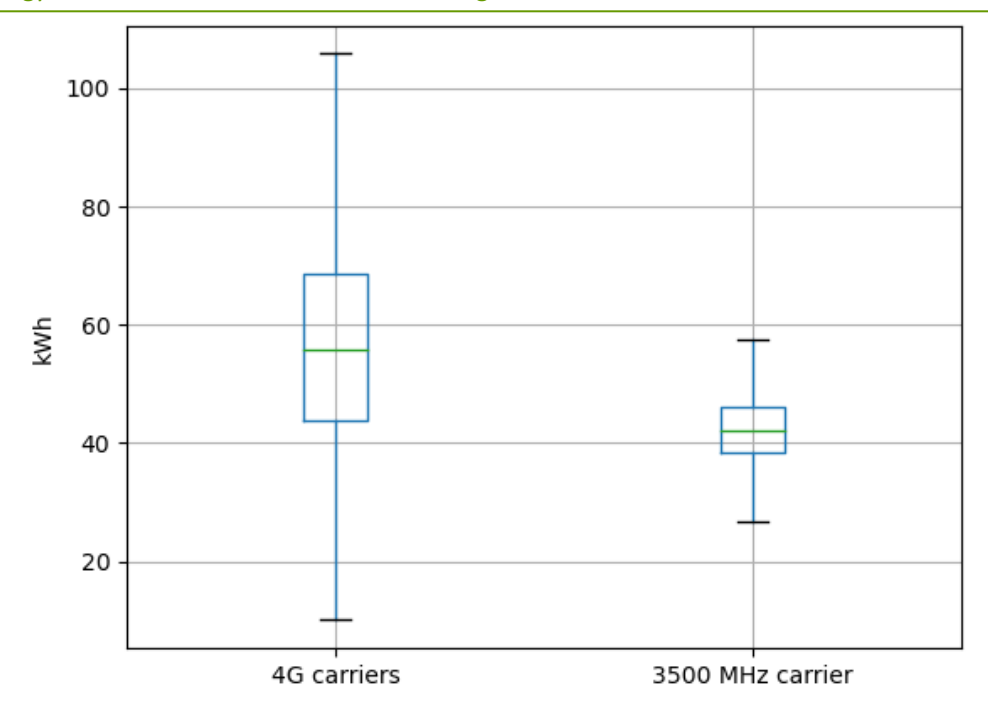


Figure 3-34 Energy consumption comparison: 4G vs 5G 3500 MHz carriers

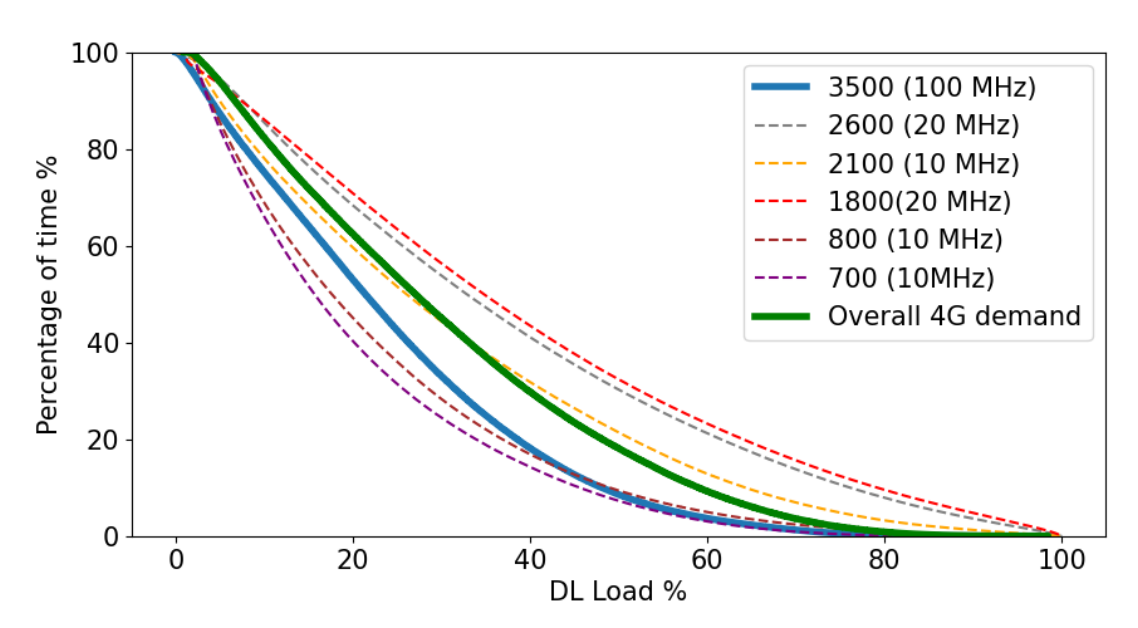


Figure 3-35 Utilization comparison: 4G vs. 5G carriers

These findings reveal that while 5G technology has the potential for higher energy efficiency compared to 4G, current 5G deployments are underutilized, leading to inefficiencies. Therefore, selectively switching off the 5G capacity layer and offloading its traffic to 4G cells could not only reduce overall RAN energy consumption but also significantly enhance its energy efficiency.

3.8.1.2 Traffic offloading strategy

The selective deactivation of 5G cells requires offloading their active traffic to 4G cells. The proposed approach considers only the 4G cells within the same sector and site, ensuring that offloaded UEs experience similar or better signal levels due to the larger coverage of 4G carriers. Note that the dataset does not include UE location data, limiting the implementation of load-balancing strategies across different sectors. Deployments incorporating advanced features like traffic steering xApps in O-RAN architectures could further enhance energy-saving opportunities by distributing traffic among sectors [31].



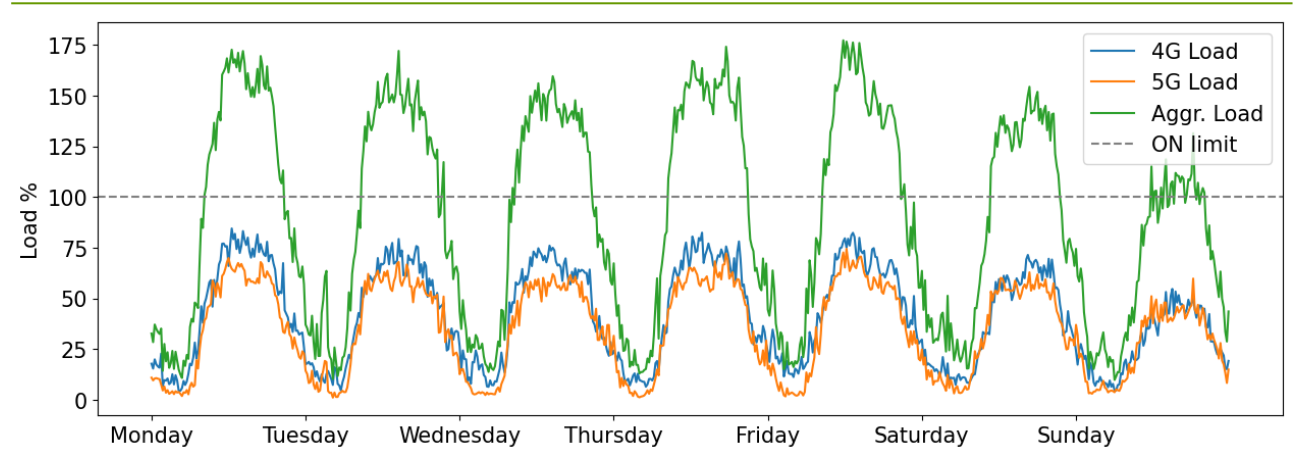


Figure 3-36 Load of a selected cell during the analysed week in percentage of total PRBs: Aggregated 4G (blue), 5G (orange), and aggregated plus offloaded demand in 4G (green)

To illustrate the designed traffic offloading strategy, Figure 3-36 depicts the load pattern of a representative urban cell with medium-high traffic demand. The blue trend represents the aggregated 4G load across all carriers, as defined in the previous section, while the orange trend shows the 5G load. Both trends exhibit a strong correlation and follow typical day-night traffic cycles. The green trend indicates the total traffic demand on the 4G cells, which includes the offloaded traffic from the 5G carrier. This value is calculated by converting 5G PRBs into 4G PRBs, considering the difference in SCS configuration reported in Table 3-3 (i.e., 5G slot duration is half that of a 4G slot). For example, a 5G average downlink demand of 60% corresponds to 123 PRBs per 5G slot (i.e., calculated as 60%×205). This translates to an equivalent 4G load of 246 PRBs per 4G slot (i.e., 123×2).

Once the aggregated 4G and offloaded 5G loads are calculated, the offloading decision becomes straightforward. If the aggregated load exceeds a predefined threshold, the 5G cell should remain active to handle the traffic demand. Otherwise, the 5G cell can be switched off to save energy and its load can be offloaded to 4G. In this analysis, usually a 100% threshold is applied to explore the upper bound of energy savings (see dashed line in Figure 3-36). However, in operational deployments, more conservative thresholds might be implemented to avoid saturation and exhaustion of 4G PRBs. Section 3.8.2 explores the effects of different thresholds on energy-saving opportunities and obtained QoS.

Using this strategy, the example cell achieved a switch-off time of 53% of the week. Given that this cell is in a high-demand area, the potential energy savings across the entire region, as discussed in Section 3.8.2, are expected to be even more significant.

3.8.1.3 Estimation of the saved energy

In this section, we discuss the methodology used to estimate the energy saved in each sector of the sites, denoted as E_{saved} , when applying the traffic offloading strategy. The estimation is based on the following:

$$E_{saved} = E_{5G,baseline} + E_{5G,traffic} - \sum_{4G cells} E_{4G,\Delta traffic}$$
 (1)

where $E_{SG,baseline}$ represents the baseline energy consumption of the selected 5G cell, $E_{SG,traffic}$ denotes the energy consumed due to the traffic demand in the 5G cell, and $E_{4G,\Delta traffic}$ accounts for the increase in energy consumption in the 4G cells as a result of the offloaded traffic. Since the dataset does not include a KPI reporting the energy consumption of the 4G nodes, we are unable to estimate this latter term directly. To address this, we simplified Equation (1), assuming that the additional energy consumption in $E_{4G,\Delta traffic}$ approximates the energy consumption attributed to the traffic demand in the 5G cells prior to the offloading, $E_{5G,traffic}$. As a result, the two terms cancel out, leaving the baseline energy consumption of the 5G cells, $E_{5G,baseline}$, as the approximation for the estimated energy savings.



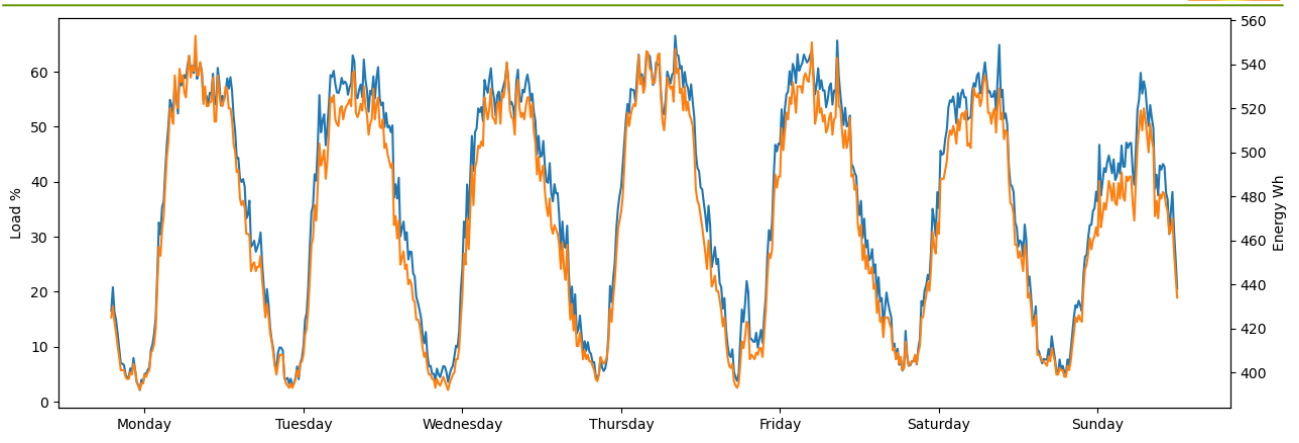


Figure 3-37 Average load (blue) and energy consumption (orange) of one 5G 3500 MHz node

Since the dataset provides only the total energy consumption per node, the baseline energy consumption of the 5G cells is estimated based on the correlation between energy consumption and load, as illustrated in Figure 3-37 for the node analysed in this section. The energy observed during the periods of lowest demand is considered an approximation of baseline consumption, as the contribution from traffic demand to energy during these times is minimal. For the analysed node, the baseline consumption is estimated at approximately 400 Wh every 15 minutes, or 1600 Wh per hour. Given that each 5G node consists of three cells, the baseline consumption per cell is calculated to be 133 Wh every 15 minutes, or 532 Wh per hour. Using this value, the switch-off time reported in the previous section translates to an energy saving of 47.4 kWh for the example cell.

Note that this estimation does not explicitly consider the division of energy usage between the Radio Unit (RU) and the Baseband Unit (BBU). According to [32], the RU typically accounts for an average of 88% of energy consumption under normal load conditions and up to 78% under maximum load conditions in 5G commercial networks. Therefore, the previously introduced energy savings estimate could be slightly adjusted to reflect these weights. However, two factors support the validity of the current approximation. First, switch-off periods mainly occur during low traffic conditions, where the RU's share of total energy consumption is higher. Second, the analysis of the complete dataset (as presented in Section 3.8.2) shows that all three cells or sectors of a 5G node are typically deactivated simultaneously during these periods, allowing for the complete shutdown of the BBU.

In any case, results in Section 3.8.2 will mainly focus on the percentage of time that 5G cells could be deactivated, offering a broader and more generalizable perspective on the energy-saving benefits and trade-offs associated with the proposed traffic offloading strategy.

3.8.1.4 QoS impact characterization

When offloading traffic from 5G cells to 4G cells, the affected UEs will experience a QoS degradation. The approach described in the previous section ensures that all offloaded 5G PRBs are fully allocated, meaning the offloaded traffic will continue to be served in the next 15-minute period. However, UEs may experience reduced uplink and downlink transmission rates due to the different capabilities of 4G and 5G cells. This can lead to slower download speeds and negatively affect services requiring specific data rates, such as video streaming. To evaluate the impact on performance, we examined the *average downlink throughput per UE* KPI, which indicates the experienced transmission rate. To illustrate the effect of cell capacity on this KPI, Figure 3-38 presents a scatter plot showing the relationship between average cell load and average throughput per UE for both a 4G 2600 MHz cell and a 5G 3500 MHz cell.

In [33], the average throughput per UE KPI is defined as the total data volume during a 15-minute interval, divided by the active time during which the scheduler assigns data to users. At lower demand levels, the scheduler allocates data sporadically.



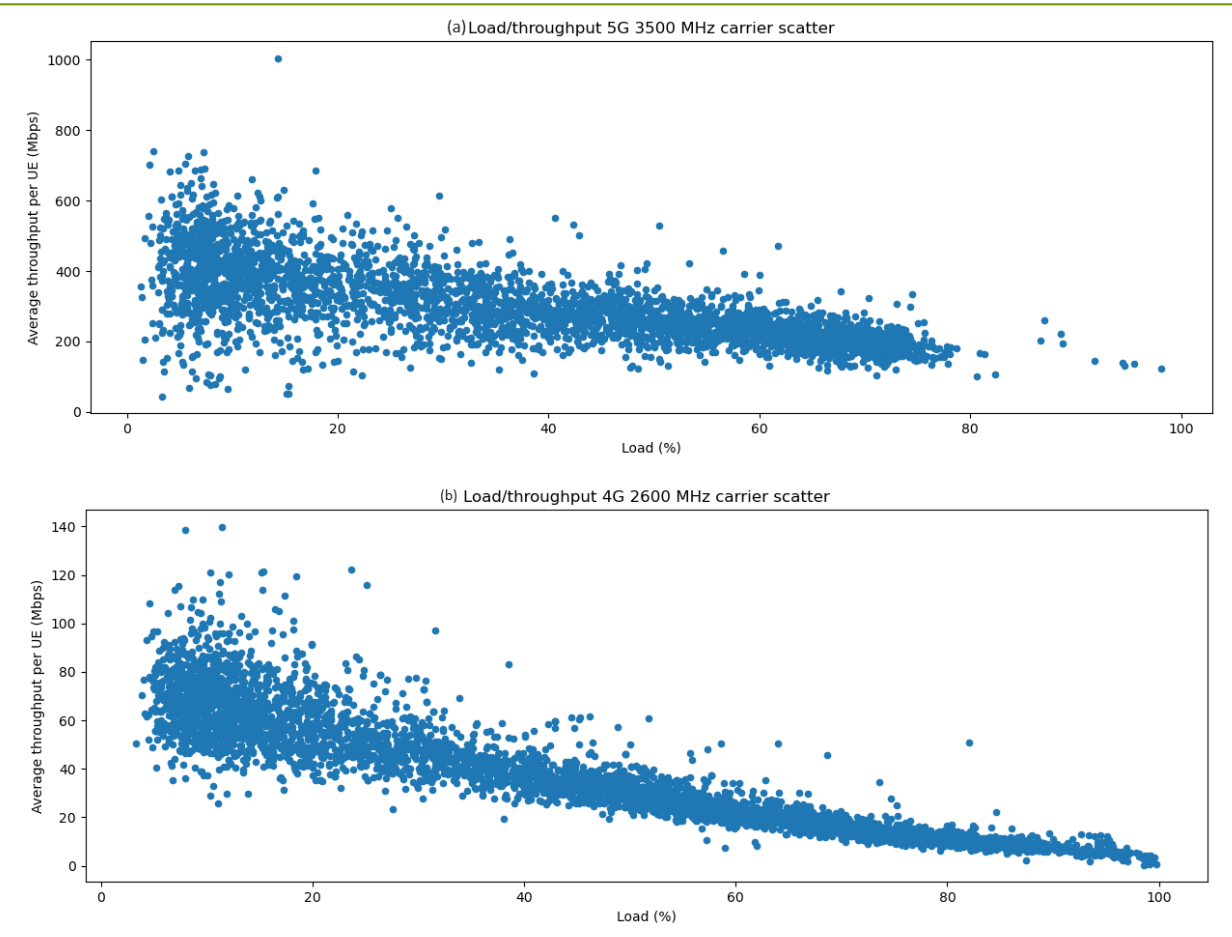


Figure 3-38 Correlation between load (% of PRBs) and average throughput per UE KPIs – (a) 5G 3500 MHz cell and (b) 4G 2600 MHz cell

This intermittent data allocation results in inflated throughput measurements, as depicted in Figure 3-38, as the data rate appears higher during brief bursts of activity. On the other hand, when the cell load approaches full capacity, the scheduler continuously assigns data to all slots to meet demand. In this case, the throughput KPI becomes a more accurate representation of the constant data rate experienced by the UEs throughout the 15-minute interval. Next, we explain how this KPI is integrated into the traffic offloading process to balance QoS and energy savings. The proposed methodology, outlined in Figure 3-39, consists of two primary phases: (i) Traffic offloading and balancing, and (ii) QoS impact estimation.

First, we verify whether offloading 5G traffic to 4G cells within the same sector and site is feasible, following the methodology described in Section 3.8.1.2. If the offloading is possible, we then apply a water-filling algorithm to distribute the 5G load and UEs evenly across all available 4G cells in the sector. This assumes a uniform distribution of PRBs among the UEs. The result of this process is an updated 4G load for each cell, reflecting the portion of 5G traffic that has been offloaded.

In the second phase, we use look-up tables to estimate the average 4G throughput per UE in each cell, based on the calculated aggregated load. These tables are specific to each cell and utilize the correlation between load and throughput, as was illustrated in Figure 3-38,, using the average throughput at each load level. Note that the variability of throughput values at a certain load value decreases under high load conditions, which is typically the case during the offloading process, allowing for the use of the average throughput value as estimation. Finally, if the estimated throughput of the cells meets or exceeds the QoS threshold (0 Mbps if no specific level is defined), we compute the energy savings based on the baseline consumption of the 5G cell, as described in Section 3.8.1.3, and the resulting QoS level.



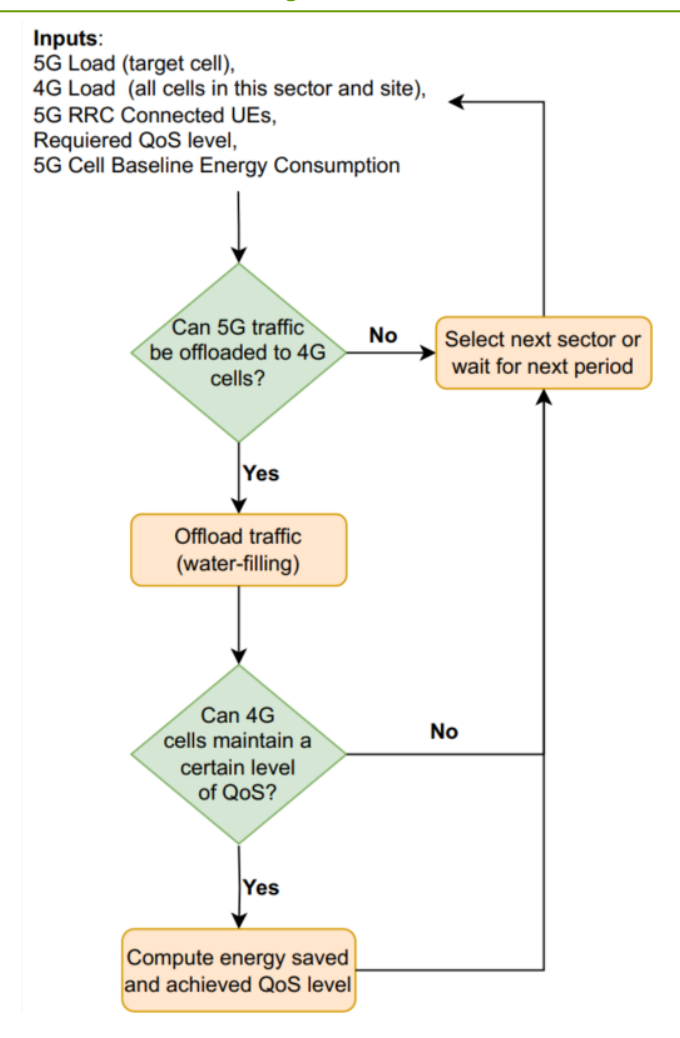


Figure 3-39 Traffic offloading and QoS impact characterization pipeline

To provide a first insight on the trade-off between switch-off opportunities and QoS, we compare the results for various QoS thresholds using the example cell from the previous section. These thresholds include: (i) 53% of the time with throughput above 0 Mbps, (ii) 53% above 5 Mbps, (iii) 45.6% above 10 Mbps, (iv) 36.6% above 15 Mbps, (v) 33.4% above 20 Mbps, and (vi) 28.6% above 25 Mbps. As anticipated, the percentage of time meeting each throughput threshold decreases notably as the required throughput level increases. Specifically, only 5 Mbps can be fully guaranteed during the switch-off period that maximizes energy savings (i.e., at 0 Mbps throughput threshold). The QoS thresholds analysed are derived from the typical requirements of popular video streaming applications like YouTube and Netflix. For example, YouTube² recommends a minimum of 5 Mbps for FHD 1080p videos and 20 Mbps for UHD 4K, while Netflix³ requires at least 15 Mbps for UHD 4K streaming.

3.8.2 Analysis of results

This section presents the results of applying the introduced methodology to the complete clusters of cells in this area (858 4G cells and 195 5G cells at 3500MHz), determining the achievable energy savings and its impact on the QoS. Additionally, we also analyze the effect of using different aggregated load thresholds when determining the on/off status of the cells.

² https://support.google.com/youtube/answer/78358?hl=en

³ https://help.netflix.com/en/node/306



3.8.2.1 Trade-off between energy savings and QoS

First, we characterized the energy-saving opportunities considering the whole cluster of cells and without QoS requirements. Figure 3-40a uses a heat map to illustrate the percentage of time each cell could be deactivated during the analysed week, based on the introduced methodology. On average, we observed that 5G cells in the deployment could be switched off during 79% of the week, leading to 13.7 MWh of energy savings. However, as shown in the figure, there is a high variability in the switch-off time of the cells, some of them reaching 100% of the time while others didn't surpass 20% of the time. Concretely, 64 cells (i.e., approximately 30% of the cells) could be switched off the whole week, representing energy savings of 5.7 MWh. Without considering these cells, the average switch-off time decreases to 68.5%. As shown in the heat map, there is no correlation between cell locations and switch-off time, not showing a distinction between urban and suburban scenarios. In general, we found that dark cells (low-opportunities cells) are found to be in social or cultural points of interest, where cell load tends to be higher during the whole analyzed period. On the other hand, residential areas show higher energy savings opportunities, probably due to the high penetration of fiber in this area that leads to a lower utilization of the cellular network.

Figure 3-40b depicts a CCDF illustrating the percentage of cells meeting each defined QoS level over a certain time period when applying the traffic offloading strategy without QoS restrictions. The values are normalized based on the time the cells are switched off (i.e., 78.8% of the week on average, as mentioned earlier). It is important to note that increasing the QoS levels significantly impacts both the percentage of cells that can meet these limits and the percentage of time they can maintain them. For example, while all cells can provide 5 Mbps for nearly 80% of the switch-off time, the percentage of cells drops to less than 60% for 10 Mbps and less than 20% for 15 Mbps. For the highest QoS limits, the reductions are even more pronounced: for instance, less than 20% of the cells can provide 20 Mbps for more than 60% of the time and 25 Mbps for more than 40% of the time.

As illustrated in Figure 3-41a (blue line), applying different defined QoS limits to control on/off switching and traffic offloading significantly reduces the opportunities for cell switch-off, i.e. the amount of saved energy. While using a 5 Mbps limit achieves energy savings comparable to the upper bound (78.3% versus 79%), increasing the QoS limit to 15 Mbps reduces them to below 50%, and at 25 Mbps, they drop to under 20%. This highlights the inherent trade-off between energy savings and the QoS experienced by users, which should be considered by operators when implementing such energy saving strategies.

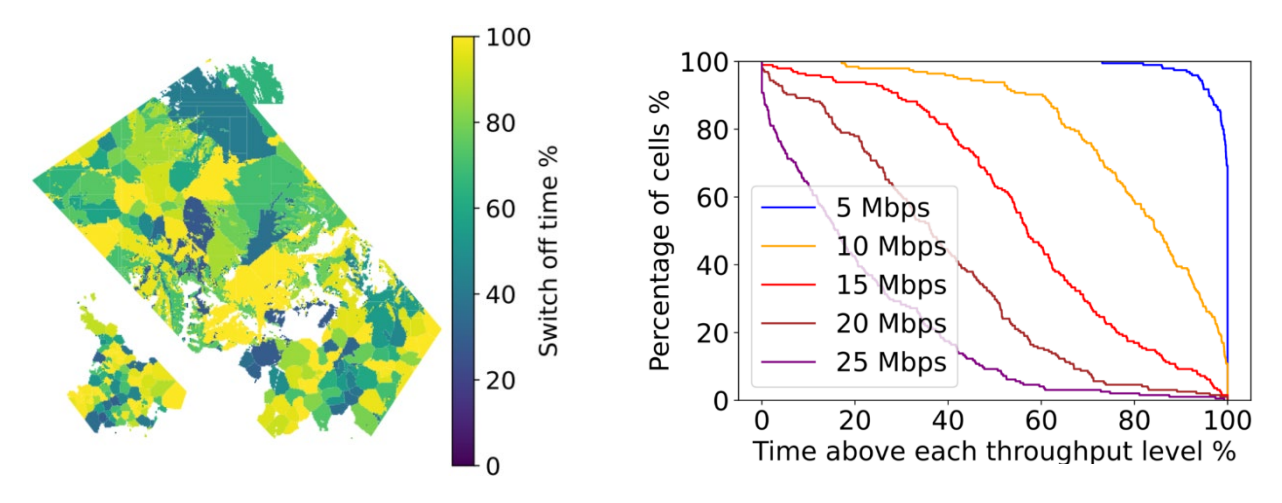


Figure 3-40 Evaluation of Energy-QoS trade-off using 100% threshold: (a) Calculated switch-off time (% of the analysed week), (b) Time above defined QoS levels per percentage of cells (CCDF)



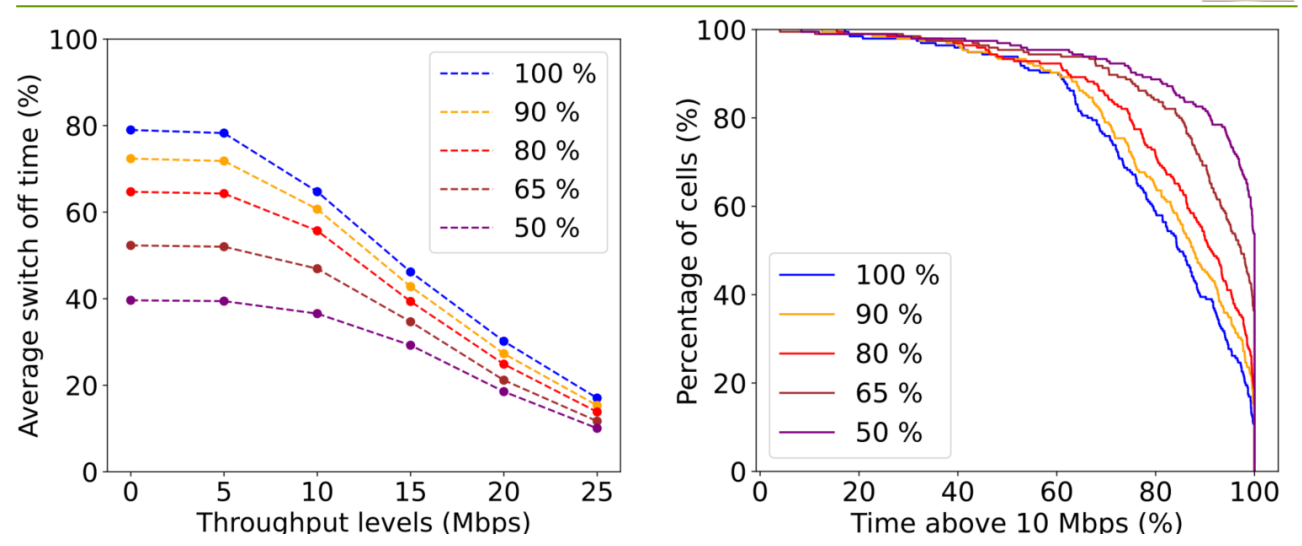


Figure 3-41 Evaluation of Energy-QoS trade-off using different thresholds: (a) Average switch-off time vs assured throughput, (b) Percentage of switching-off time above 10 Mbps level per percentage of cells (CCDF)

3.8.2.2 Threshold study

In this section, we analyze the impact of varying the aggregated load threshold of 4G cells on the energy-QoS trade-off when deciding cell switch-off and traffic offloading. The objective is to determine whether reducing the overall threshold can achieve specific QoS limits without the need to estimate the QoS of each individual 4G cell during offloading. Simplifying this process could make the application of the proposed framework more practical.

As shown in Figure 3-41a, while decreasing the throughput level generally reduces the difference between the switch-off time achieved by the upper bound (i.e., 0 Mbps) and that obtained when applying QoS limits, the penalty in terms of wasted energy-saving opportunities is significant. For instance, in the case of a 10 Mbps limit, Figure 3-41b illustrates that lowering the threshold effectively increases the percentage of cells able to maintain this throughput for a greater portion of their switch-off time. However, this comes at the cost of reducing the overall percentage of time the cells are switched off. As shown in Figure 3-41a, applying a 100% threshold considering a QoS limit of 10 Mbps achieves approximately 65% average switch-off time, but this drops to less than 40% when the threshold is reduced to 50%. This highlights the importance of assessing the QoS achievable by individual cells before applying the traffic offloading decision.

Figure 3-42 illustrates the distribution of throughput levels across cells required to achieve the specified QoS limits throughout the entire switch-off time period. As expected, the average throughput decreases as the QoS limits increase, aligning with the intuitive notion that reducing thresholds increases the probability of meeting certain QoS levels. However, the significant dispersion observed within each QoS limit emphasizes the need to set cell-specific thresholds to maximize energy-saving opportunities while meeting the QoS constraints. This is aligned with the results extracted from Figure 3-40a, which demonstrated a significant variability in the achievable energy savings across the different cells of the analyzed area.

We can conclude that, since each cell operates within a unique context, such as the utilization trend and the characteristics of 4G carriers, energy efficiency strategies considering the energy-QoS trade-off should rely on per-cell approaches such as per-cell load thresholds or QoS estimation. Alternatively, clustering methods could be employed to group cells with similar behavior, reducing the complexity by enabling the application of common strategies to each cluster.



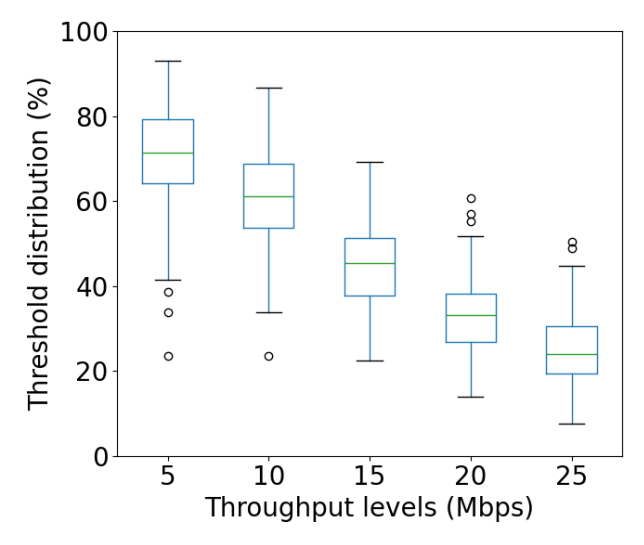


Figure 3-42 Threshold distribution of the cells for each throughput level. For each throughput level, cases where the 5G cell remains off continuously due to low load are not considered (i.e., no threshold can be inferred)

3.9 Performance assessment of energy savings via A1 policies at Adastral Park

This section presents the proposed scenario for the BeGREEN simulation at Adastral Park, leveraging a SFN to enhance coverage and optimize energy consumption. The Energy Management Subsystem (EMS) plays a crucial role in integrating data from the VIAVI AI RSG simulator, which emulates the radio environment and its various scenarios. The primary goal is to manage the radio environment effectively, ensuring a reduction in energy consumption while maintaining the required QoS.

The proposed deployment consists of six cells in the Adastral scenario or seven cells in the reference scenario, each positioned at an elevation of five meters. The transmission power per cell is set at 35 dBm, supporting 20 users with an individual data requirement of 5 Mbps each. The system operates with a bandwidth of 40 MHz within the 3.8 GHz TDD band (7D2U1S configuration), covering an area of approximately 1.5 km².

The use case focuses on the implementation of a SFN environment that aims to minimize energy consumption by dynamically adjusting transmission power and selectively deactivating radio units during periods of low traffic, based on A1 policies provided by the intelligence plane. When traffic demand increases, deactivated cells can be reactivated to maintain adequate coverage and service levels. The scenario considers various traffic patterns and mobility behaviours, including pedestrians, stationary indoor users, and mobile users traveling by bike or car. The simulation environment is modelled based on the geographical characteristics and infrastructure of Adastral Park, utilizing predefined site locations and configurations.



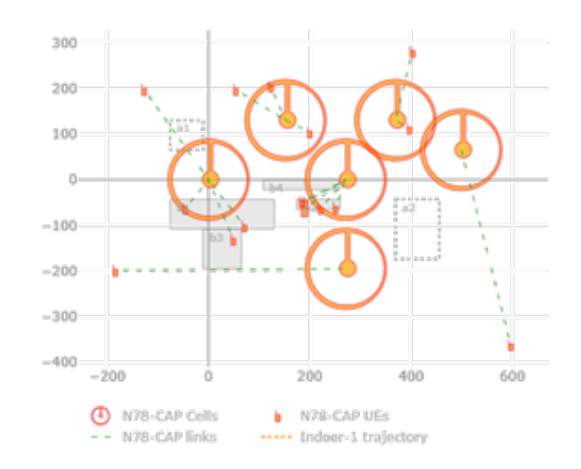


Figure 3-43 General location of sites in Adastral Park, b) mapping of sites on the VIAVI AI RSG Tester.



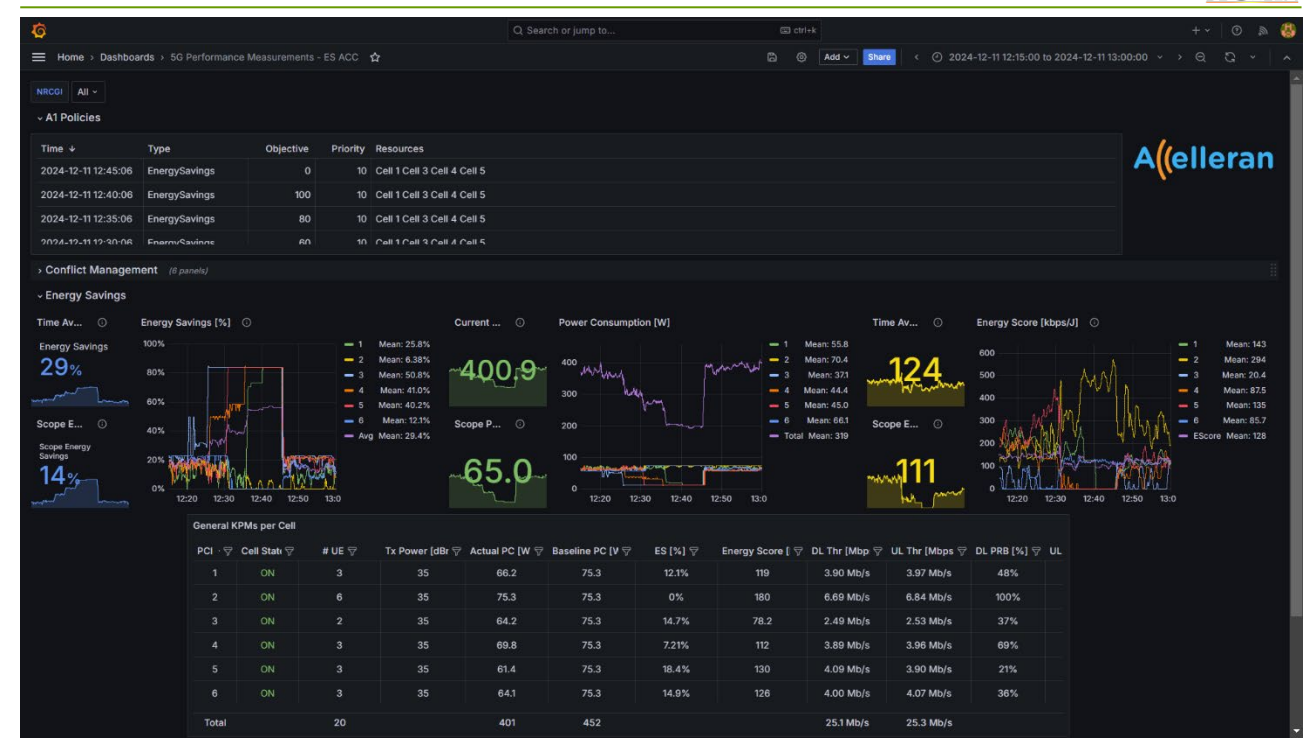


Figure 3-44 Dashboard providing energy savings metrics, policies and general cell metrics.

The test plan consists of two key scenarios designed to validate the proposed approach. The baseline scenario serves as a benchmark to establish initial energy consumption levels and collect telemetry data for performance evaluation. In contrast, the EMS-activated scenario employs predictive AI/ML algorithms to dynamically optimize energy efficiency by managing cell power in response to varying traffic conditions. These tests are conducted changing the energy saving objective from 0% to 80%. Figure 3-44 depicts the results dashboard where the policies, the energy savings metrics and general system metric can be investigated.

3.9.1 Results

Figure 3-45 presents a time-based analysis of energy savings across multiple cells in the Adastral Park simulated scenario. Several coloured lines describe the specific cell's energy savings performance over time (Cell 1 through Cell 6), while the dotted line shows the averaged Energy Savings for the whole system and the dashed line the average of the cells in the scope of the policy. In the early stages of the simulation, energy savings for most cells are relatively low and fluctuate between 10% and 30%, reflecting optimizations in the base line while no policies are applied. The first policy arrives at 12:20 requesting Cells 1, 3, 4 and 5 to provide an energy savings of 20% and since the energy savings are already close ot this value, nothing changes. Around the 12:25 mark, the next policy requesting 40% energy savings. Here, the ES algorithm decides to turn-off Cell 3 (orange line) moving the Scope ES to 40% and leave it for the rest of time until a new policy arrives. Five minutes later, at 12:30 a new policy arrives requesting 60% which the system complies by shutting down Cell 5 and reducing Tx power of Cell 4. At 12:35 a policy for 80% is issued and the algorithm complies by switching Cell 4 off. Then at 12:40 the 100% ES policy arrives and turn-on off Cell 6, increasing into the maximum possible energy savings which is nearly 84%. This confirms the activation of energy-saving mechanisms, such as cell power adjustments or traffic load redistribution strategies. Following this increase, the energy savings values for certain cells, including Cell 1 and Cell 6, rise more gradually, showing a steady improvement in performance. The system-wide average, represented by the dotted line, follows an upward trend, indicating an overall improvement in energy efficiency across the network.



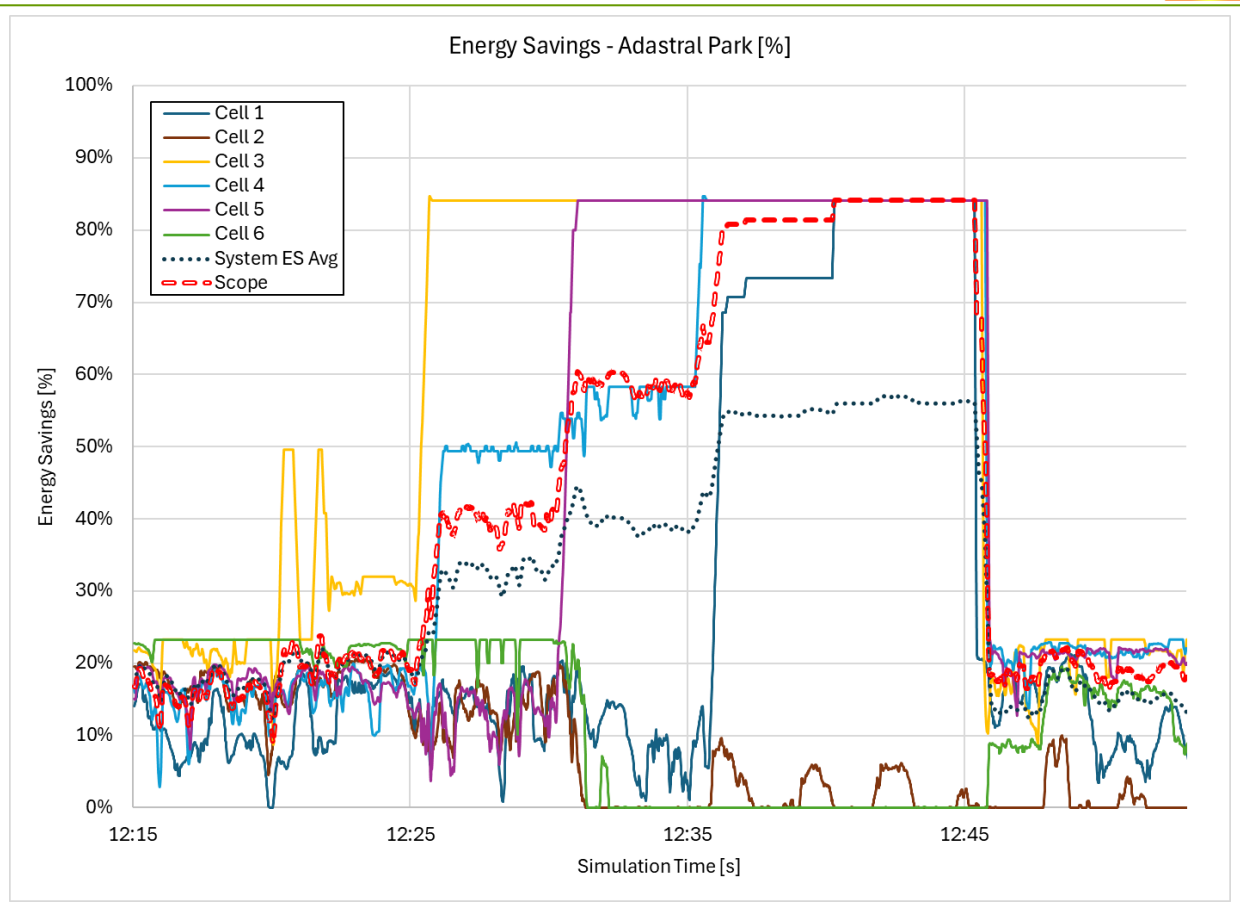


Figure 3-45 Energy Saving results for the Adastral Park use case.

Closer to 12:45, all energy savings values exhibit a sharp decline, after the reception of the 0% ES policy returning to lower Energy Savings levels, due to the activation of all the cells. Overall, the graph illustrates the dynamic adjustments in energy savings across different cells within the Adastral Park scenario, highlighting the effectiveness of the energy management strategies being tested.

Conversely, the total network power consumption over time in the Adastral Park simulation scenario is presented in Figure 3-46. The dotted line represents the total system power consumption, while individualcoloured lines correspond to the power consumption of each cell (Cell 1 through Cell 6), providing a detailed breakdown of the system's energy usage. Initially, total power consumption fluctuates around 350 to 400 watts, with all cells contributing to the overall power demand. Around 12:20, a policy is applied, requesting specific cells to reduce energy consumption. Cell 3 (yellow line) is the first to exhibit a noticeable drop in power consumption as it is turned off. By 12:25, further energy-saving policies are implemented, leading to the shutdown of additional cells, including Cell 4 (cyan line), which results in a significant decline in total power consumption. As the simulation progresses, at 12:30, Cell 5 (purple line) experiences a reduction in transmission power, followed by a complete shutdown. At this time, the power consumption of the remained cells slightly increases to compensate for the new users allocated. Finally, Cell 1 (blue line) is powered down and the further driving down overall power usage to around 200 watts, showing energy savings larger than 50%. This demonstrates the impact of dynamic power management strategies in optimizing energy consumption. After 12:45, a policy change leads to the reactivation of previously deactivated cells, causing a sharp rise in total system power consumption. The power values for each cell return to their previous levels, restoring the network to full operational capacity.





Figure 3-46 Power consumption results from the Adastral Park use case.

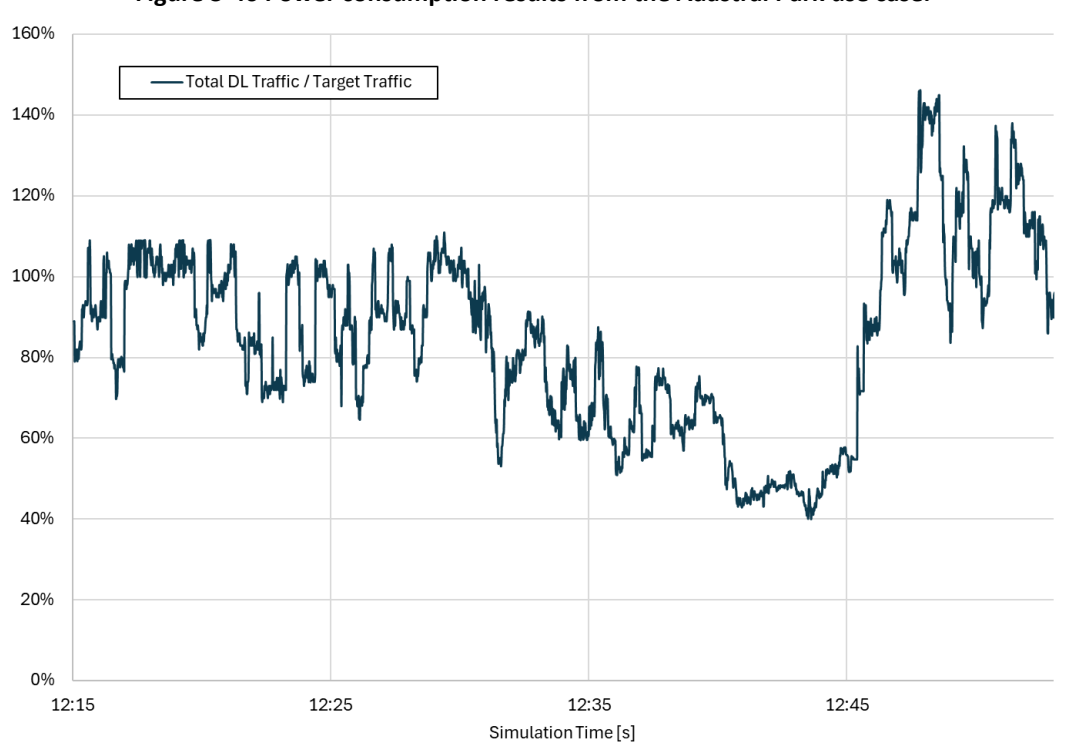


Figure 3-47 Ratio between the requester traffic and the served traffic in the Adastral Park use case.

Figure 3-47 presents the QoS Score defined as the ratio of actual DL traffic to target traffic over the simulation period for the Adastral Park scenario. A value of 100% indicates that the actual traffic matches the requested traffic, while values below or above 100% represent under-provisioning, while values higher, represent traffic that is delayed in the buffer of the network. Initially, the ratio fluctuates around the 90-100% range, suggesting that the system is mostly meeting traffic demands. However, around 12:25, the ratio begins to



decline, reaching levels as low as 60%. This drop coincides with the activation of energy-saving policies that reduce available capacity by switching off cells or lowering transmission power. Between 12:35 and 12:45, the ratio remains low, indicating a significant mismatch between provided and requested traffic, likely due to aggressive energy saving measures. After 12:45, the ratio rapidly increases, surpassing 100%, indicating that system capacity has been restored, potentially due to the reactivation of previously disabled cells, and serving storage traffic in a delay basis. Overall, the graph highlights the trade-off between energy savings and service quality, showcasing how network adjustments impact the ability to meet user traffic demands showing and average of 97% for the whole simulation time.

Finally, Figure 3-48 presents the Energy Score for the Adastral Park scenario, measured in kilobits per second per joule (kbps/J), which quantifies the relationship between the traffic served by each cell (or the overall system) and the energy consumed by the respective cells. The dotted line represents the system-wide Energy Score, fluctuating between approximately 100 and 200 kbps/J throughout the simulation with an average of 127 kbps/J. This indicates a general energy efficiency of the network, but still the Energy Score diminishes during the higher energy savings policies, showing that the policies algorithm is not optimized towards Energy Score. Looking at individual cell performance, Cell 2 (brown line) demonstrates a significant increase in energy efficiency, reaching values as high as 500 kbps/J. This peak occurs when Cell 2 is serving most of the network users, highlighting its effectiveness in delivering traffic with optimal energy consumption. This trend suggests that Cell 2 is efficiently utilizing its resources during high-load periods, contributing positively to the overall system performance having an average of 293 kbps/J for the simulation time. In contrast, other cells such as Cell 3 (yellow) and Cell 4 (blue) exhibit relatively lower Energy Score values (20 kbps/J and 87 kbps/J in average) and eventually drop to zero when they are deactivated as part of the energy-saving strategies. The remaining active cells show fluctuating scores, reflecting changes in traffic distribution and energy usage across the network.

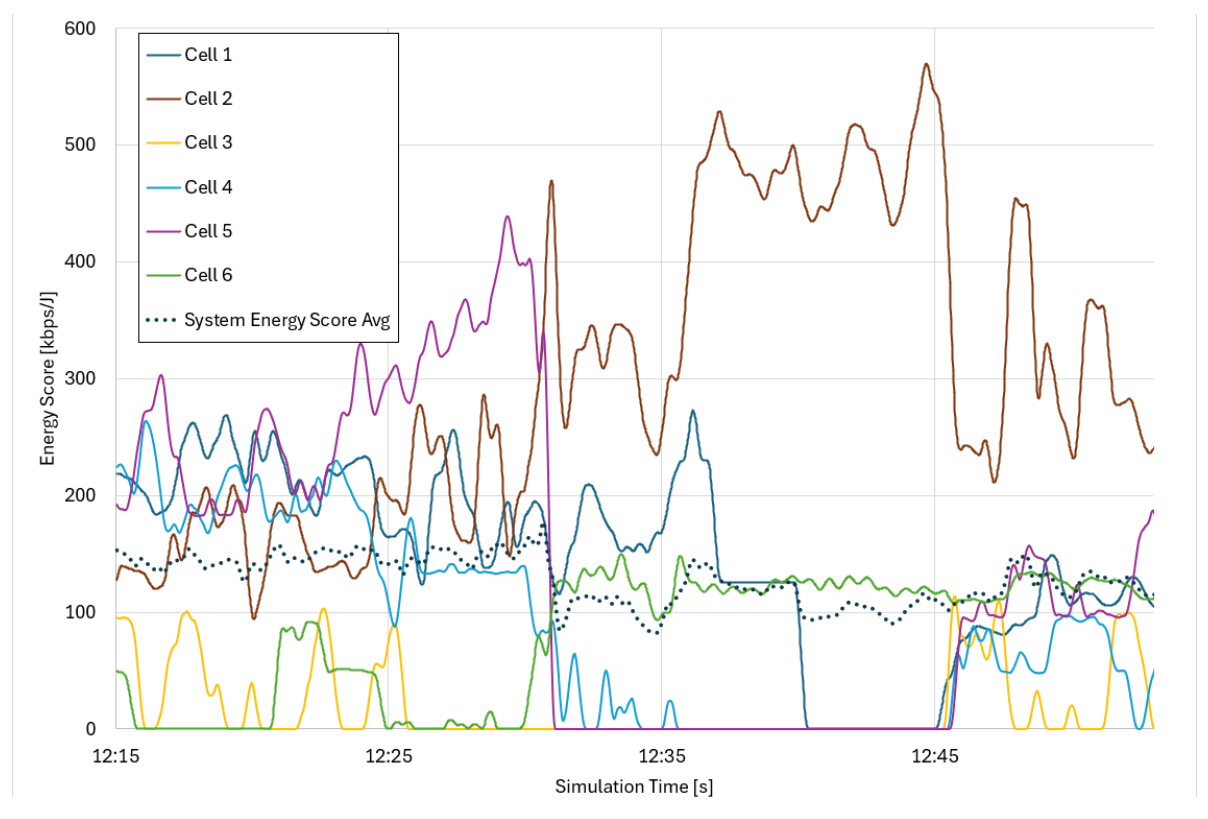


Figure 3-48 Energy score in kbps/J results for the Adastral Park use case.



3.9.2 Conclusions

The BeGREEN simulation at Adastral Park demonstrates the effectiveness of an SFN in optimizing coverage and reducing energy consumption through intelligent management strategies. The EMS, utilizing data from the VIAVI AI RSG simulator, enables dynamic adjustments of transmission power and selective deactivation of radio units based on traffic demands. The simulation results show that energy savings can reach up to 84% by progressively shutting down cells while maintaining an acceptable quality of service. However, reactivation of cells is required when traffic increases, highlighting the balance between energy efficiency and service availability.

The test scenarios validate the proposed energy-saving strategies, with total power consumption initially fluctuating between 350 and 400 watts before gradually reducing to 200 watts under active energy-saving policies, demonstrating more than 50% reduction. The system effectively adapts to varying traffic patterns, including pedestrians, stationary users, and mobile users, ensuring operational efficiency. The actual QoS Score ratio remained satisfactory at an average of 97%, although significant drops were observed during aggressive energy-saving measures, indicating potential trade-offs in service quality.

Furthermore, the Energy Score metric, which evaluates traffic delivery efficiency relative to energy consumption, showed an overall system average of 127 kbps/J. Cell 2 demonstrated outstanding efficiency, reaching peaks of 500 kbps/J when serving most users, whereas other cells displayed lower efficiency values and were deactivated when necessary. These findings underscore the impact of intelligent energy management policies on balancing performance and sustainability in 5G network environments.



4 KPI results

This chapter shows how the results obtained in this deliverable align with our project's KPIs. This mapping is crucial to demonstrate the real-world impact of the project and how it contributes to the attainment of our defined KPIs. Particularly the work in WP2 provides a high-level analysis of the KPIs that underpin our BeGREEN project, helping us to navigate toward a more energy-efficient future in mobile networks.

Table 4-1 outlines all BeGREEN project's KPIs, as done in BeGREEN D2.2, but at this stage we are able to provide additional (simulation) results that are able to complete the table.

Table 4-1 BeGREEN KPI Evaluation (based on that in BeGREEN D2.2 [2], and to BeGREEN D5.2 [34]).

#	WP	Verification	Spec and Ref. Value	Description	Measured Value
		Method	for 6G Use Cases	2 2 3 2 1 3 1 3 1	(Results Obtained)
1	2	Simulation	Energy consumption, N/A	Energy consumption model for 5G/B5G base-stations and proposing energy efficiency enhancements	50-100% improvements in energy score are achievable in the cellular reference model.
2	2	Simulation	Energy consumption, N/A	System level simulator (AIMM) to enable area-wide assessment of energy consumption over time.	As in the previous row, 50- 100% improvements in energy score are achievable in the cellular reference model.
3	2	Simulation	Energy efficiency optimization across BeGREEN components, N/A	Balance between different network evolution strategies to optimize energy efficiency in different target service areas	30 dB of energy reduction of transmit power by using a cell-free architecture compared with C-MIMO.
10	2,3	Simulation and In-lab test (PoC2)	Angle and range precision for localisation	Precision of the developed sensing algorithm for detecting potential users	20º angular resolution, 1 m range resolution (with Sub-6 ISAC system)
11	2,3	Simulation	Use identification with 20% less wireless medium (channel) usage	Sensing-assisted beam search – 20% performance improvement with respect to extensive search and hierarchical search.	30% improvement of performance improvement (detailed results are included in Section 4.1.3 in BeGREEN D3.3 [35])
12	3	Simulation and measurement results	50% accuracy improvement in user estimation	Detection of users/user density in order to estimate the presumed network load – at least 50% accuracy of estimation of potential mobile users	60% accuracy depending on the range at which the user(s) are and the area to be covered. To be assessed fully in BeGREEN D5.3.
19	4	Simulations and in-lab tests (NEC)	Energy consumption, N/A	>20% power consumption reduction on the server that runs the edge AI service AI service power consumption	Energy saving up to 29.24%, depending on the constraints in terms of accuracy and delay set in for the use case.
20		Analytical analysis based on lab tests with x86 and ARM servers with the same test scenario. The	Scenario for low throughput 1 UE Both Energy Consumption and Energy Performance (Joules/bit) must fulfil the 20% reduction.	>20% power consumption reduction on running CU on ARM and HW accelerating PDCP of CU- UP	22% energy savings for UC1 (15% ES for UC2) as described in D3.2.



8
BEGREEN

	metric used	
	will be	
	Joules/bit to	
	include the	
	performance	
	improvement	
	of the system	
	in this test.	



5 Summary and conclusions

Nine different energy-saving studies have been carried out and their findings are summarized below.

Section 3.1 has explored how cell-free architecture reduces energy consumption. In particular, a cell-free system was compared to a traditional C-MIMO deployment in a realistic urban-dense scenario. It was concluded that a cell-free architecture reduces the transmit power by 30 dB compared with a traditional MIMO deployment. In addition, the cell-free system provides functional BER for 8 streams which makes this technology suitable for high-data-rate applications.

Section 3.2 has studied the evaluation of the energy savings and energy efficiency improvements achievable through the usage of relay nodes considering a realistic university campus scenario. The study has analyzed the placement of indoor relays in floors of different buildings with coverage limitations and studied the effect of different parameters such as the required bit rate or the power consumption model parameters. This analysis has demonstrated that an energy saving of up to 90% was achieved by properly placing relays on the floors of buildings with poor indoor coverage conditions.

In section 3.3 a comparison between the use of a RIS or a relay has been presented focused on assessing their achievable energy savings concerning the case in which none of these elements is used to enhance the coverage in certain areas. It has been found that in general, the RIS provides higher energy savings when its pathloss with the base station is lower than 90 dB and for UEs located in a relatively narrow angular region for the RIS pointing direction, while for larger pathlosses or outside this region the relay outperforms the RIS. Also, an analysis in a realistic university campus scenario in which most of the poor coverage areas are found indoors has led to the observation that in most of the studied situations, the relay provides higher energy savings than the RIS, while the RIS only outperforms the relay in very specific conditions where it can be placed outdoors.

Section 3.4 has researched the impact of increasing, from sub-6 GHz to mmWaves, the operating frequency of the base stations in terms of total power consumption. The results found in the UPC campus scenario have revealed that to keep the same coverage conditions when moving from 3.72 GHz to 26 GHz, a transmitted power increase of 27 dB is required to compensate the higher propagation losses. This leads to increasing the power consumption per base station in a factor 94. This increase can be substantially reduced by exploiting features such as beamforming. In this case, results have shown that it is possible to keep the same coverage with a power consumption increase factor of only 1.28.

The findings in the network optimization given sensing data, presented in section 3.5, provide an idea of power consumption savings by turning off some of the BSs and turning on the optimal BS given a certain scenario. The results show that, given a performance metric to optimize, the power consumption can be reduced by up to 50%.

Section 3.6 studied fundamental limits (that is, those obtained from information theory) on energy score improvements obtainable in a cellular reference model of 7 cells, with these being compared to simulator results for a realistic 5G system. These are intended as a benchmark or basis for comparison with less theoretical models.

Section 3.7 analysed and presented the DU uplink energy consumption results. It was shown that the energy optimized UL scenarios fit the cellular reference model. Hence, a DU energy score improvement of approximately 40% compared to legacy architectures can be expected for these scenarios.

Section 3.8 presented BeGREEN approach to investigating energy-saving opportunities in a real 5G NSA deployment, utilizing a dataset provided by a European MNO, as described in Section 2.5.4. A data-driven framework was detailed to evaluate the energy-saving and QoS trade-off when selectively deactivating underutilized 5G cells and offloading their traffic to 4G cells with enough resources within the same sector



and site. Results demonstrate network-wide cell switch-off opportunities ranging from 17% to 79% while ensuring data rates of 25 Mbps and 5 Mbps, respectively. The importance of considering site-specific characteristics and KPIs was also highlighted, discouraging the use of global fixed strategies for effective optimization. This framework is being leveraged in WP4 to propose practically implementable AI/ML-driven strategies that effectively balance QoS and energy saving.

Section 3.9 demonstrated the ability to optimize energy consumption while maintaining service quality. This analysis was done by utilizing a Single Frequency Network (SFN) and the EMS with data from the VIAVI AI RSG simulator. By dynamically adjusting transmission power and selectively deactivating radio units during low-demand periods, energy savings of up to 84% were achieved, reducing the total power consumption from 400W to approximately 200W. However, these strategies impact the actual-to-target traffic ratio, which drops to 60% at certain points but averages 97% throughout the simulation. Energy efficiency fluctuates between 100 and 200 kbps/J, with a system-wide average of 127 kbps/J, while Cell 2 stands out with a peak efficiency of 500 kbps/J when serving most users. These results highlight the effectiveness of energy management strategies in balancing efficiency and network adaptability.



6 References

- [1] BeGREEN D2.1, "BeGREEN Reference Architecture", July 2023, https://www.sns-begreen.com/deliverables?id=971369
- [2] BeGREEN D2.2, "Evolved Architecture and Power Enhancement Mechanisms", July, 2024.
- [3] ETSI standard TR 138.901, 3GPP standard TR 38.901 v18.0.0 R18, available at https://www.etsi.org/deliver/etsi_tr/138900_138999/138901/18.00.00_60/tr_138901v180000p.p df.
- [4] 3GPP standard 36.873. Available at https://portal.3gpp.org/desktopmodules/Specifications/SpecificationDetails.aspx?specificationId=2
 574.
- [5] 36873-c70.doc from https://portal.3gpp.org/desktopmodules/Specifications/SpecificationDetails.aspx?specificationId=2 574.
- [6] BeGREEN D4.2, "Initial evaluation of BeGREEN O-RAN intelligent plane, and AI/ML algorithms for NFV user-plane and edge service control energy efficiency optimization", September 2024.
- [7] O. Ruiz, J. Sánchez-González, J. Pérez-Romero, O. Sallent, I. Vilà, "Space and time user distribution measurements dataset in a university campus", Computer Networks, 243, March, 2024.
- [8] M. Matalatala Tamasala *et al.*, Multi-objective optimization of massive MIMO 5G wireless networks towards power consumption, uplink and downlink exposure. *APPLIED SCIENCES-BASEL*, vol. 9, no. 22, 2019.
- [9] 3GPP technical specification 38.214, https://www.3gpp.org/ftp/Specs/archive/38 series/38.214/38214-hc0.zip
- [10]GSMA. 5G TDD synchronization: Guidelines and recommendations for the coexistence of TDD networks in the 3.5 GHz range. Technical report, GSMA, April 2020.
- [11]Ngo, H. Q., Tran, L. N., Duong, T. Q., Matthaiou, M., & Larsson, E. G. (2017). On the total energy efficiency of cell-free massive MIMO. IEEE Transactions on Green Communications and Networking, 2(1), 25-39.
- [12] Demir, Ö. T., Méndez-Monsanto, L., Bastianello, N., Fitzgerald, E., & Callebaut, G. (2024). Energy Reduction in Cell-Free Massive MIMO through Fine-Grained Resource Management. arXiv preprint arXiv:2405.07013.
- [13] Jayaweera, N., Manosha, K. S., Rajatheva, N., & Latva-aho, M. (2024). Minimizing Energy Consumption in Cell-free Massive MIMO Networks. IEEE Transactions on Vehicular Technology.
- [14] E. Björnson, M. Kountouris and M. Debbah, "Massive MIMO and small cells: Improving energy efficiency by optimal soft-cell coordination," ICT 2013, Casablanca, Morocco, 2013, pp. 1-5, doi: 10.1109/ICTEL.2013.6632074.
- [15] G. Auer et al., "How much energy is needed to run a wireless network?", in IEEE Wireless Communications, vol. 18, no. 5, pp. 40-49, October 2011, doi: 10.1109/MWC.2011.6056691.
- [16] R. Fantini, D. Sabella, M. Caretti, "An E3F-based assessment of energy efficiency of Relay Nodes in LTE-Advanced networks", PIMRC, 2011.
- [17] BeGREEN D3.2, "Initial developments and evaluation of the proposed enhancements and optimization strategies", August 2024.



- [18] C. Huang, A. Zappone, G. C. Alexandropoulos, M. Debbah, C. Yuen, "Reconfigurable intelligent surfaces for energy efficiency in wireless communication," *IEEE Trans. on Wir. Comm.*, Vol. 18, No. 8, 2019.
- [19] A-A. A. Boulogeorgos, A. Alexiou, "Performance analysis of reconfigurable intelligent surface-assisted wireless systems and comparison with relaying," *IEEE Access*, Vol. 8, 2020.
- [20] E. Björnson, Ö. Özdogan, E. G. Larsson, "Intelligent reflecting surface versus decode-and-forward: How large surfaces are needed to beat relaying?," *IEEE Wir. Comms. Letters*, Vol. 9, No. 2.
- [21] I. Chatzigeorgiou, "The impact of 5G channel models on the performance of intelligent reflecting surfaces and decode-and-forward relaying", *IEEE 31st Annual International Symposium on Personal, Indoor and Mobile Radio Communications (PIMRC)*, 2020.
- [22] M. Di Renzo, et al. "Reconfigurable intelligent surfaces vs. relaying: Differences, similarities, and performance comparison", IEEE Open Journal of the Communications Society, 1, 2020, pp. 798-807
- [23] A. Bazrafkan, et al., "Performance comparison between a simple full-duplex multi-antenna relay and a passive reflecting intelligent surface," *IEEE Trans. on Wir. Comms.*, Vol. 22, No. 8, 2023.
- [24] J. Ye, et al., "Spatially-distributed RISs vs relay-assisted systems: A fair comparison," *IEEE Open Journal of the Communications Society*, 2021.
- [25] M. Rossanese, et al., "Data-driven analysis of the cost-performance trade-off of reconfigurable intelligent surfaces in a production network," *Proceedings of the ACM on Networking*, Vol. 1, CoNEXT3, 2023.
- [26] M. Rossanese, et al., "Designing, building, and characterizing RF switch-based reconfigurable intelligent surfaces," ACM Workshop on Wireless Network Testbeds, Experimental evaluation & CHaracterization, 2022.
- [27] L. M. Guerrero, "Study of macro and small cell deployment options in 5G mmWave bands using ATOLL radio planning tool", Master Thesis of UPC, February, 2020, available at https://upcommons.upc.edu/handle/2117/178151.
- [28] Annu and P. Rajalakshmi, "Towards 6G V2X Sidelink: Survey of Resource Allocation—Mathematical Formulations, Challenges, and Proposed Solutions," IEEE Open Journal of Vehicular Technology, vol. 5, pp. 344-383, 2024.
- [29] N. Baskar et al., "A Survey on Resource Allocation and Energy Efficient Maximization for IRS-Aided MIMO Wireless Communication," IEEE Access, vol. 12, pp. 85423-85454, 2024.
- [30] L. M. P. Larsen, H. L. Christiansen, S. Ruepp and M. S. Berger, "Toward Greener 5G and Beyond Radio Access Networks—A Survey," in IEEE Open Journal of the Communications Society, vol. 4, pp. 768-797, 2023, doi: 10.1109/OJCOMS.2023.3257889.
- [31] O-RAN Alliance. O-RAN WG1 Use Cases Detailed Specification. Technical report, 2024.
- [32] SK Telecom and NTT Docomo. Green mobile network: Energy saving efforts, 2023. Accessed: 2023-12-18
- [33] Ericsson. Key Performance Indicators NR, User Guide, 2020. Accessed: 2024-12-18.
- [34] BeGREEN D5.2, "Solution Integration and Validation", March 2025.
- [35] BeGREEN D3.3, "Final evaluation and benchmarking of the implemented solutions", March 2025.